Characterization of Flax Fibres for Application in the Resin Infusion Process

By
Steven Phillips

A thesis submitted to McGill University in partial fulfillment of the requirements of the degree of Doctor of Philosophy in Engineering

Structures and Composite Materials Laboratory
Department of Mechanical Engineering
McGill University, Montreal

Abstract

Increasing concerns over depleting natural resources has led to the development of so-called biocomposites based on fibres from renewable resources such as flax. Although these fibres are seeing use in some applications, there is a lack of understanding concerning their processing requirements in relation to their unique physical and chemical properties. Furthermore, there is limited information regarding the links between their processing behaviour and mechanical performance. With the aim of addressing these missing links, this thesis presents a methodology for characterizing flax fibres for application in the resin infusion process and considers two important case studies with the overall goal of improving the state-of-the-art for this class of materials.

Flax fibres were first characterized at the fibre level by advancing contact analysis, thermal gravimetric analysis, scanning electron microscopy and helium pycnometry. The advancing contact analysis revealed a reduction in the polar component of surface free energy after the application of silane and diluted epoxy treatments. A methodology was then developed for the characterization of the compaction and permeability of flax-based fabrics for the modelling of the resin infusion process. These parameters were quantified and used as input in a 1D process model that included capillary pressure. The model predictions for flow front evolution were shown to be in good agreement with experimental data. Alkaline treatments were shown to increase the required compaction pressure for a given porosity due to an increase in fibrillation. This had direct implications in the context of resin infusion processing due to the coupled nature of flow and compaction in this process. Consequently, a mechanical characterization revealed a decrease in flexural properties for alkaline-treated flax/epoxy composites manufactured by resin infusion due to a decrease in fibre volume fraction. A decrease in flexural properties was also noted with increasing void content.

In an effort to improve the state-of-the-art for this class of materials, a case study was carried out on the incorporation of nano-modifiers in the resin infusion process. Nanocellulose was incorporated by two novel techniques; a 'grafting' method and a wet-layup method that incorporated an aqueous NC solution in the resin infusion pre-filling stage. Both methods were shown to lead to an increase in damage to the composites after subjection to a drop-weight impact event which suggested that the nano-modifier did not increase the interlaminar properties. However, an increase in interlaminar shear strength was observed by a short beam test due to an increase in fibre volume fraction as a result of softening and lubrication effects arising from the use of the aqueous NC solution.

A second case study addressed the primary source of voids in a class of flax/epoxy prepregs which are generally used as a benchmark for composites manufactured by the resin infusion process. A series of compaction tests and thermal gravimetric analysis suggested that moisture and resin starvation were the primary source of voids in commercially available prepregs. Panels manufactured in an autoclave at varying pressures suggested that the latter of these issues was the dominant problem for the studied materials. The presence of voids was finally shown to lead to increased moisture sorption for flax/epoxy composites.

This study stresses the coupled nature of the resin infusion process and the full implications of the use of chemical treated flax fibres. Additionally, it demonstrates the negative consequences of process-induced voids on the performance of flax/epoxy composites. It also provides useful data on the fibre surface chemistry, permeability, compaction and mechanical performance of flax-based composites. This assists in furthering the development of this class of materials with the goal of increasing their potential for use in load-bearing structures.

Résumé

La préoccupation avec l'épuisement des ressources naturelles a conduit à l'élaboration des bio-composites à base de fibres renouvelables telles que le lin. Bien que ces fibres sont utilisées dans certaines applications, il y a un manque de compréhension au sujet de leurs besoins de traitement par rapport à leurs uniques propriétés physiques et chimiques. En outre, il y a peu d'information sur les liens entre leur comportement et la performance des traitements mécaniques. Dans le but de répondre à ces liens inconnus, cette thèse présente une méthodologie de caractérisation des fibres de lin pour une utilisation dans le procédé d'infusion de résine et tient compte de deux études de cas importantes dans le but d'améliorer l'état-de-l'art pour cette classe de matériaux.

Les fibres de lin ont d'abord été caractérisé au niveau des fibres en faisant l'analyse de l'angle de contact, analyse thermique gravimétrique, microscopie électronique à balayage et la pycnométrie hélium. L'analyse de l'angle de contact a révélé une réduction de la composante polaire de l'énergie de surface après l'application des traitements silane et époxy dilué. Une méthode a été ensuite développée pour la caractérisation de la compression et de la perméabilité de lin à base de tissus, pour la modélisation du processus d'infusion de résine. Ces paramètres ont été quantifiés et utilisés comme input dans un modèle de processus 1D qui comprenait la pression capillaire. Les prédictions du modèle d'évolution du front d'écoulement étaient en bon accord avec les données expérimentales. Le traitements alcalin a démontré une augmentation de la pression de compactage nécessaire pour une porosité donnée, en raison de l'augmentation de la fibrillation. Ce résultat a des implications directes dans le cadre du traitement d'infusion de résine en raison de la nature couplée de l'écoulement et de compactage dans ce processus. Par conséquent, une caractérisation mécanique a révélé une baisse de propriétés de flexion pour le lin/époxy composites fabriqués par infusion de résine pour des tissus traités avec alcalines en raison d'une diminution de la fraction

volumique de fibres. Une diminution des propriétés en flexion a également été notée quand le contenu de vide augmente.

Dans un effort pour améliorer l'état-de l'art pour cette classe de matériaux, une étude de cas a été réalisée sur l'incorporation de nano-modificateurs dans le procédé d'infusion de résine. Du nano-cellulose a été constituée par deux nouvelles techniques; une méthode de greffage et un procédé <<wet layup>> qui intègre une solution aqueuse NC avant l'infusion. Les deux méthodes ont démontré une augmentation de l'endommagement des composites après avoir été soumis à des impacts, qui suggère que le nano-modificateur n'a pas augmenté les propriétés interlaminaires. Toutefois, une augmentation de la résistance au cisaillement interlaminaire a été observée par un faisceau de test court en raison d'une augmentation de la fraction volumique des fibres à la suite d'effets de ramollissement et de lubrification provenant de l'utilisation de la solution aqueuse NC.

Une deuxième étude de cas a abordé la principale source de vides dans une classe de lin/époxy préimprégnés qui sont généralement utilisés comme point de repère pour les composites fabriqués par le procédé d'infusion de résine. Une série d'essais de compactage et d'analyse thermique gravimétrique suggère que la manque d'humidité et de résine ont été la principale source de vides dans préimprégnés disponibles. Des panneaux fabriqués dans un autoclave à pression variant suggére que le dernier de ces questions était le problème dominant pour les matériaux étudiés. La présence de vides a finalement causé une dégradation des propriétés d'absorption d'humidité pour les composites lin/époxy.

Cette étude souligne le caractère couplé du procédé d'infusion de résine et les implications de l'utilisation de traitement chimique des fibres de lin. En outre, il met en évidence les conséquences négatives de vides sur la performance des composites lin/époxy. Il fournit également des données utiles sur la chimie de surface des fibres, perméabilité, le compactage et la performance mécanique des

composites à base de lin. Cette aide favorise le développement de cette classe de matériaux dans le but d'augmenter leur potentiel d'utilisation dans des structures portantes.

Acknowledgements

There are several people and organizations who made this thesis work possible. I would first like to thank my supervisor **Prof. Larry Lessard** for giving me the opportunity to pursue this work and for his support throughout my studies. I would also like thank **Prof. Pascal Hubert** for fruitful collaborations and his support during my studies. In addition, I would like to give a special thanks to **Dr. Joris Baets** and **Prof. Ignaas Verpoest** from the Catholic University of Leuven for giving me the opportunity to carry out part of my studies at their facilities. Similarly, I would like to thank **Prof. Mohini Sain** for allowing me to carry out experiments at the University of Toronto and also for fruitful collaborations.

Regarding the thesis experimental and modelling work, there were several people who provided invaluable assistance whom I would like to thank including:

- **Pei-Yu Kuo** for her assistance with the chemical treatments, scanning electron microscopy and analysis-of-variance.
- **Manuël Adams** and **Kris Van de Staey** who provided training on the autoclave and universal testing machines respectively.
- **Carlos Fuentes Rojas** and **Le Quan Ngoc Tran** for training on contact angle measurements and fruitful discussions.
- **Jim Kratz** and **Cyrill Cattin** for training on the rheometer.
- **Xavier Gagné Brulotte** for training on the thermal gravimetric analyzer.
- **Timotei Centea** for training on polishing and microscopy.
- **Romain Dufaur** for his assistance with microscopy in Chapter 6.
- **Dr. Arthur Levy** for his aid with the modelling component of this work.
- **Benedikt Schlager**, **Marc-Palardy Sim** and **Dr. Cristian Demaria** for helping with the design and assembly of the permeability apparatus.
- **Richard Desnoyers** for training and assistance with drop-weight impact testing.

Funding from the following organizations is kindly acknowledged; **Network for Innovative Plastic Materials and Manufacturing Processes**, **McGill Engineering Doctoral Award** and the **Ministry of Economic Innovation and Exportation Development**. The following material suppliers are also kindly acknowledged; **Libeco-Lagae®**, **Lineo NV®** and the **Composite Innovation Center**.

I would finally like to extend my gratitude to the members of the **Structures and Composite Materials Laboratory** at McGill University as well as the **Natural Fibre Group** at the Catholic University of Leuven for providing excellent working environments and their invaluable support along the way. I am also indebted to my family who helped me in countless ways throughout my studies.

Contents

1. Introduction 1
1.1 Processing flax fibre-reinforced composites 4
1.2 Resin infusion process 6
1.3 Thesis motivation and objectives 6
2. Literature review 8
2.1 Flax fibre properties 8
2.1.1 Physical 9
2.1.2 Chemical 11
2.1.3 Tensile 15
2.2 Resin infusion process modelling 17
2.2.1 Process modelling 17
2.2.2 Compaction 23
2.2.3 Permeability 27
2.3 Mechanical characterization of flax/epoxy composites 29
2.3.1 Tensile 30
2.3.2 Flexural 31
2.4 Summary 32
3. Fibre characterization 33
3.1 Material selection 33
3.2 Thermal gravimetric analysis 34
3.3 Chemical treatment 37
3.3.1 Alkaline 37
3.3.2 Silane 37

3.3.3 Diluted epoxy 37
3.3.4 Scanning electron microscopy 37
3.4 Density measurement 39
3.5 Contact angle measurement 39
3.6 Summary 43
4. Fabric characterization 44
4.1 Permeability measurement 44
4.1.1 Test fixtures 44
4.1.2 Test fluids 46
4.1.3 Unsaturated 48
4.1.4 Saturated 53
4.2 Compaction 58
4.2.1 Test methods 58
4.2.2 Dry compaction 61
4.2.3 Wet unloading 63
4.2.4 Wet compaction 63
4.2.5 Comparison of compaction stages 64
4.3 Summary 65
5. Composite processing and characterization 67
5.1 Composite processing 67
5.2 Process model 68
5.2.1 Model development 68
5.2.2 Model validation 70
5.3 Mechanical characterization 74
5.3.1 Void analysis 74

5.3.2 Flexural behaviour 75
5.3.3 Charpy impact behaviour 77
5.4 Summary 78
6. Case studies 79
6.1 Multi-scale composites by resin infusion 79
6.1.1 Fabric treatment 80
6.1.2 Laminate manufacturing 80
6.1.3 Mechanical characterization 85
6.2 Flax/epoxy prepregs 93
6.2.1 Materials 94
6.2.2 Uncured prepreg characterization 95
6.2.3 Cured prepreg characterization 99
6.3 Summary 108
7. Conclusions 110
7.1 Contributions 112
7.2 Future work 113

List of Figures

Figure 1-1: Categories and examples of bio-fibres (compiled from [4]) 2
Figure 1-2: Early example of flax usage in composite materials: fuselage for a Spitfire manufactured from a unidirectional flax/phenolic prepreg [11] 3
Figure 1-3: Hybrid flax/carbon racing yacht set to participate in a transatlantic race; hull comprises of 50% flax fibres [12] 4
Figure 1-4: Steps involved in the resin infusion process; (a) lay-up, (b) pre-filling, (c) filling and (d) post-filling 6
Figure 2-1: Illustration of the microstructure of flax (adapted from [31]) 9
Figure 2-2: Illustration of the hierarchical structure of fibres within the flax stem (adapted from [32]) 10
Figure 2-3: Representative control volume for resin infusion process model [83] 19
Figure 2-4: Illustration of dual-scale flow that can occur during liquid composite moulding processes; inter-tow region are filled first followed by intra-tow regions leading to two flow fronts (adapted from [97]) 22
Figure 2-5: Illustration of compaction behaviour during the resin infusion process (adapted from [87]); (a) dry compaction (pre-filling stage) (b) wet compaction (filling and post-filling stage) and (c) wet relaxation (filling stage) 25
Figure 2-6: Tensile modulus and strength versus fibre volume fraction for published data on untreated unidirectional flax/epoxy composites 31
Figure 3-1: Dry 2x2 twill flax weaves used in this thesis a) CL001 b) CL015 34
Figure 3-2: Representative TGA mass loss curves for untreated flax exposed to 25, 75 and 100% ambient relative humidity values 35
Figure 3-3: Solubility data for untreated flax fibres (error bars represent maximum and minimum values) 36
Figure 3-4: SEM images of treated flax fibres: (a) as supplied, (b) acetone, (c) alkaline, (d) silane and (d) diluted epoxy 38

Figure 3-5: Representative force-displacement diagram for Wilhelmy contact angle measurement of untreated flax fibres (probe liquid = pure H_20): note negative slope due to buoyancy effects 40
Figure 3-6: Example cross-section of technical flax fibres used to measure contact angle by Wilhelmy method 41
Figure 3-7: Owens-Wendt plot used to deduce fibre surface free energy components; line coefficient R^2 varied between 0.88 and 0.99 (error bars represent maximum and minimum values) 42
Figure 4-1: Schematic of tool plate for permeability test apparatus #1 (where L=laser thickness gauges and T=thermocouples); (a) top view and (b) side view 46
Figure 4-2: Tool plate design for in-plane permeability measurement apparatus #2 (where L=laser thickness gauges and p=pressure sensors); (a) side view schematic and (b) actual setup 46
Figure 4-3: Viscosity versus temperature for Araldite LY1564/Aradur 3486 epoxy immediately after mixing determined on a rheometer using a 2° cone and 40mm diameter plate type geometry (error bars represent maximum and minimum values) 47
Figure 4-4: Viscosity versus temperature for Dow Corning® Fluid 200 silicone oil determined on a rheometer using a 2° cone and 40mm diameter plate type geometry (error bars represent maximum and minimum values) 48
Figure 4-5: Flow front position squared versus time for resin infusion of untreated CL015 flax fabric with epoxy 49
Figure 4-6: Permeability test apparatus #1 for unsaturated measurements during infusion: note that apparent unsaturated flow front was observed to be very small (about 5mm) 51
Figure 4-7: Cross-section of compacted CL015 flax fabric at 100 kPa of pressure: note similarity in inter-yarn and intra-yarn length scales 52
Figure 4-8: Equivalent in-plane permeability and porosity values for treated flax fabrics measured during the resin infusion process (error bars represent maximum and minimum values) 52

Figure 4-9: Evolution of resin mass during in-plane saturated permeability measurement 55
Figure 4-10: Representative spatial variation of pressure and thickness during saturated permeability measurement during saturated regime of infusion 55
Figure 4-11: Representative permeability versus fibre volume fraction relationship for saturated permeability measurement 57
Figure 4-12: Average of models for saturated permeability versus fibre volume fraction for untreated CL015 flax fabrics (error bars represent maximum and minimum values) 57
Figure 4-13: Test fixture used to measure the transverse compliance of fibre beds 59
Figure 4-14: Sample acquisition data during infusion experiments; 1=pre-filling stage, 2= filling stage and 3=post-filling stage 60
Figure 4-15: Representative compaction curve and power law model; R^2 value was a minimum of 0.95 for all experimental data..... 61
Figure 4-16: Average compaction pressure versus fibre volume fraction for dry treated CL015 flax fabric (3 layers total)..... 62
Figure 4-17: Wet unloading behaviour of untreated CL015 flax fabric (error bars represent maximum and minimum values)..... 63
Figure 4-18: Wet compaction behaviour of CL015 flax 2/2 twill weave fabric (error bars represent maximum and minimum values) 64
Figure 4-19: Average compaction curves for flax 2/2 twill weave fabrics during dry compaction, wet unloading and wet compaction (error bars represent maximum and minimum values) 65
Figure 5-1: Sample thermocouple data during curing stage of flax/epoxy processing by resin infusion..... 68
Figure 5-2: Comparison of model predictions and experimental results for flow front evolution of epoxy through untreated CL015 flax fabric (error bars represent maximum and minimum values) 71
Figure 5-3: Capillary pressure versus fabric porosity as calculated from Eq. 4 for untreated fabric 72

Figure 5-4: Predicted pressure distribution along CL015 flax fabric preform length during resin infusion for untreated fabric 72
Figure 5-5: Model predictions for flow front evolution during resin infusion of treated flax fabrics..... 73
Figure 5-6: Example cross-section of untreated flax/epoxy for void analysis after 25 kPa post-fill vent pressure a) before thresholding and b) after thresholding... 75
Figure 5-7: Void content versus post-fill pressure for flax CL015 fabric/epoxy composites; note that lower post-fill pressures resulted in degassing of resin and an increase in voids in the final laminates 75
Figure 5-8: Flexural properties of flax/epoxy composites manufactured by resin infusion at different post-fill pressures using common chemical treatments: a) modulus and b) strength (error bars represent maximum and minimum values) . 76
Figure 5-9: Flexural properties versus void content of flax/epoxy composites manufactured by resin infusion at different post-fill pressures using common chemical treatments: a) modulus and b) strength..... 76
Figure 5-10: Charpy impact properties of flax/epoxy composites manufactured by resin infusion at different post-fill pressures using common chemical treatments (error bars represent maximum and minimum values) 77
Figure 6-1: Bagging arrangement for resin infusion laminate manufacturing..... 81
Figure 6-2: Scanned surface of cured laminate using grafting technique; note agglomerations of nanocellulose are clearly visible 81
Figure 6-3: Flow front position squared versus time for single-scale composite manufactured from initially wet preform: note deviation from linearity due to end of distribution media 83
Figure 6-4: Infusion of flax fabric after MS (Wet-layup) preparation; note the rapidly advancing flow front in the distribution medium indicating low in-plane and through-thickness permeability of the modified fabric 84
Figure 6-5: Fibre volume fraction for single- and multi-scale nanocellulose, flax and epoxy composites manufactured by the resin infusion process (error bars represent maximum and minimum values)..... 85

Figure 6-6: Cross-sections of single- and multi-scale composites consisting of flax, nanocellulose and epoxy manufactured by resin infusion (± standard deviation) 86
Figure 6-7: Interlaminar shear strength for single- and multi-scale composite manufactured by resin infusion; incorporation of nanocellulose fibres did not lead to an increase in interlaminar shear strength (error bars represent maximum and minimum values) 88
Figure 6-8: Representative histories for drop-weight impact testing for single- and multi-scale composites manufactured from flax, epoxy and nanocellulose by resin infusion (a) force, (b) velocity, (c) displacement and (d) energy 91
Figure 6-9: Dent depth and maximum dent diameters of single-scale and multi-scale flax, nanocellulose and epoxy composites after being impacted by 1.6cm diameter hemispherical striker head with 7J of impact energy (error bars represent maximum and minimum values) 92
Figure 6-10: Representative bag-side damage areas after drop-weight impact testing for single- and multi-scale composites manufactured from flax, nanocellulose and epoxy by resin infusion; (a) SS (Dry), (b) MS (Grafted), (c) SS (Wet) and (d) MS (Wet-layup) 93
Figure 6-11: Typical mass loss curves obtained by thermal gravimetric analysis for BL200 prepreg, BL550 prepreg and LY5150 epoxy 96
Figure 6-12: Representative compaction curves for 2x2 twill weave fabrics used in BL200 and BL550 flax/epoxy prepregs with holds applied at 1, 3, 5, 7 and 9 bars (3rd order polynomial curve fit represents relaxed fibre bed)..... 98
Figure 6-13: Processing cycle applied during manufacturing of studied flax/epoxy prepregs in an autoclave..... 100
Figure 6-14: Vacuum bag arrangement used in prepreg case study 100
Figure 6-15: Representative cross-sections of flax/epoxy prepregs processed at varying pressure and void contents as determined by image analysis (± standard deviation). 101
Figure 6-16: Void content versus applied autoclave pressure for cured BL200 and BL550 prepregs (error bars represent maximum and minimum values) 102

Figure 6-17: Representative stress/strain curves for balanced twill weave flax/epoxy prepregs (a) BL200 and (b) BL550 104
Figure 6-18: Tensile modulus and strength versus number of layers in the warp direction (error bars represent maximum and minimum values) 105
Figure 6-19: Void content versus interlaminar shear strength for BL200 and BL550 flax/epoxy prepregs processed a 1, 3 and 5 bars (error bars represent maximum and minimum values) 106
Figure 6-20: Void content versus mass gain after 24 hours in water absorption test (error bars represent maximum and minimum values) 107

List of Tables

Table 1: Reported values for surface energy components of untreated flax fibres13
Table 2: Summary of published 1D resin infusion models for filling stage 18
Table 3: Published tensile properties for untreated woven and unidirectional flax/epoxy composites 30
Table 4: Published flexural properties for untreated woven and unidirectional flax/epoxy composites 32
Table 5: Physical properties of 2/2 twill weave flax fabrics studied in this thesis (± standard deviation) 34
Table 6: Surface energy components of selected probe liquids [142] 40
Table 7: Surface free energies for treated flax fibres (± standard deviation) 42
Table 8: Sample parameters in computation of saturated permeability 56
Table 9: Power-law constants for dry compaction behaviour of CL015 fabric 62
Table 10: Test matrix for laminate manufacturing for nanocellulose experiments 83
Table 11: Measured sample geometries for short beam strength specimens (± standard deviation) 87
Table 12: Summary of tensile testing results for cured BL200 and BL550 flax/epoxy prepregs (± standard deviation) 103
Table 13: Mass gain after 2 and 24 hours submersion in water of cured flax/epoxy prepreg samples processed at varying pressure (± standard deviation) 107

Nomenclature

F	Force
l	Wetted perimeter
γ	Surface tension
γ_t	Total surface energy
γ_p	Polar component of surface energy
γ_d	Dispersive component of surface energy
$\cos\theta$	Contact angle
K	In-plane permeability
u	Superficial velocity
ν	Interstitial velocity
μ	Viscosity
p	Pressure
p_c	Capillary pressure
Ca	Capillary number
σ	Compaction stress
σ_f	Fibre bed stress
σ_r	Resin stress
h	Thickness
t	Time
φ	Porosity
V_f	Fibre volume fraction
η	Number of layers
α	Fabric areal weight
ρ	Density
β	Form fitting factor
D	Fibre diameter
A	Compaction power-law constant
B	Compaction power-law exponent

Chapter 1

Introduction

In the last century, the development of advanced composite materials (i.e. fibre-reinforced polymers) has led to significant advancements in the limits of performance for many engineering applications. Composite materials are lightweight, strong and versatile which has made them attractive for applications ranging from primary aircraft structures to hockey sticks. Concurrently with their development, the world has recognized a need for sustainability including a reduced dependence on fossil fuels. In line with this need, the composite materials community has begun to develop eco-friendly alternatives that no longer depend on petroleum-derived fibres and resin systems. Directives set forth by the European union, which require that over 50% of an automobile chassis be recyclable by 2015, have further stressed the need for research in this area [1]. Within a couple of decades, research has led to the use of bio-based composite materials in notable applications such as automotive interior components [1, 2] and construction supplies [3].

Bio-based composite materials cover a broad range of fibre/resin combinations. Several types of so-called bio-fibres have been successfully sourced from animal, plant and minerals. Some examples of fibres in these categories are shown in

Figure 1-1. The mechanical properties of some cellulose-based fibres are provided in Appendix A.

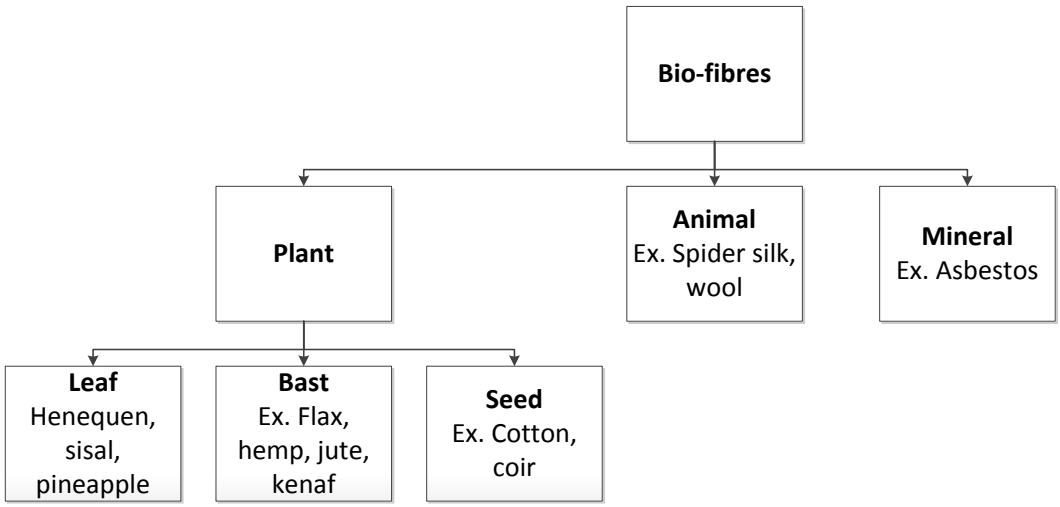

Figure 1-1: Categories and examples of bio-fibres (compiled from [4])

As with man-made fibres, the diversity of bio-fibres gives rise to unique properties and each has particular applications for which they are best suited. In general, the best combination of abundance and mechanical properties are possessed by bast fibres which are derived from the stems of certain plant species. Among the types of bast fibres, flax (*Linum usitatissimum*) is particularly interesting as a result of its large production rate in Canada. At the time of this writing, Canada was the leading producer and exporter of this agricultural crop [5]. Flax fibres have a combination of low density (~1.5 g/cm^3) as well a high specific modulus that can exceed that of glass fibres [6]. Among bast fibres, they possess close to the highest strength and modulus values as shown in Appendix A. Furthermore, they possess interesting damping and insulation properties that make them desirable in some automotive and sporting goods applications [1, 7].

Unlike man-made fibres, many exceptional factors affect the performance of flax fibres such as the cultivation method, seasonal quality and fibre extraction process. Flax is by and large not produced for its fibre (sometimes referred to as 'linen') and is normally cultivated as an oilseed crop to produce industrial oils and edible seeds [8]. As a result, the mechanical properties of oilseed flax fibres are

not as high as those varieties that are cultivated for fibre [6]. Furthermore, the process of extracting the flax fibres from the plant stem consists of several stages and has been shown to affect the mechanical properties [6, 9]. Therefore, flax cultivators and weavers play a key role in improving the reinforcing ability of these fibres in composite materials.

The use of flax fibres in composite materials is not an entirely new notion. One of the earliest examples was an experimental fuselage for the Spitfire in the 1940's (Figure 1-2). To address the scarcity of other materials during the second world war, unidirectional flax was combined with a phenolic resin to produce a prepreg product that was known as 'Gordon Aerolite' [10].

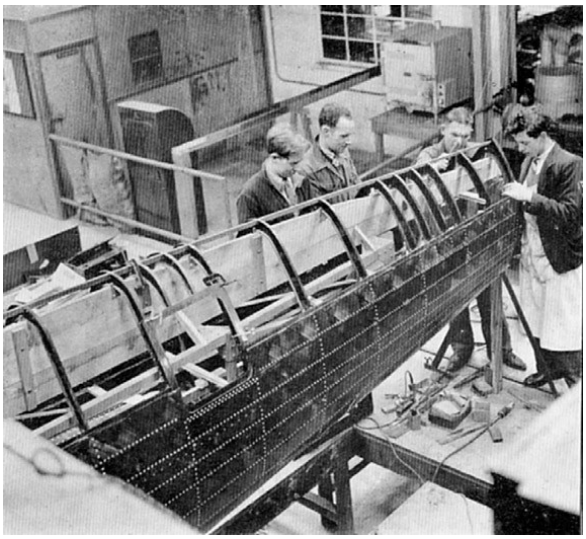

Figure 1-2: Early example of flax usage in composite materials: fuselage for a Spitfire manufactured from a unidirectional flax/phenolic prepreg [11]

Modern applications of flax-reinforced polymers include sporting goods such as bicycles, tennis racquets and wind surf boards [7]. The state-of-the art for this type of composite material at the time of this writing was a yacht developed in France that was set to join a transatlantic race (Figure 1-3).

Figure 1-3: Hybrid flax/carbon racing yacht set to participate in a transatlantic race; hull comprises of 50% flax fibres [12]

1.1 Processing flax fibre-reinforced composites

Most composite manufacturing processes that have been developed for conventional composites have also been applied to flax-reinforced composites and bast fibre-based composites in general. Compression moulding is currently the dominant method in the automotive industry due to its rapid cycle times and ability to mould complex shapes [1]. Traditionally, parts have been compression moulded with glass-mat-thermoplastics (GMT), long-fibre thermoplastics (LFT) or sheet moulding compound (SMC). In order to replace these conventional materials with those based on natural fibres, variations of compression moulding have been developed. One of the most commercially successful methods was developed by Daimler AG and is known as 'express' processing. This process involves the automated deposition of bio-fibre chopped strand mats and thermoplastic films on a tempered mould [2].

The above processes typically use low performance commodity thermoplastics which have the advantages of being inexpensive and recyclable. However, these commodity thermoplastics also have limited mechanical properties and require high tooling cost (especially when high consolidation pressures are involved). Furthermore, the above processes use short flax fibres that are randomly oriented

(i.e. nonwoven mats) which do not fully utilize the directional properties of the fibres. In an effort to expand the use of bio-fibres such as flax, many researchers have started to consider aligned fabric architectures combined with high performance thermosetting resins such as epoxy [13-20]. Although epoxies are generally expensive, they possess excellent mechanical properties, are available in a wide array of forms and their processing science is relatively well understood. In addition, the development of bio-epoxies is becoming more common which raises the possibility of producing so-called 'green' composites (i.e. a bio-fibre combined with a bio-resin [21]).

Thermosetting matrix composite processes generally involve three major steps. First, the fibrous reinforcement (a.k.a. 'preform') is placed on the surface of a mould (or tool) that is shaped to the desired part geometry (usually referred to as the 'layup' step [22]). Secondly, the resin is infiltrated into the fibrous reinforcement. Thirdly, chemical crosslinking of the resin is facilitated under heat, pressure and/or ambient conditions (known as the 'curing' step). The method of infiltration in step 2 can be separated into two main classes [23]; consolidation processes and liquid composite moulding (LCM) processes. The former includes preimpregnated textiles (known as 'prepregs') that are typically cured in an autoclave. This is the industry standard for applications that require high part quality with a low part count (e.g. aerospace) [22]. The second group of processes all involve the infusion of resin (a.k.a. 'matrix') by means of a pressure gradient into the dry preform. LCM processes are interesting because they combine the low cost of the basic wet-layup process (since the fibres and resin can be purchased separately) along with the ability to achieve higher fibre volume fractions, on the order of those achieved by an autoclave. Additionally, they significantly reduce the release of volatile organic compounds (VOCs) which improves workplace health and safety.

1.2 Resin infusion process

Among the various LCM process, resin infusion (a.k.a. VARTM, SCRIMP) is particularly attractive since it involves low tooling costs (since only a one-sided tool is required) and can achieve more consistent and higher fibre volume fractions when compared to wet-layup [22]. A schematic of the main steps involved in the process is presented in Figure 1-4.

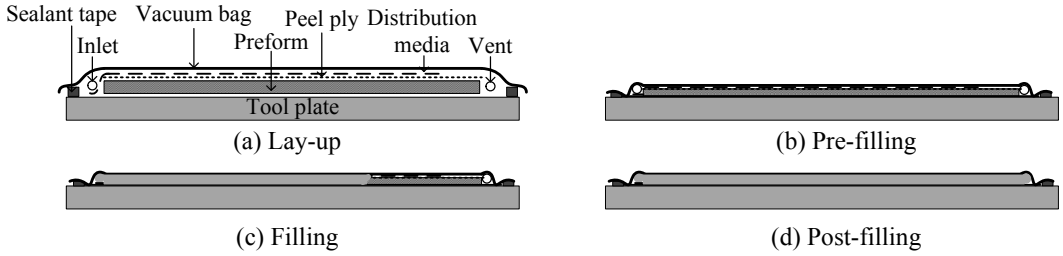

Figure 1-4: Steps involved in the resin infusion process; (a) lay-up, (b) pre-filling, (c) filling and (d) post-filling

The process begins with the preform placement onto the tool surface along with a layer of peel ply (a permeable release film). This is sometimes accompanied by a distribution media which is an optional layer that speeds up the process when the permeability of the preform is low [24]. Spiral tubing is then often incorporated in the bagging arrangement to act as the resin inlet and outlet (a.k.a. 'vent'). The layup is then covered with a vacuum bag and vacuum is drawn on the dry preform, initiating the 'pre-filling' stage. The inlet tube is then opened which initiates the flow of resin and the 'filling' stage. Following saturation of the preform, the inlet tubing is typically clamped and the 'post-filling' stage commences. After the system reaches equilibrium, the curing of the resin is carried out after which the part is removed from the tool.

1.3 Thesis motivation and objectives

Although researchers have made large steps in the advancement of processing flax-based composite materials, this class of materials is still not widely accepted primarily due to their large variability, low strength and susceptibility to moisture absorption [6, 25]. In addition to faults in performance, there is a lack of understanding in the relationships between their distinctive features (e.g. complex

fibre structure and chemistry) and the processing requirements that lead to the manufacturing of high quality composite parts. The current thesis aims to contribute to the understanding of these relationships for the case of flax fibre/epoxy composites manufactured by the resin infusion process.

The overall objective is to link the distinctive nature of flax fibres to their behaviour during processing and ultimately the quality and performance of their composite parts. It will delve into the science behind the resin infusion process as a base in understanding these relationships. A case study will also be presented on the autoclave curing of flax/epoxy prepregs, since this process is generally used as a benchmark for mechanical properties comparison with other processes. In both cases, epoxy resin has been selected as the matrix. In order to focus this thesis, only aligned arrangements of flax have been studied as these architectures represent the next generation of flax-reinforcements that could be used in load-bearing composites. Specifically the objectives of the current thesis were to:

1) Perform a literature review on flax fibre properties, resin infusion process modelling and the mechanical characterization of flax/epoxy composites (Chapter 2).
2) Characterize flax fibres to better understand their behaviour during composite processing (Chapter 3).
3) Develop and implement a methodology to characterize flax fabrics and determine material input parameters for a resin infusion process model (Chapter 4).
4) Manufacture and characterize flax/epoxy composites produced by resin infusion and compare processing data with a process model (Chapter 5).
5) Perform case studies with the aim of improving the state-of-the-art for this class of materials (Chapter 6).

Chapter 2

Literature review

Although flax-reinforced polymers are a relatively new development in the field of modern composite materials, there have been considerable efforts over the past couple of decades in their development. The following subsections present a literature review relevant to the processing and mechanical characterization of flax fibre composites by resin infusion. It is divided into three parts; flax fibre properties, resin infusion process modelling and mechanical properties of flax/epoxy composites. It should be noted that in some cases, studies related to similar cellulose-based fibres (e.g. hemp, jute and wood) were included when the results were deemed relevant.

2.1 Flax fibre properties

Understanding the physical and chemical properties of reinforcing fibres such as flax is critical in developing suitable processes for their incorporation in composite materials. These properties directly affect the flow kinetics [26, 27] during LCM processes as well as the adhesion properties with the matrix. The following sections present a background in the physical, chemical and tensile properties of flax fibres.

2.1.1 Physical

The physical properties of flax fibres that contribute to the understanding of their processing and performance in composite materials include microstructure and density as discussed below.

2.1.1.1 Microstructure

Unlike conventional reinforcement fibres such as carbon and glass, flax has a highly complex hierarchical microstructure consisting of four walls of microfibrils based on cellulose held together by hemi-cellulose and lignin [25] (Figure 2-1). The center of the flax fibre is hollow and is known as the lumen. The fibres themselves come from bast fibre bundles located in the stem of the flax plant (Figure 2-2). Several 'elementary' flax fibres are tightly packed in these bast fibre bundles to form larger so-called 'technical' fibres (Figure 2-2). Technical fibres are typically the basis for producing flax yarns and have an average length of approximately 50 centimetres [28]. This span makes them more useful than elementary fibres which have an average length of only 3.3 centimetres [29].

It is clear that due to the unique morphology of cellulose-based fibres, there are implications in terms of LCM processing. In particular, the hollow structure means more possible channels for flow to occur and a complex transverse elastic behaviour that could result in plastic deformation such as the collapse of the lumen [30].

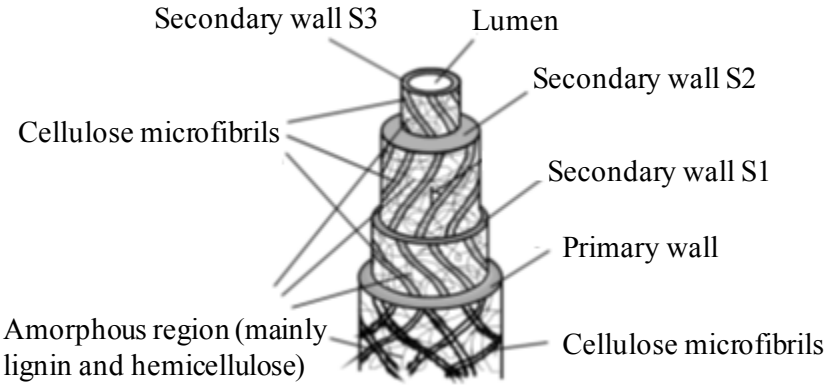

Figure 2-1: Illustration of the microstructure of flax (adapted from [31])

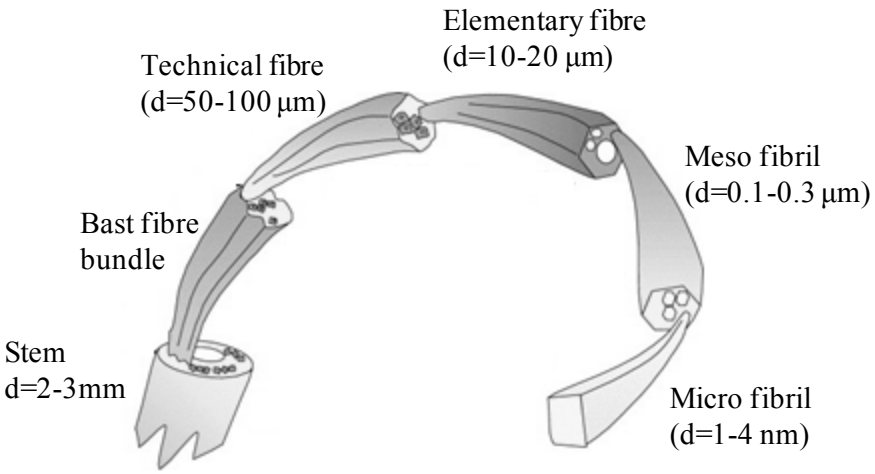

Figure 2-2: Illustration of the hierarchical structure of fibres within the flax stem (adapted from [32])

2.1.1.2 Density

Another important physical property is density, especially for calculating fibre volume fraction and void content (according to ASTM D3171 and ASTM D2734 respectively). In general, the mechanical properties of a composite material increase with fibre volume fraction [33] and the quality of a part is evaluated based on void content [34, 35]. Therefore, fibre density is a critical parameter for predicting the performance of composite parts.

Although several density values have been reported in the literature, they differ widely (ranging from 1.4 g/m^2 to 1.6 g/cm^3 [36]) in part due to the method of measurement. Troung *et al* compared several methods to measure the density of cellulose-based fibres and determined that gas pycnometry was the most effective [36]. Another factor that further complicates the accuracy of density is the lumen. Batra *et al* measured an 'apparent' density (which assumed that the quasi-cylindrical structure of the flax fibre is solid) and found it to be 1.38 g/cm^3 whereas the actual density was found to be 1.53 g/m^3 [4]. It should also be noted that use of apparent dimensions leads to an underestimation of the elastic properties of the fibre since they are calculated based on cross-sectional area [6].

2.1.2 Chemical

Equally as important as physical properties, are chemical properties which directly relate to the bonding characteristics as well as the wetting behaviour of the fibres. In the case of cellulose-based fibres, it is common to use chemical treatments to alter physical and chemical properties to encourage more favourable processing and adhesion conditions [37]. The following subsections discuss the surface chemistry of flax as well as common chemical treatments that are used to improve the interfacial properties.

2.1.2.1 Surface chemistry

The surface chemistry of reinforcement fibres dictates their wetting behaviour and is thus of great importance in the study of liquid composite moulding processes [38]. Closely coupled with the study of surface chemistry is the measurement of contact angles. Prior to discussing the published literature for the surface characterization of flax fibres, an overview of contact angle measurement will be presented.

2.1.2.1.1 Contact angle measurement

Contact angle is an effective parameter that relates to the intermolecular interaction between the interface of a vapour, liquid and solid [39]. Contact angles are typically used as a tool to quantify the wettability for a given fibre and resin combination [40]. Contact angles can either be measured directly (Sessile drop technique) or deduced using the modified Wilhelmy method [41]. The Wilhelmy method involves measuring the force caused by the submersion of a single fibre in a probe liquid. The contact angle (θ) can then be computed from [42]:

$$\cos\theta = \frac{F}{\gamma \cdot l} \qquad (1)$$

where F is the force measured by the micro-balance, l is the wetted perimeter of the fibre and γ is the surface tension of the liquid. Another method of indirectly determining contact angles is known as the capillary-rise method (a.k.a Washburn

technique). This method involves dipping a fabric in a liquid of known surface tension and measuring the time the fluid takes to rise to a certain height. This method is particularly well suited for cellulose-based fibres as the non-uniform perimeter along the length of single fibres can lead to erroneous results for the Wilhelmy technique [38, 41].

Contact angles can be used to quantify the total surface free energy of a given solid which directly relates to the wetting and adhesion characteristics. During the measuring of contact angles, several types of molecular interactions are known to take place including dispersive (van der Waals), hydrogen bonding, polar and acid/base [43]. Several theories exist that describe the make-up of surface energies that differ mainly in the number of these interactions that they take into account [44-47]. One of the most common theories, that takes into account two of these interactions, was developed by Owens and Wendt [45]. This theory relates the polar and dispersive components of the total surface energy to the contact angle by:

$$\gamma^L \frac{(\cos\theta + 1)}{2\sqrt{\gamma_d^L}} = \frac{\sqrt{\gamma_p^S}\sqrt{\gamma_p^L}}{\sqrt{\gamma_d^L}} + \sqrt{\gamma_d^S} \qquad (2)$$

where γ is the surface energy and θ is the contact angle. Superscripts *S* and *L* represent the solid and liquid respectively. Subscripts *p* and *d* represent the polar and dispersive components respectively. Upon examination of Eq. 2, it can be seen that a linear plot can be used to deduce the polar and dispersive surface free energies based on the contact angle obtained with several probe liquids.

2.1.2.1.2 Surface energy components of flax

Using the above contact angle measurement techniques, some past studies have investigated the surface free energy components of untreated flax. The data from these studies are summarized in Table 1.

Table 1: Reported values for surface energy components of untreated flax fibres

	Method	**γ_p (mJ/m^2)**	**γ_d (mJ/m^2)**	**γ_t (mJ/m^2)**
Arbelaiz *et al* [48]	Wilhelmy	19.87	23.85	43.72
Baley *et al* [49]	Sessile drop	26.6	35.9	62.5
Aranberri-Askargorta *et al* [38]	Capillary rise	17.6	12.9	30.5
Van De Velde *et al* [50]	Wilhelmy	11.68	22.57	34.25

It is clear that there is a fairly large range of surface energy values in the literature for untreated flax fibres. There are several possible reasons for this, including variation in measurement techniques, sample preparation and fibre extraction methods. Taking this into account, it can be concluded that it is best to measure contact angles for a given batch of flax fibres to ensure correct values for use in modelling.

There are a few studies that have looked at the effect of chemical treatments on the surface chemistry of flax. Arbelaiz *et al* investigated the effect of alkaline, vinyltrimethoxy silane and maleic anhydride-polypropylene (MAPP) chemical treatments and observed a reduction of the polar component of the surface free energy (20%, 93% and 83% reductions respectively) [48]. The alkaline concentration was 20% and the treatment time was one hour. Baley *et al* studied separately the effect of a mild (1%) alkaline treatment and formic acid treatment. The alkaline treatment was found to have a very small effect on the surface free energy components likely due to the low concentration [49]. The formic acid treatment on the other hand was found to reduce the polar component by almost 40%. Van De Welde *et al* studied the effect of propyltrimethoxysilane, phenylisocyanate and MAPP treatments and found notable reductions in the polar component of surface energy in all cases [50].

In comparison to carbon, flax fibres are very hydrophilic. Carbon fibres have been reported to have dispersive and polar components of surface energy of 28 and 1 mJ/m^2 respectively [51]. Due to the hydrophobic nature of epoxy (γ_d = 41.2; γ_p = 5.0 mJ/m^2 [52]), it is well known that carbon fibres adhere better to epoxy than

untreated cellulose-based fibres. In contrast, E-glass has been reported to have dispersive and polar components of surface energy of 19.5 and 28.8 mJ/m^2 respectively [53]. For this reason, coupling agents such as silane are commonly used with glass fibres. The dispersive and polar components of surface energy for pure cellulose have been reported to be 27.5 and 41 mJ/m^2 respectively [49]. The reason for the increase in polar component compared to flax fibres is likely due to the absence of lignin, hemicellulose and other components of the flax fibre.

2.1.2.2 Treatments

It is well known that chemically treating flax and other bast fibres is beneficial to the adhesion properties as well as to reduce moisture uptake of the hydrophilic fibres [25, 37]. The current literature review will cover two of the most common and cost effective; alkaline and silane. For other chemical treatments, the reader is directed to a review paper by Kabir *et al* [37].

2.1.2.2.1 Alkaline

Alkaline (also known as mercerization) is one of the most common chemical treatments for cellulose-based fibres and has long been applied to cotton [54]. This treatment is normally applied by soaking fibres or fabrics in an aqueous NaOH solution [55]. Several factors including treatment concentration, time, temperature and tension in the fibres have been shown to influence the final outcome [25, 56]. Alkaline treatments have been reported to impart several changes to the fibre including:

- Surface roughening [25, 27]
- Removal of lignin, wax and oils from surface [25]
- Increase in amount of cellulose exposed on fibre surface [25]
- Increase in fibre tensile modulus due to better alignment of the cellulose chains [25]
- Increase in fibrillation [25]
- Increase in resistance to moisture absorption [37]
- Better thermal stability [37]

Most of the above changes improve the final properties of the composite by either improving the adhesion with the matrix or else increasing the fibre tensile modulus. However, high concentrations of NaOH have been shown remove excess amounts of lignin and consequently degrade the fibre and composite properties [57].

2.1.2.2.2 Silane

Silane is a commonly used coupling agent for glass fibres to facilitate good adhesion with polymer resin systems [58]. In the case of cellulose-based fibres, silane also reduces the number of available hydroxyl groups on the fibres surface and renders the fibre more resistant to moisture absorption [59]. The following changes to cellulose-based fibres have also been reported after application of silane treatments:

- Reduction of moisture sensitivity in fibres and composite [37]
- Improvement in fibre/matrix adhesion [37]
- Increase in thermal stability [59, 60]
- Restraining effect of fibre swelling into the matrix [56]

Some studies suggest that application of an alkaline treatment prior to the silane treatment enhances the its effectiveness since the former treatment increases the number of available hydroxyl groups to which the silane groups can bond [61].

2.1.3 Tensile

The single most important property for a reinforcing fibre in a composite material is its tensile mechanical properties. Due to the relatively short length of technical flax fibres, it is necessary to spin them into a yarn which leads to a decrease in effective tensile properties [62, 63]. In the following section, a background is presented on the tensile behaviour of flax fibres as well as flax yarns.

2.1.3.1 Fibre

The stress-strain behaviour of elementary flax fibres has been shown to be quite complex. Baley studied the tensile behaviour of elementary flax fibres and

determined that the Young's modulus increased with increasing strain due to the progressive alignment of the cellulose microfibrils [29]. In addition, Baley found that the Young's modulus decreased with increasing fibre diameter due to the relative size of the lumen. Overall, the study found an average Young's modulus of 54.1±15.1 GPa and strength of 1339±486 MPa. In another study by Baley *et al*, the transverse Young's modulus of flax was estimated to be a mere 8 GPa which stresses the need to align this class of fibres and load them in the fibre direction [64]. Bos *et al* studied the tensile properties of technical flax fibres and found the strength to largely depend on the clamping length [65]. Clamping lengths over 25 mm resulted in a tensile strength of around 500 MPa whereas for clamping lengths less than 25 mm, the strength increased precipitously up to 1522 ± 400 MPa. This clamping length was roughly the length of the elementary flax fibres so it was concluded that below this length the failure mode was fracture of the elementary fibres and above this length the failure mode was debonding of the elementary fibres.

It is interesting to note that the position of the fibre along the flax stem length has also been shown to affect the tensile properties [13]. Fibres located in the middle of the stem possess the highest tensile properties. Hence, along with variability due to cultivating and harvesting methods there are also variations in the plants themselves.

2.1.3.2 Yarn

In reality, due to the short length of flax fibres it is necessary to twist many short so-called 'staple' fibres into yarns. The level of twist in these yarns inherently affects the mechanical properties of the impregnated composite similar to the behaviour of off-axis plies. Yarns with a very low degree of twist have lower strength in air and are consequently difficult to process using conventional textile equipment or processes such as pultrusion [62]. Yarns with a high degree of twist inherently lead to lower properties in the composite [62, 63, 66]. Additionally, high twisted yarns lead to impregnation difficulties for the resin and a higher risk

of voids within the yarns [67]. Overall, it can be said that for justifiable comparison of experimental results in the literature, the degree of twist should be taken into account.

2.2 Resin infusion process modelling

The science involved in the processing of thermoset composite materials is an area that has received considerable attention over the past couple of decades [68, 69]. This is in part due to a need for numerical models that can eliminate costly trial and error methods in the development of manufacturing processes. A background is presented below related to the process modelling of the resin infusion process along with the characterization of two important model parameters; the compaction and permeability of the fibre bed.

2.2.1 Process modelling

The modelling of the resin infusion process is very similar to its close relative the resin transfer moulding (RTM) process for which there have been modelling efforts for almost three decades [70-76]. Similar to RTM, incompressible flow in the resin infusion process is generally modelled using Darcy's law given by [77]:

$$u = \frac{K}{\mu}\nabla p \qquad (3)$$

where u is the superficial velocity, K is the permeability, μ is the viscosity of the fluid and p is the pressure. A critical material property in this relationship is permeability, which is a measure of the resistance to flow through a porous medium.

The primary difference between RTM and resin infusion is that the latter process employs a one-sided tool and flexible vacuum bag to consolidate the preform. This leads to a time variation of pressure and thickness in the preform. This behaviour can be described by Terzaghi's law, borrowed from soil mechanics, that states that the applied load is shared between the resin and fibre bed according to [78]:

$$\sigma = \sigma_f + \sigma_r \qquad (4)$$

where σ, σ_f and σ_r are the applied, fibre bed and resin pressures respectively. During the filling stage, the stress in the fibre bed gradually decreases as some of the applied load is carried by the resin according to Eq. 4. This causes a change in fibre volume fraction according to the compaction behaviour of the fibre bed which in turn results in a change in permeability (a known function of fibre volume fraction [79-82]). Therefore, unlike the RTM process, resin pressure, fibre volume fraction and permeability are closely coupled parameters during the resin infusion process.

The overall governing equation of the resin infusion process is the continuity of the resin over a representative control volume (Figure 2-3). Although several variations of the continuity equation for the resin infusion process exist in the literature, Correia *et al* [83] demonstrated that all followed the form of that derived by Hammami *et al* [84], given by:

$$-\frac{\partial(hu)}{\partial x} = \frac{\partial h}{\partial t} \qquad (5)$$

where h is the preform thickness and u is the fluid velocity. A summary of existing 1D models in the literature is presented in Table 2.

Table 2: Summary of published 1D resin infusion models for filling stage

Authors	Numerical method	Governing equations
Hammami *et al* **[84]**	Finite volume	$\frac{\partial}{\partial x}\left(\frac{Kh}{\mu}\frac{\partial p}{\partial x}\right)=0$
Kang *et al* **[85]**	Finite element	$\frac{\partial}{\partial x}\left(\frac{K}{\mu}\frac{\partial p}{\partial x}\right)=-\frac{1}{V_f}\left(\frac{\partial V_f}{\partial t}\right)$
Correia *et al* **[83]**	Finite difference	$\frac{\partial}{\partial x}\left(\frac{Kh}{\mu}\frac{\partial p}{\partial x}\right)=\frac{\partial h}{\partial t}$
Govignon *et al* **[86]**	Finite element	$\frac{\partial}{\partial x}\left(\frac{Kh}{\mu}\frac{\partial p}{\partial x}\right)=\frac{\partial h}{\partial t}$

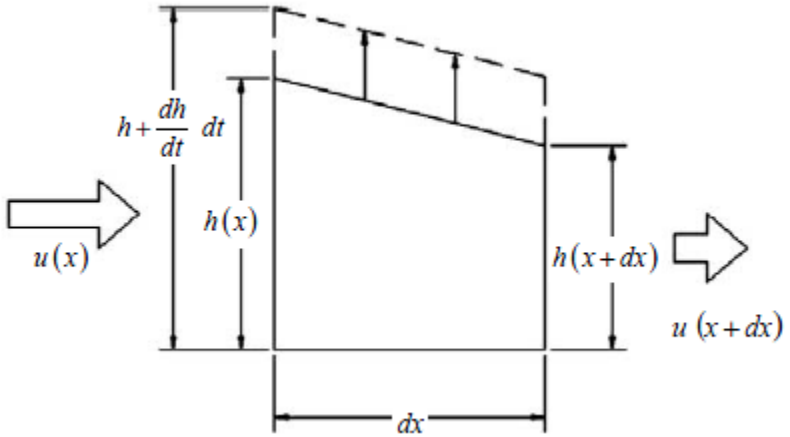

Figure 2-3: Representative control volume for resin infusion process model [83]

There have also been efforts to develop more complex 2 and 3D models that account for the effect of the distribution media. These models are generally solved by the finite element/control volume method [87-89]. Sun *et al*, showed that incorporation of a distribution media reduced the infiltration time significantly and reduced the influence of the preform permeability on fill time [89]. Mathur *et al* studied the through-thickness flow with a distribution media and found a steady lag between the top and bottom of the preform [88]. Grimsley *et al* also developed a 3D finite element/control volume model that was able to predict this lag well [87].

The primary differences between the 1D models summarized in Table 2 lie in the assumptions. The main assumptions that the majority of resin infusion models share in common are:

1) Isothermal and incompressible flow
2) The fibres do not shift during the process
3) Shear stresses are negligible when the fibre bed is compacted
4) The fibre bed is completely saturated after the flow front ('slug-flow assumption' [23])
5) Capillary pressure is insignificant compared to applied pressure

In the case of a model by Han *et al*, the variation of thickness along the length was additionally neglected and the initial thickness value (after the pre-filling

stage), h_0, was assumed [90]. Carreia *et al* investigated the implications of this assumption and found that it resulted in the same trend for the pressure field but led to an underestimate of the pressure values [83]. Hammami *et al* made a quasi-static assumption (i.e. the preform will reach its equilibrium height at every instant) to simplify the numerical solution [84].

2.2.1.1 Modelling cellulose-based fibres during resin infusion

In the case of cellulose-based fibres, there is very little existing research with respect to modelling their behaviour during the resin infusion process. A study by Francucci *et al* on the resin infusion of jute fabrics revealed that swelling and fluid absorption by the cellulose-based fibres resulted in a lower permeability for the saturated fabrics compared to when they were unsaturated [91]. The degree of transverse swelling was shown to be almost three times as high when the jute fibres were exposed to a polar solution (water and glycerin) as opposed to non-polar (vinylester and phenolic resin). In the case of the non-polar fluids, the transverse swelling was found to be minimal (<2%) for exposure times less than 10 minutes.

A later study by Masoodi *et al* proposed a model to account for these swelling and sink effects during the resin transfer moulding process [92]. This was done by incorporating a sink and swelling rate term in the governing flow equation for RTM as follows:

$$-\frac{\partial u}{\partial x} = -S - \frac{\partial \varphi}{\partial t} \qquad (6)$$

where S is the rate of liquid absorbed by the fibres and φ is the fibre bed porosity. It was later shown that the rate of fluid absorption is approximately equal to the swelling rate of the fibre which simplifies Eq. 6 to the standard governing equation for RTM flow. The only difference with the flow model was then the dependence of permeability on time in Darcy's law for polar matrices. This was accounted for by assuming the time-dependent permeability to lie linearly

between the permeability measured with a polar fluid (diluted corn syrup) and a non-polar fluid (motor oil) as described by:

$$K(t) = K_0 + \frac{K_0 - K_{end}}{t_{end}} t \qquad (7)$$

where K_0 is the permeability measured with a non-polar fluid and K_{end} is the permeability measured with a polar fluid after time, t_{end} (when the test liquid reaches the end of the preform in the permeability measurement).

2.2.1.2 Dual-scale modelling

One of the more questionable assumptions in the above models is the slug-flow assumption. Several studies have shown that flow in liquid composite moulding processes in reality occurs at two scales; inter-tow and intra-tow flow [93-95]. This results in an unsaturated regime behind the flow front where the inter-tow regions are filled but the intra-tow regions are partially saturated (Figure 2-4) [96]. Depending on the properties of the reinforcement and resin, this can lead to the entrapment of air during the infusion and consequently voids in the final part [97]. Neglecting this behaviour has been suggested to lead to discrepancies between resin infusion models and experiments [98]. Therefore, some recent resin infusion models have taken these issues into account. Acheson *et al* developed a model that incorporated tow impregnation phenomena and carried out a parametric study [99]. It was found that neglecting dual-scale behaviour did not result in significant differences in predicted pressure and fill times for resin infusion. Bayldon *et al* also modelled this dual-scale nature in the resin infusion process and found good agreement with experimental results [100].

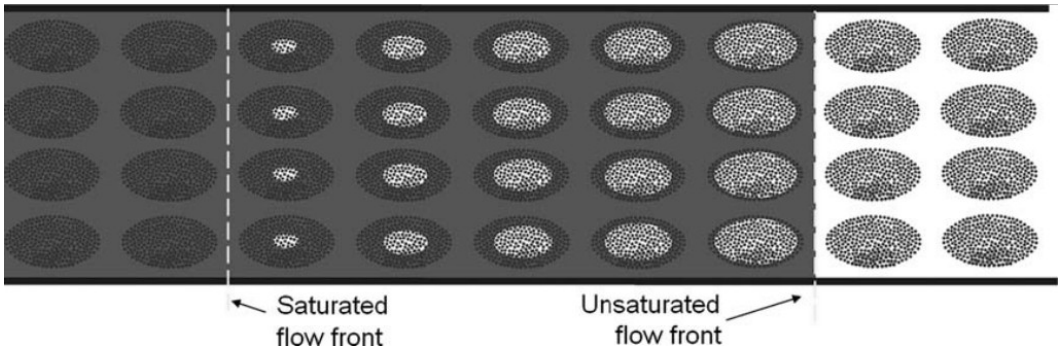

Figure 2-4: Illustration of dual-scale flow that can occur during liquid composite moulding processes; inter-tow region are filled first followed by intra-tow regions leading to two flow fronts (adapted from [97])

2.2.1.3 Role of capillary pressure

Another questionable assumption is neglecting capillary pressure due to the relatively low pressures involved in the resin infusion process. Some authors have shown that the magnitude of capillary pressure can be comparable to the applied pressure gradient [101], especially in the case of bast fibres due to the small channels located within the fibres themselves [102].

For orthotropic fibre textiles, capillary pressure can be calculated from a modified Young-Laplace equation given by [103]:

$$p_c = \frac{\beta}{D} \cdot \frac{(1-\varphi)}{\varphi} \cdot \gamma_r \cdot \cos\theta \qquad (8)$$

where D is the diameter of a single fibre, φ is the porosity, γ_r is the surface tension of the resin, cos θ is the contact angle and β is a form fitting factor which depends on the textile architecture. Capillary pressure has been shown to be rate-dependant and its value can change over the course of the process in relation to the capillary number (Ca) given by [104]:

$$Ca = \frac{\mu \cdot u}{\gamma} \qquad (9)$$

In general, contact angles measured for Ca values of below 10^{-5} are equivalent to those measured at equilibrium [104].

2.2.2 Compaction

One critical property in all resin infusion models is the transverse deformation behaviour of the fibre bed (commonly referred to as 'compaction'). Compaction behaviour has been shown to be quite complex and it is strongly influenced by many factors including the textile architecture, number of layers, compaction rate and lubrication effects [105-107]. Viscoelastic phenomena such as hysteresis and stress relaxation are also common due to rearranging, sliding and/or breaking of the fibres [105-110]. At the time of this writing, no models existed that could simultaneously account for all of these complexities. However, several analytical and empirical models had been developed that were adequate in resin infusion process modelling. Some of the key examples in the literature are presented in the following paragraphs.

One of the earliest works on compaction was a study by Van Wyk on the compressibility of wool [111]. Van Wyk developed an analytical model that described the compaction of a random bundle of wool fibres based on beam theory and assumed bending was caused by the applied pressure transmitted through fibre-fibre contact points. A later pioneering model in the field of composite materials (also based on beam theory) was proposed by Gutowski *et al* who described the consolidation of unidirectional fibre beds by [112].

$$\sigma = \frac{3\pi E_f}{\lambda^4} \frac{\sqrt{\frac{V_f}{V_0}} - 1}{\left(\sqrt{\frac{V_a}{Vf}} - 1\right)^4} \qquad (10)$$

where E_f is the fibre flexural modulus, λ is the waviness ratio, V_f is the fibre volume fraction, V_a is the maximum achievable V_f and V_0 is the fibre volume fraction at a compaction stress (σ) of zero. This model assumed the fibres to be curved beams in bending and was validated using special prepregs made with constant viscosity oils. Chen *et al* later studied the single- and multi-layer preforms in liquid composite moulding [113, 114]. An analytical compaction model was proposed based on a 3D model of a textile unit cell and beam theory

[114]. Saunders *et al* carried out compaction experiments on resin impregnated woven cloths and observed that compaction deformation occurs in three modes: fabric nesting, yarn waveform deformation and deformation of the yarn cross-section [115, 116]. Based on these compaction modes, Lomov and Verpoest proposed a model developed from textile mechanics to predict the compaction behaviour and found good agreement with experimental results [117]. Kelly *et al* proposed a viscoelastic model that could account for both the compaction and time-dependant relaxation phase [109].

Although several analytical models have developed, the majority of resin infusion process models in the literature (e.g. [83, 84, 86]) have employed empirical models due to their simplicity. One of the most widely used empirical models was proposed by Robitaille et al [105]. In a study on the compaction behaviour of several types of reinforcements, a power-law fit was found of the form:

$$V_f = A\sigma^B \qquad (11)$$

where A and B are fitting constants and σ is the applied compaction stress. It should be noted, that this empirical model assumes that the compaction behaviour is not time dependant which is contrary to many experimental observations [105, 110, 118]. Kang *et al* proposed an exponential curve fit for compaction data in the development of a resin infusion process model [85]. Polynomials have also been successfully fit to compaction data [119].

2.2.2.1 Compaction during the resin infusion process

It is widely accepted that the compaction behaviour of a preform is different in dry and saturated states [86, 100, 106, 118]. Similarly, the behaviour is different in loading and unloading of the fibre bed due to plastic deformation. As a result of this complex behaviour, a preform undergoes three different types of compaction during the resin infusion process; dry compaction, wet relaxation and wet compaction [86, 100]. Dry compaction refers to the initial consolidation of the preform during the pre-filling stage (Figure 2-5a). Wet relaxation occurs

when the resin wets the preform and starts to carry some of the applied load, reducing the amount pressure on the fibre bed according to Eq 4. Due to lubrication effects, the wet relaxation occurs at higher fibre volume fractions for a given pressure, as illustrated in Figure 2-5b. The third type of behaviour is wet compaction which primarily occurs during the post-filling stage when the inlet is closed and excess resin is drawn off while the part thickness reaches equilibrium. There is also a small period of wet compaction when the resin first wets the fibre bed due to the lubrication effect [87]. The wet compaction follows a similar compaction curve to the wet relaxation due to the lubrication effect as illustrated in Figure 2-5c.

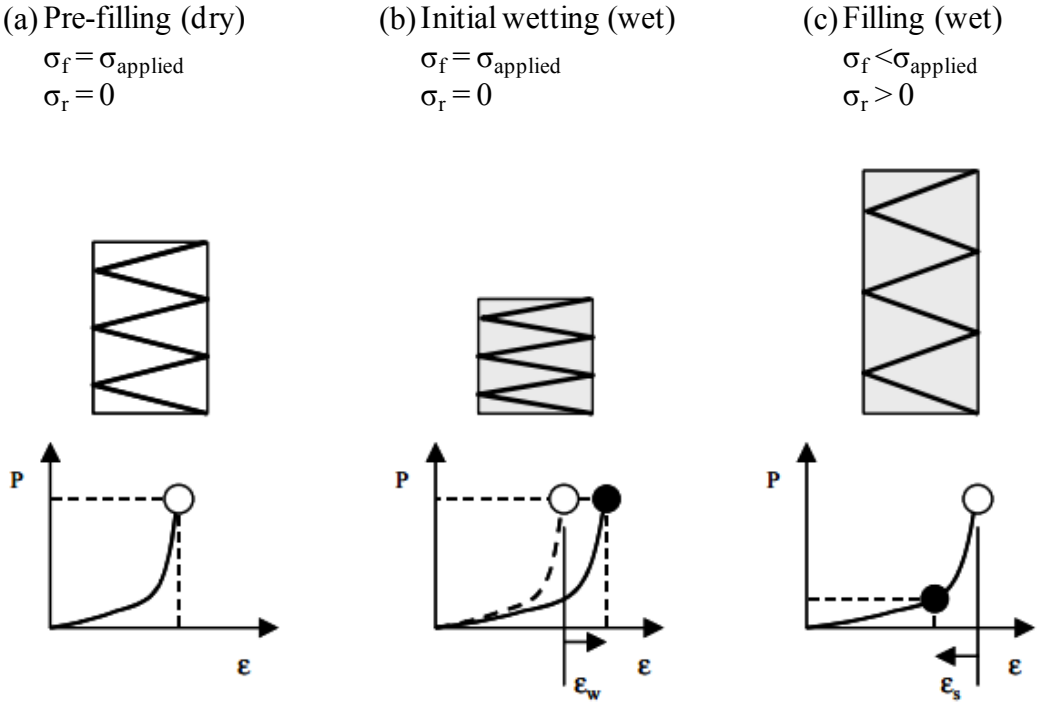

Figure 2-5: Illustration of compaction behaviour during the resin infusion process (adapted from [87]); (a) dry compaction (pre-filling stage) (b) wet compaction (filling and post-filling stage) and (c) wet relaxation (filling stage)

Typically to account for the various types of compaction that are experienced during the resin infusion process, empirical models are determined for all cases and incorporated into the process model [86, 100]. However, in many studies this variation in compaction behaviour is neglected [83-85, 90]. Baydon *et al*

proposed a compaction model that provides a better fit for the relaxation portion of the compaction curves in the resin infusion process given by [100]:

$$\frac{p}{p_{\max}} = \left(a - \frac{V_f}{V_{f\max}} \right)^n - \left(a - \frac{V_0}{V_{f\max}} \right)^n \qquad (12)$$

where a is a constant, p_{max} is the maximum applied pressure and V_{fmax} is the fibre volume fraction at p_{max}. Hammami later studied the compaction of various fibrous reinforcements and distribution medias at the low compaction pressures involved in resin infusion (< 1atm) [118]. It was found that the distribution media can strongly affect the compaction behaviour under dry and wet conditions.

2.2.2.2 Compaction of cellulose-based reinforcements

In general, the required compaction forces for cellulose-based fibre reinforcements are much higher than for similar man-made fibre reinforcements for a given fibre volume fraction. Ouagne *et al* studied the transverse infiltration of flax nonwoven mats and by means of compaction experiments determined that the required clamping forces were almost an order of magnitude higher for the flax mats [120]. This was attributed to the higher amount of fibre entanglement and consequently fibre-fibre contact points in the flax mats. Umer *et al* assessed the potential of various wood fibre mats to replace glass fibre mats in liquid composite moulding (LCM) processes by comparing their permeability and compaction behaviour [121]. It was shown that the wood fibre mat architecture and the testing fluid (polar vs. non-polar) both strongly influenced the compaction behaviour. The wood fibre mats required much higher compaction forces to achieve comparable fibre volume fractions. In another study by Umer *et al*, the effect of flax yarn length and diameter on permeability and compaction of non woven mats was investigated. It was found that larger diameter yarns required much lower compaction forces to attain a given fibre volume fraction. Furthermore, longer yarns were found to require higher compaction forces due to a greater number of yarn cross-over points [122]. Francucci *et al* studied the compaction response of jute fabrics used in liquid composite moulding processes

[123]. The jute fibre lumen was shown to collapse after the application of the compaction pressure. Moreover, saturation of the preform with water/glycerin was shown to soften the fibres as apparent by a reduction in compaction stress for a given fibre volume fraction. This observation was similar to that of Umer *et al* for the case of wood fibre mats [121]. Xue *et al* studied the compaction of flax mats at low pressures (< 1 atm) and found the fibre volume fractions to be very low (around 20%) at the pressures involved during the resin infusion process [124].

2.2.3 Permeability

Another critical property in modelling the resin infusion process is the preform permeability. As discussed in Section 2.2.1, permeability is a material property that describes the resistance of flow through a porous media. Permeability is a tensor property and thus can be different in all the principal directions in a porous media [125]. For the purpose of this thesis, discussions will be limited to in-plane permeability.

To fit permeability data, one of the most commonly employed models is the Kozeny-Carmen equation given by [69, 80]:

$$K = \frac{r_f}{4k}\frac{(1-V_f)^2}{V_f{}^2} \qquad (13)$$

where r_f is the fibre radius, k is the Kozeny constant (different for varying stack orientation) and V_f is the fibre volume fraction. Gerbert derived a very similar equation to the Kozeny-Carmen equation given by [81]:

$$K = \frac{8r_f{}^2}{c}\frac{(1-V_f)^2}{V_f{}^2} \qquad (14)$$

where c is a shape factor. It is apparent from Eq. 13 and Eq. 14 that the shape factor, c, is related to the Kozeny constant, k, by a factor of 32. Gebert revealed that Eq. 13 is strictly only valid for flow parallel to unidirectional reinforcements and derived a separate relationship for transverse flow. In addition, it was shown

that *k* is a weak function of fibre volume fraction. The Kozeny constant has also been observed to vary with fibre volume fraction in other studies [69].

Although Eq 13 is the most widely used permeability model, other approaches have been explored in the literature. For example, Bruschke and Advani developed a permeability-porosity relationship based on flow across a bed of aligned cylinders that could be applied to several fibre packing arrangements [79].

2.2.3.1 Unsaturated versus saturated permeability

As discussed in Section 2.2.1.2, LCM processes can give rise to unsaturated effects due to the dual-scale porous nature of many fibrous reinforcements. These effects can also arise in the measurement of permeability and has led to the distinction of two types of permeability; unsaturated and saturated [91, 126]. Saturated permeability is measured under steady-state conditions when the fibre bed is completely saturated and the flow rate is constant. Thus, it can be determined directly from Darcy's law with knowledge of the pressure gradient, flow rate and fluid viscosity at steady state. Unsaturated permeability is the apparent permeability when the fluid is initially wetting the dry fibre bed and as such it is subject to sink effects caused by saturation of the dry tows as illustrated in Figure 2-4. Furthermore, the pressure gradient has the addition of capillary pressure since air at the flow front is being replaced by a liquid [126]. Unsaturated permeability is typically measured by tracking the flow front [91, 101] and can be calculated from a form of Darcy's law given by:

$$K = \frac{m \cdot \varphi \cdot \mu}{2 \cdot (p_{applied} + p_c)} \qquad (15)$$

where m is the slope of flow front position squared versus time, φ is the porosity, μ is the viscosity, $p_{applied}$ is the applied pressure gradient and p_c is the capillary pressure given by Eq 8.

2.2.3.2 Permeability of cellulose-based fibre reinforcements

Some previous studies have studied the permeability of cellulose-based fibrous reinforcements. Umer *et al* studied the permeability of various wood fibre mats and it was shown that the wood fibre mat architecture and the testing fluid (polar vs. non-polar) both influenced the measured permeability [121]. In general, the wood fibre mats had a permeability of two orders of magnitude lower than that of similar glass fibre mats at comparable fibre volume fractions. Permeability tests were also carried out by Rouison *et al* on hemp fibre mats and it was reported that the permeability was an order of magnitude lower than that of glass fibre mats used in resin transfer moulding [127]. Similarly, it has also been reported by Re *et al* that the permeability of a bi-axial +45/-45 flax fabric is about five to six times lower that a similar glass fabric at the same fibre volume fraction [128]. Umer *et al* looked at the effect of yarn diameter and length on the permeability of flax mats and found the permeability to increase with increasing length and decreasing diameter [122]. In a study on jute fabrics, Francucci *et al* observed a lower saturated permeability compared to unsaturated which was attributed to fibre swelling and fluid absorption [91].

In contrast to the above studies, Rodriguez *et al* found higher permeability for bast fibre mats compared to glass mats for a given porosity which was attributed to the ability of bast fibres to create more flow channels [129]. This contradictory evidence suggests that more work is required in this area in order to understand what mechanisms are unique to bast fibres during LCM processes.

2.3 Mechanical characterization of flax/epoxy composites

The end goal of understanding the processing of composite materials is to maximize the mechanical properties of the final product by producing a high quality composite part. In developing this thesis, a background in the two most commonly tested mechanical properties is presented; tensile and flexural. It should be noted that only data for untreated flax fibres was included due to the large variation in chemical treatment methods.

2.3.1 Tensile

Tensile testing is one of the most common mechanical tests for composite materials and least controversial [130]. ASTM D3039 is a very common testing standard for this property [131]. Currently, tensile testing data for woven and unidirectional (UD) flax/epoxy is limited. The published data for the tensile properties of flax/epoxy composite is summarized in Table 3. Figure 2-6 shows the reported tensile properties versus fibre volume fraction for UD fabric architectures.

Table 3: Published tensile properties for untreated woven and unidirectional flax/epoxy composites

	Fabric type	**V_f (%)**	**Epoxy type**	**Process**	**E_x (GPa)**	**S_x (MPa)**
Oksman **[18]**	UD	47	Ciba XB5082	RTM	39	279
Oksman **[18]**	UD	42	Ciba XB5082	RTM	35	280
Oksman **[18]**	UD	21	Ciba XB5082	RTM	22	193
Oksman **[18]**	UD	32	Ciba XB5082	RTM	15	132
Charlet *et al* [13]	UD	20.1	Axson 2015	Wet layup	16.7	127
Van De Weyenberg *et al* **[20]**	UD	40	Hexcel HM 533	Film stacking	26	190
Van De Weyenberg *et al* **[20]**	UD	48	Hexcel HM 533	Filament winding	32	268
Heijanrath *et al* **[132]**	UD	50	Araldite LY556	Pultrusion	24	325
Gning et al **[15]**	UD	42	SR 8200	Wet layup	15.6	150
Goutianos *et al* **[67]**	Warp knit	28	Araldite MY-750	Hand layup	15	160
Liu *et al* **[17]**	Plain weave	34	Ampreg 20	Resin infusion	9	127

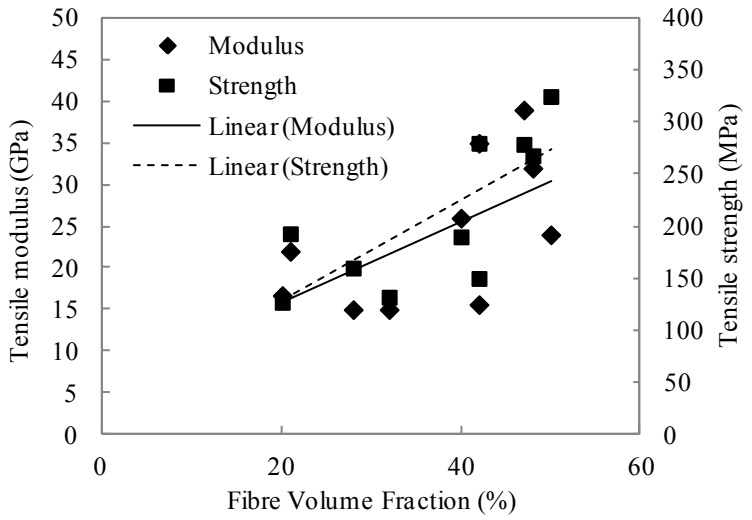

Figure 2-6: Tensile modulus and strength versus fibre volume fraction for published data on untreated unidirectional flax/epoxy composites

It is apparent from Figure 2-6 that there are noticeable deviations from linearity in the fibre volume fraction versus tensile property relationship. This is likely due in part to differences in yarn twist as discussed in Section 2.1.3.2. In addition, variations in fabric crimp (the amount of waviness in the yarns) can affect the mechanical properties of woven fabric composites [133]. Nonetheless, it is apparent that the tensile strength for flax/epoxy is significantly lower than typical values for E-glass/epoxy (800-1000 MPa [18, 67]). However, the moduli are comparable especially in terms of specific moduli due to the lower density of flax fibres [67]. In comparison to typical modulus and strength values for unidirectional carbon fibre/epoxy (207 GPa and 1276 MPa [134]), flax/epoxy is far inferior. Thus, it is unlikely that flax/epoxy could ever effectively replace carbon fibre/epoxy.

2.3.2 Flexural

Flexural testing is popular due to its relatively small sample size and ability to apply compressive, tensile and shear loads in a single test [130]. For this reason, it is also particularly sensitive to the presence of voids and is useful for studying the link between process-induced and mechanical properties [34, 135]. The published data for flexural properties of untreated flax/epoxy is provided in Table

4. Similar to the tensile properties, the strength values were inferior to those of E-glass/epoxy composites but the moduli were comparable.

Table 4: Published flexural properties for untreated woven and unidirectional flax/epoxy composites

	Fabric type	**V_f (%)**	**Epoxy type**	**Process**	**E_x (GPa)**	**S_x (MPa)**
Goutianos *et al* **[67]**	Warp knit	28	Araldite MY-750	Hand layup	16	190
Van De Weyenberg *et al* [20]	UD	40	Hexcel HM 533	Film stacking	18	218
Van De Weyenberg *et al* [20]	UD	48	Hexcel HM 533	Filament winding	23	282
Yan *et al* **[136]**	2/2 Twill	55	SP 20LV	Resin infusion	5.5	120

2.4 Summary

The physical and chemical properties of flax fibres are distinct in comparison to man-made fibres and have direct implications in the processing behaviour of LCM processes as well as in the adhesion with polymer resin systems. To incorporate these fibres into the resin infusion process requires a thorough understanding of the closely coupled nature of the pressure, permeability and compaction in this process. Furthermore, cellulose-based fibres require chemical treatments to promote adhesion with common resin systems which can alter the surface chemistry and consequently the process kinetics. This is further complicated by the fact that cellulose-based fibres such as flax have been shown to exhibit swelling and sink behaviour during LCM processes especially when a polar fluid is used. Most available resin infusion models do not account for these complexities or the capillary pressure which is intimately tied to the chemical treatment of these fibres. All of this processing science directly links to the performance of this class of composites and thus the two are intimately tied. The following chapters will reflect the links between the fibre level, processing and performance aspects of flax/epoxy composites manufactured by resin infusion.

Chapter 3

Fibre characterization

This chapter will discuss the methodology for characterization of flax fibres for the purpose of understanding their behaviour during composite processing. It will begin with material selection details followed by the characterization of the moisture absorption properties of flax fibres. This is followed by a description of selected chemical treatment methods and characterization of the fibre surface chemistry by advancing contact angle analysis. A description of the fibre density measurement method is also included.

3.1 Material selection

The flax fibres that were characterized were obtained from the same textiles that were used in the proceeding chapters. The fabrics were based on linen flax and were produced by the Belgian company, Libeco-Lagae®. Unlike textiles based on conventional reinforcements, there were only a handful of companies producing fabrics with aligned fibres from flax at the time of this writing. Based on availability, two fabric systems were selected which were used in the experiments in this thesis; CL001 and CL015. Selected properties of these fabrics relevant to the experimental results are provided in Table 5. The former fabric was not subjected to a complete characterization in Chapter 4, due to its inferior

filling rate (i.e. the total area filled with fibres) as can be observed in Figure 3-1. However, the CL001 fabric was studied more completely in the prepreg case study presented in Chapter 6. Both fabrics were not subjected to any chemical treatments by the manufacturer. It is interesting to note that for the CL015 fabric, that although the percentage of fibres in the warp in weft direction was similar, the difference in crimp is substantial. This was expected to lead to a large difference in mechanical properties between the two directions for this fabric.

Table 5: Physical properties of 2/2 twill weave flax fabrics studied in this thesis (± standard deviation)

	Areal weight (g/m^2)	**Fibres in Warp Direction (%)**	**Warp Crimp[a] (%)**	**Weft Crimp[a] (%)**	**Yarn Linear Density (Tex)**	**Yarn Twist (twists/m)**
CL001	196±2	51.2	1.2±0.1	1.6±0.1	104	452±98
CL015	543±2	51.3	2.1±0.5	7.9±0.7	385	138±39

[a] Crimp measured by image analysis on samples processed at 3 bars
b from textile specifications
c measured by image analysis and calculated from $TPM = \frac{\tan\beta}{\pi D}$ using 10 samples (β = helix angle)

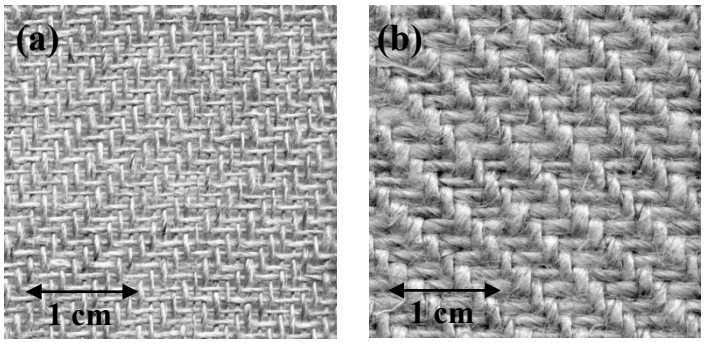

Figure 3-1: Dry 2x2 twill flax weaves used in this thesis a) CL001 b) CL015

It should be noted that the areal weight quoted in Table 5 was the average of five 20x35 cm^2 untreated fabric sections conditioned at 110 °C in a convection oven for 1 hour. This 'dry' areal weight was used to compute the fibre volume fractions quoted in the remainder of this thesis.

3.2 Thermal gravimetric analysis

Thermal gravimetric analysis (TGA) was first carried out on the untreated fabrics to determine the amount of moisture absorption for a range of equilibrium relative

humidity values. It is well known that the presence of moisture in fibres and resin is a critical factor in the formation of voids during composite processing [35]. Thus, understanding how storage and processing conditions affect the moisture uptake in fibres helps to understand how to regulate these two factors. Thermal gravimetric analysis (TGA) was carried out on a TA Q500 in order to obtain the overall moisture content for a range of equilibrium relative humidity values. A ramp cycle was run with 5°C/min up to 100 °C followed by 10 °C/min up to 300°C. Nitrogen was selected as a purge gas.

Three environmental conditions were exposed to the fibres in order to achieve various ambient relative humidity values. The first was ambient laboratory conditions which averaged about 25%. The second was obtained by exposure to a saturated solution of sodium chloride (a.k.a table salt) which is known to provide a relative humidity of 75% [137]. The third was a relative humidity of 100% as obtained by exposure to distilled water in a closed container. For the later two conditions, small samples (5x5 mm^2) were placed on a screen above the solution in a small sealed container (measuring 2x2x3cm^3). The samples were exposed to their respective conditions for one week prior to testing. Typical results in the range of interest (below 300°C) for the CL015 fabric after exposure to the above conditions are plotted in Figure 3-2.

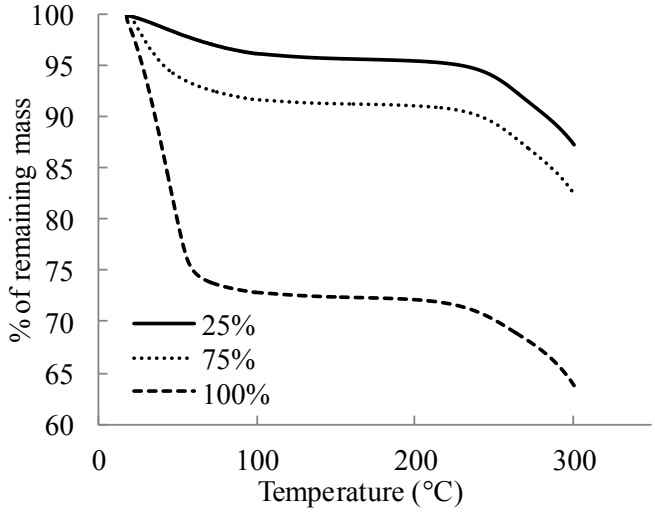

Figure 3-2: Representative TGA mass loss curves for untreated flax exposed to 25, 75 and 100% ambient relative humidity values

Figure 3-2 reveals that the environmental relative humidity had a dramatic effect on the moisture uptake. This is most dramatic for the samples exposed to 100% relative humidity where a mass loss of almost 30% was recorded at 100 °C which was presumably a result of moisture loss. Around 230 °C, the fibres themselves started degrade which is in agreement with other studies [25]. Although this temperature is beyond that required to cure the majority of thermosetting resins, it is below that required to melt most high performance thermoplastics. This was another motivation to use high performance epoxy resins that can be cured at relatively low temperatures.

Taking a temperature of 146°C as when the moisture had completely evaporated (see Section 6.2.2.1 for the calibration method), it was possible to estimate the solubility data for the untreated flax fibres (Figure 3-3). The equilibrium moisture contents agree well with the results from other studies [138, 139].

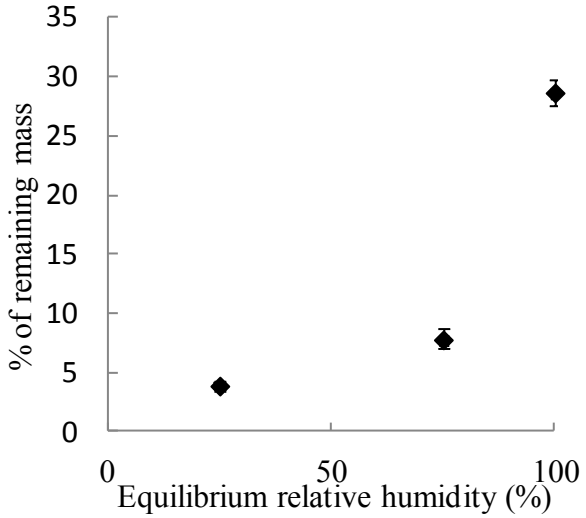

Figure 3-3: Solubility data for untreated flax fibres (error bars represent maximum and minimum values)

It is clear that flax fibres are highly susceptible to moisture absorption which has direct consequences in the context of composite processing. Due to the direct link between moisture and void formation, it is necessary to extract the moisture prior to processing. The resin infusion process lends itself well to this, as a vacuum

hold (sometimes termed 'debulk') can be incorporated prior to infusion to assist with moisture evacuation.

3.3 Chemical treatment

Based on the literature review, two chemical treatments were applied to the fabrics; alkaline and silane. A third was also investigated based on a diluted epoxy solution, which has been shown to be promising [55]. Additionally, fabrics were cleaned by acetone in a separate case to investigate the influence of cleaning surface impurities. All treatments involved a 2-hour soak in a corresponding solution. Further details of the chemical treatments are provided in the following sections.

3.3.1 Alkaline

The alkaline treatment was performed in a solution of 4% NaOH in distilled water. Following the 2-hour soak, the fabrics were rinsed with distilled water until a balanced pH was measured with the litmus paper. The fabrics were then dried in a convection oven at 80 °C for 12 hours.

3.3.2 Silane

The second treatment was a 1% silane of type gamma-glycidoxypropyltrimethoxysilane in a solution of 60% ethanol and 40% distilled water (pH between 3.5 and 4). This treatment was also followed by 12 hours of drying in a convection oven.

3.3.3 Diluted epoxy

The final treatment was a 3% diluted epoxy in acetone. The epoxy monomer and hardener (Huntsman Araldite LY1564 and Aradur 3486 respectively) were first mixed in acetone into which the fabrics were added. The fabrics were then dried at ambient laboratory conditions.

3.3.4 Scanning electron microscopy

Scanning electron microscopy (SEM) was carried out to observe the effect of the treatments on the fibre surface morphology. Small sections of the fabrics were

gold-coated and images were captured in an SEM (Figure 3-4). The SEM images provided some insight into the nature of the treatment on the fibre surfaces. Most distinct was the diluted epoxy treatment which displayed clear epoxy droplets in a non-uniform manner. The acetone, alkaline and silane treatments did not reveal any significant differences from the untreated fabrics. Alkaline treatments have been observed by other authors to roughen the surface of bast fibres [49]. However, this outcome was not obvious in the current study likely due to the relatively low concentration of the NaOH solution. The SEM imaging suggested that the uniformity of the treatments (especially in the case of the diluted epoxy) was a factor.

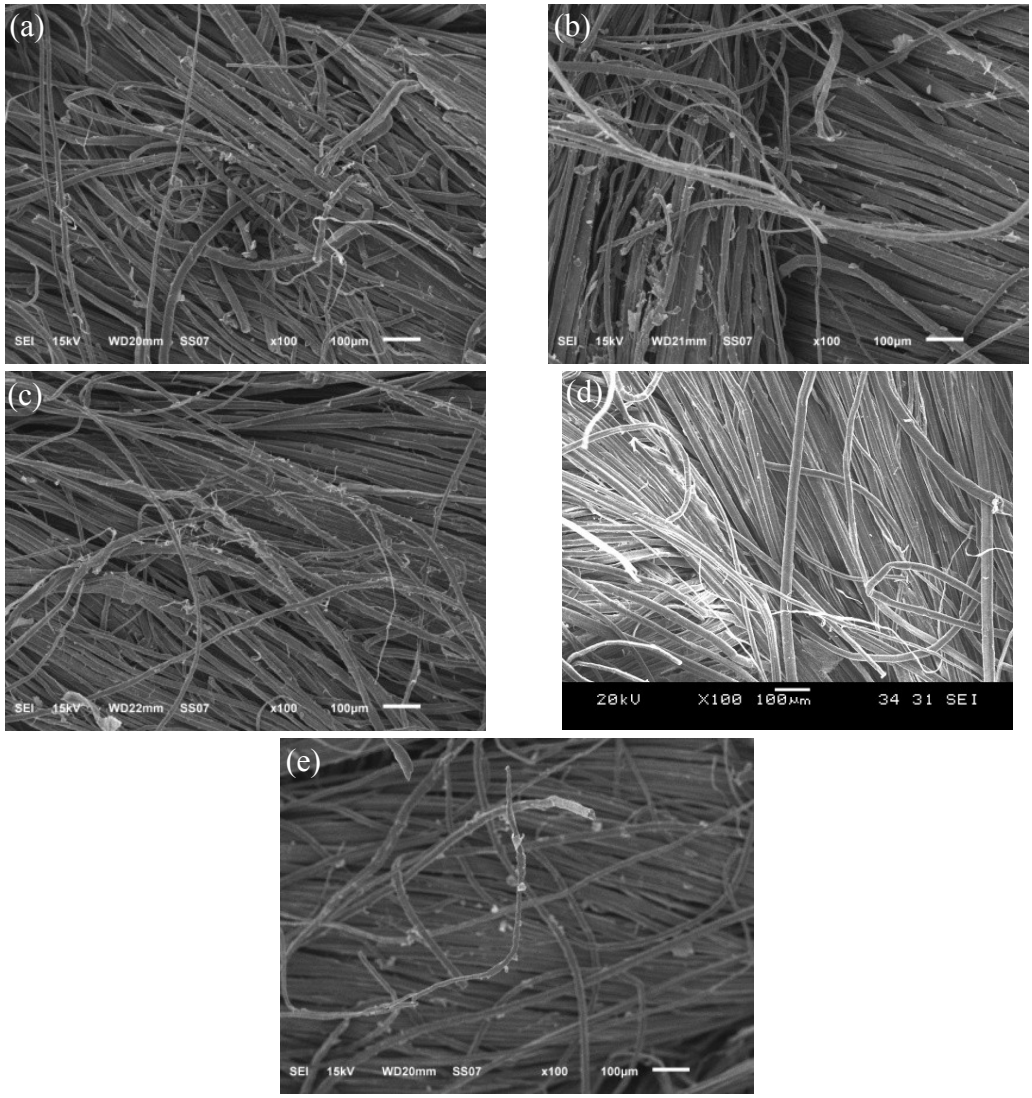

Figure 3-4: SEM images of treated flax fibres: (a) as supplied, (b) acetone, (c) alkaline, (d) silane and (d) diluted epoxy

3.4 Density measurement

Based on the work of Truong et al [36], helium pycnometry was selected for the determination of the fibre density on a Model 930 Beckman® Pycnometer. To minimize closed porosity in the volume measurement, untreated fibres were first ground into a powder using a Retsch® ultracentrifugal mill (ZM 100). Five samples were tested with an average sample mass of 2.1±0.3g. The density of the untreated fibres was determined to be 1.51±0.03 g/cm3. This value for density was used to calculate fibre volume fraction given by:

$$V_f = \frac{\eta \cdot \alpha}{\rho \cdot h} \qquad (16)$$

where η is the number of layers, α is the areal weight of the fabric, ρ is the density of the fibre and *h* is the thickness of the panel. This expression was used to determine the fibre volume fractions quoted in the remainder of this thesis. The terms fibre volume fraction (V_f) and porosity (φ) are used interchangeably throughout this thesis, where $V_f = 1 - \varphi$.

It should be noted that the chemical treatments were assumed not to affect the density or areal weight of the flax fabrics in computing the fibre volume fraction. The latter was determined for the treated fabrics from an average measurement of four 10 x15 cm^2 sections after 48 hours exposure in a desiccant chamber and was found to vary negligibly (< 2%). Since the treated fabrics did not change in areal weight, the constant fibre density assumption was deemed acceptable. It should be noted that some studies have shown a change in 'apparent' density due to the alkaline treatment of cellulose-based fibres [140, 141]. However, the apparent density does not account for the porosity that is created due to the removal of pectin, lignin and hemicelluloses from the fibre and would thus be misleading in the computation of fibre volume fraction.

3.5 Contact angle measurement

To understand the change in fibre surface energy, advancing contact angle analysis was carried out on a Kruss K100 dynamic tensiometer using the

Wilhelmy plate method. Technical flax fibres composed of five to ten elementary fibres were removed from the treated flax yarns for testing. The fibres were fixed vertically and a platform supporting the probe liquid was raised to wet the fibre. The force was zeroed prior to the test to account for the weight of the fibre and test fixture in the calculations. A displacement rate of 1.5 mm/min was applied during the advancing contact angle measurement. The receding angle was not used in the contact angle calculation since, during this stage, the fibre was already wet by the test fluid and the contact angle approached zero. The force data was recorded for a depth range from 0.5 to 2.5 mm. The test fluids that were selected were pure water, diodomethane and ethylene glycol to give a range of x-axis values in Figure 3-7. The surface energy components of these fluids are given in Table 6. A representative force-displacement curve is shown in Figure 3-5 for the described measurement technique.

Table 6: Surface energy components of selected probe liquids [142]

	γ_P (mJ/m^2)	γ_d (mJ/m^2)	γ_t (mJ/m^2)
Pure H_20	26.25	46.55	72.8
Diodomethane	0	50.8	50.8
Ethylene glycol	14.1	33.9	48

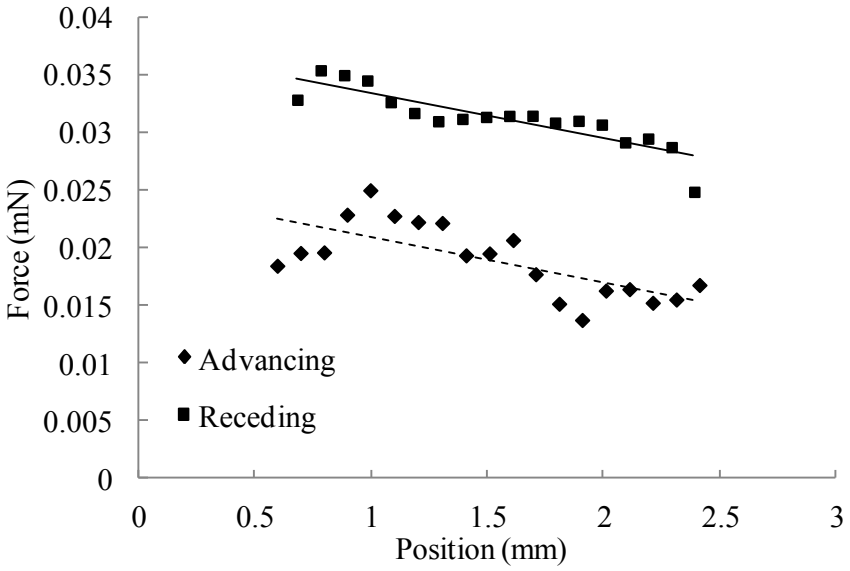

Figure 3-5: Representative force-displacement diagram for Wilhelmy contact angle measurement of untreated flax fibres (probe liquid = pure H_20): note negative slope due to buoyancy effects

It is apparent from Figure 3-5 that there is a distinct negative slope in the force-displacement relationship. This was due to buoyancy forces which increased as the fibre immersion depth increased. To account for this, the force-displacement line was extrapolated to zero in order to determine the equivalent force at zero displacement.

To determine the wetted perimeter, a fully wetting fluid (n-hexane) was used in order to approach a contact angle of zero. The diameter was then deduced using Eq.1. To verify this method, ten fibre cross-sections were also measured by optical microscopy. The two methods were found to be within 15% of each other which was deemed acceptable due to the inherent variability in diameter of flax fibres along their length. A sample cross-section measured by this method is shown in Figure 3-6.

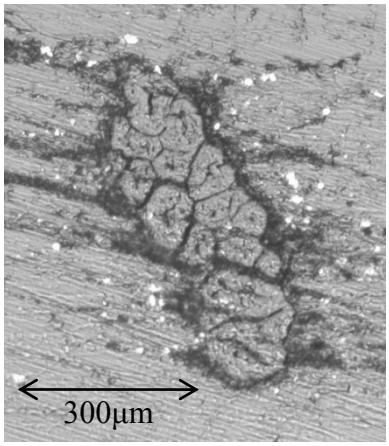

Figure 3-6: Example cross-section of technical flax fibres used to measure contact angle by Wilhelmy method

Based on the above experimental method, the contact angle was determined from the Wilhelmy equation given by Eq. 1. Owens-Wendt theory (Eq. 2) was then applied to deduce the polar and dispersive components of the total surface energy. In accomplishing this, a linear plot was created whereby the polar and dispersive components could be determined from the slope and y-intercept (Figure 3-7). The line coefficient, R^2, of this plot varied between 0.88 and 0.99 which was deemed acceptable. The surface energies determined from the slope and y-intercept are given in Table 7.

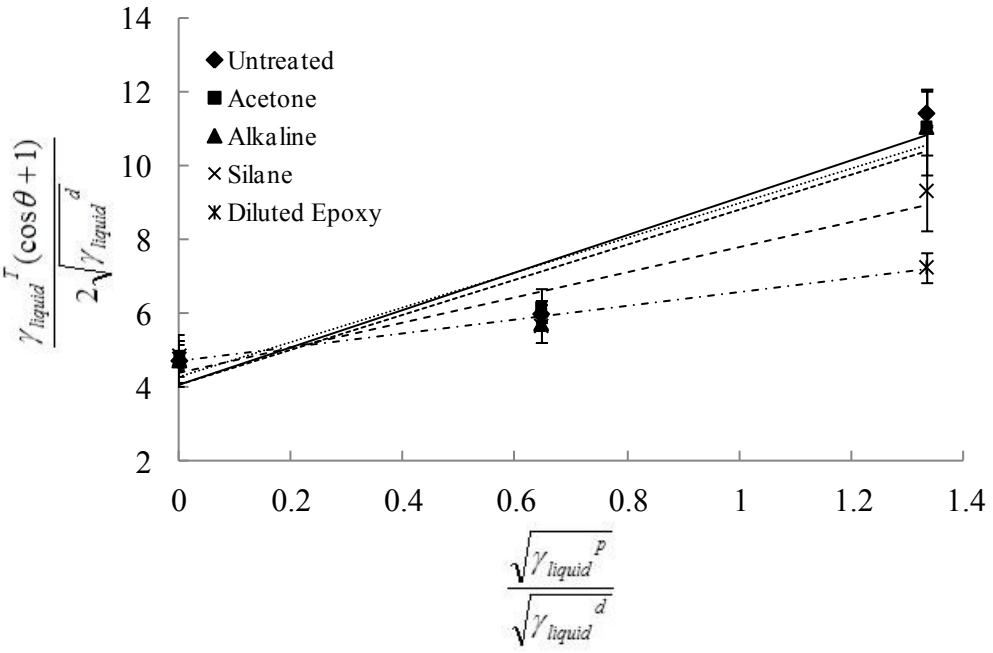

Figure 3-7: Owens-Wendt plot used to deduce fibre surface free energy components; line coefficient R^2 varied between 0.88 and 0.99 (error bars represent maximum and minimum values)

Table 7: Surface free energies for treated flax fibres (± standard deviation)

	γ_P (mJ/m^2)	γ_d (mJ/m^2)	γ_t (mJ/m^2)
Untreated	25.6 ± 2.6	16.5 ± 1.0	42.1 ± 3.6
Acetone	22 ± 3.0	18.4 ± 0.9	40.5 ± 3.9
Alkaline	22.9 ± 3.4	16.3 ± 0.7	39.2 ± 4.1
Silane	11.4 ± 3.9	19.5 ± 2.0	30.8 ± 5.9
Diluted epoxy	3.5 ± 0.8	22.2 ± 0.9	25.7 ± 1.7

The results indicate that, for the majority of the selected treatment parameters, there was not a significant change in fibre surface chemistry. Exceptions were the silane and diluted epoxy treatment which showed a large reduction in the polar component. This suggests that the fibres became more hydrophobic and thus more compatible with epoxy resin systems. The alkaline treatment did not show a large change likely due to the relatively low concentration of the NaOH solution [49]. The untreated fabric surface energy values agreed well with those reported by Cantero *et al* [143].

3.6 Summary

In summary, this chapter focused on the characterization of flax fibres for the purpose of understanding their behaviour during the resin infusion process. This was done by investigating the surface chemistry and morphology of flax fibres subject to common chemical treatments. Of the treatment methods studied, silane and diluted epoxy resulted in a noticeable decrease in the polar component of the fibre surface energy. A 4% alkaline treatment did not show any significant difference in surface free energy values due to the relatively low concentration.

In addition, the water absorption behaviour over a range of equilibrium relative humidity values was studied. Water intake (measured in mass) was shown to approach 30% for high values of environmental relative humidity values (about 100%). This stressed the need for moisture evacuation during the design of composite manufacturing process incorporating flax fibres.

Chapter 4

Fabric characterization

Following the fibre characterization, the flax fabric was characterized to determine material input parameters for a resin infusion process model. The two necessary properties required by the model were the permeability and compaction response of the fibrous preform. The determination of these parameters is described in the following sections.

4.1 Permeability measurement

To measure the in-plane permeability, two different test fixtures were employed. The first setup was designed to measure unsaturated permeability and was compatible with the use of epoxy as the test fluid. The second setup was designed to measure saturated permeability but was limited to non-curing test fluids.

4.1.1 Test fixtures

The first apparatus consisted of an instrumented tool plate with heating capabilities and compatibility with curing resin systems (Figure 4-1). However, this setup could not measure the saturated permeability since it was not equipped

with resin pressure sensors. The tool plate material for this setup was Aluminum 6061. The entire setup was attached to a hot plate in order to facilitate curing at elevated temperatures. To avoid bonding between the tool plate and cured composite part, a layer of release film was first placed on the tool plate. Spiral tubing (Heli-Tube® ¼ inch diameter polyethylene) acted as the resin inlet and vent. The rest of the bagging arrangement was standard for resin infusion (Figure 1-4) without the use of distribution media or peel ply. In addition, two lines of sealant tape were added to the sides of the preforms in order to avoid "race tracking" (i.e. rapid flow of the resin along the sides of the preforms). The tubing for both setups was Hitech® polyethylene (¼ inch diameter). The thickness of the laminate at two points (5 cm and 15 cm from the inlet) was measured using laser thickness transducers (Banner LG5A65NIQ). A resin trap was used at the vent and the trap pressure was monitored with a Wika® Eco-tronic® pressure transducer. The calibration procedures for all pressure and laser sensors are provided in Appendix B.

The second apparatus was similar to the first with two key differences; it employed five pressure sensors (Omega® PX26) and did not have heating capabilities. This setup was based on the work of Croteau-Labouly [144]. It made use of changes in porosity experienced by the fibre bed during infiltration to compute saturated permeability values over a limited range of fibre volume fractions. The tool plate material for this setup was selected as acrylic glass. The inlet and outlet were tube fittings that facilitated direct connection with ¼ inch tubing. The bagging arrangement was the same as the first setup without the release film. A silicone sealer (DAP® AlexPlus®) was used on the sides of the preforms since there were no resin compatibility issues. To measure the flow rate in this apparatus, the resin container was placed on a scale (Ohaus® Scout® Pro SP2001) and the mass change was recorded by a LabView® program. Laser thickness transducers (Banner LG5A65NIQ) were also used in this setup at positions of 10 and 30 cm from the inlet. A schematic of the tool plate design for this test setup is shown in Figure 4-2.

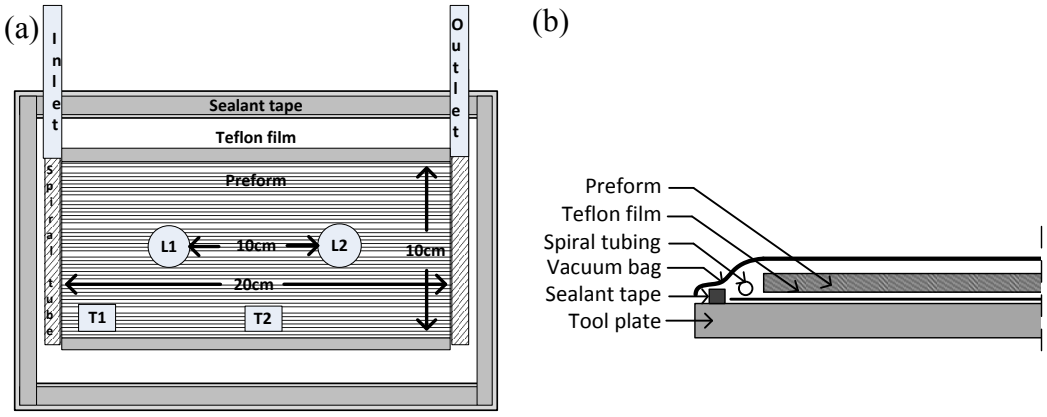

Figure 4-1: Schematic of tool plate for permeability test apparatus #1 (where L=laser thickness gauges and T=thermocouples); (a) top view and (b) side view

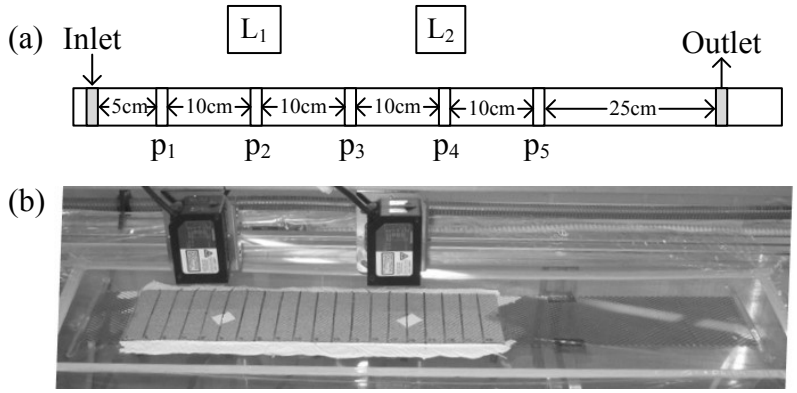

Figure 4-2: Tool plate design for in-plane permeability measurement apparatus #2 (where L=laser thickness gauges and p=pressure sensors); (a) side view schematic and (b) actual setup

4.1.2 Test fluids

Two test fluids were used in the permeability experiments. The first was the same epoxy resin (Araldite LY1564/Aradur 3486) that was used in the manufacturing of the mechanical characterization samples presented in Chapter 5. The second was silicone oil (Dow Corning® Fluid 200) which was selected due to its stability and hydrophobic nature. The epoxy and silicone oil were used with test setups #1 and #2 respectively.

The viscosity of both fluids was determined in the temperature range of interest (Figure 4-3 and Figure 4-4) with a TA AR2000 rheometer equipped with a 2°

cone and 40mm diameter plate type geometry. A flow test employing a frequency sweep from 10 to 500 Hz was carried out and the viscosity was taken to be that measured at 500Hz. The viscosity (μ) in Pa·s over the given temperature range was then fit using an Arrhenius model of the form:

$$\mu = \mu_0 e^{-\frac{E}{RT}} \qquad (17)$$

where T is the absolute temperature (K), μ_0 is a constant (Pa·s), R is the universal gas constant (8.314 J/K/mol) and E is the activation energy (J/mol). For the epoxy resin, the constant and activation energy were determined to be 7.268×10^{-10} Pa·s and -5.001×10^{4} J/mol respectively. For the silicone oil, they were determined to be 5.013×10^{-4} Pa·s and -1.292×10^{4} J/mol respectively.

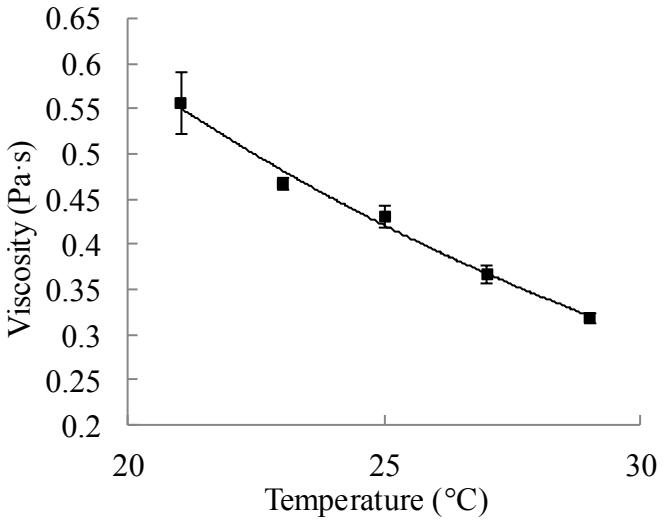

Figure 4-3: Viscosity versus temperature for Araldite LY1564/Aradur 3486 epoxy immediately after mixing determined on a rheometer using a 2° cone and 40mm diameter plate type geometry (error bars represent maximum and minimum values)

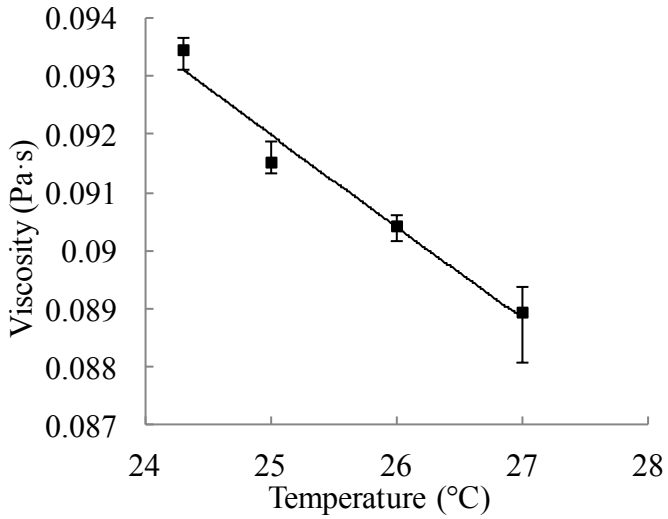

Figure 4-4: Viscosity versus temperature for Dow Corning® Fluid 200 silicone oil determined on a rheometer using a 2° cone and 40mm diameter plate type geometry (error bars represent maximum and minimum values)

4.1.3 Unsaturated

The unsaturated permeability was first measured on test setup #1. Due to changes in porosity experienced by the fibre bed during infiltration, the concept of equivalent permeability was applied for the unsaturated permeability [145-147]. The equivalent resin infusion permeability neglects the thickness change during the process and assumes the porosity which is measured prior to infusion in Eq. 15. Although this inherently over predicts the permeability value (since the porosity actually increases during the process) it is still a valuable comparative tool and has even been shown to have applicability in modelling [145-147].

4.1.3.1 Experimental procedure

The experimental procedure for the equivalent unsaturated permeability measurement on test setup #1 was as follows:

1) Three layers of CL015 with an area of 10 x 20 cm^2 were stacked in the center of the tool plate (warp direction parallel to direction of flow).

2) The sides of the preform were lined with sealant tape.

3) The appropriate consumables (i.e. vacuum bag, sealant tape etc.) were added.

4) A 30 min vacuum debulk was carried out to evacuate moisture.

5) Lines were drawn with permanent marker at 2 cm intervals on the top of the vacuum bag to facilitate tracking of the flow front.
6) The vacuum pump was then disconnected to check for leaks (a pressure drop of less than 0.5 kPa over 10 minutes was deemed passable).
7) The system was vented and vacuum was applied promptly during which the dry compaction behaviour was measured (discussed in Section 4.2.2)
8) The inlet was opened and the position of the flow front was tracked by means of the marks from step 5 and a LabVIEW® program.
9) Once the resin reached the outlet, the inlet was clamped and the post-fill thickness evolution was monitored.

From step 8, the graph of the flow front position squared versus time could be obtained (Figure 4-5). The slope of this graph is equal to *m* in Eq. 15. It should be noted that in cases where the flow front was uneven, the data point was registered when the centre of the flow front passed the marks from step 8. The thickness evolution data for all measurements is presented in Appendix C.

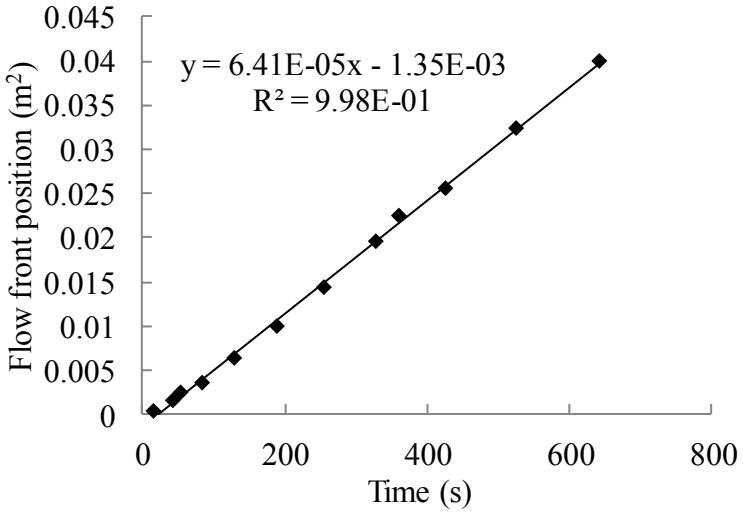

Figure 4-5: Flow front position squared versus time for resin infusion of untreated CL015 flax fabric with epoxy

4.1.3.2 Permeability of untreated fabrics

Based on the above procedure, the equivalent unsaturated permeability values were calculated from Eq. 15 for the untreated fabrics. The porosity was taken to be that which was measured prior to infusion by the method described in Section 4.2. A total of three samples were tested in each of the permeability experiments.

The contact angle was computed from Eq. 8. To determine the contact angle with the epoxy resin, the Owens-Wendt equation (Eq. 2) was used with literature surface energy values for a similar epoxy system reported by Comyn [52] (γ_d = 41.2; γ_p = 5.0 mJ/m^2). Another unknown in Eq. 8 was the form fitting factor, β, which depended on the architecture and orientation of the fibrous preform. For the case of a plain weave carbon fabric, it has been shown that this form fitting factor is approximately equal to 3.84 [148]. Assuming the same form fitting factor for the CL015 fabric, a fibre diameter of 17.8 μm [29] and constant porosity, the capillary pressure was estimated to be about 4 kPa for the untreated fabrics. Upon examination of Eq. 8, this low value of capillary pressure was mainly a result of the high porosity values. The equivalent unsaturated permeability was determined to be 9.42x10^{-11} m^2 for a porosity of 68.4% for the untreated fabrics.

One vital observation was made during the unsaturated permeability experiments. From visual inspection, the apparent unsaturated regime was observed to be very small (Figure 4-6). One cause of this could have been the similarity in length scales between the inter-yarn and intra-yarn spacing for the studied fabric architecture in the observed porosity ranges (Figure 4-7). Thus, a significant difference in time scales between the impregnation of the intra-yarn and the inter-yarn regions would not be expected. However, this conclusion neglects the impregnation of the technical fibres themselves where the spacing of the elementary fibres is very small (about 1 μm). If impregnation of the technical fibres did occur, fabrics from cellulose-based fibres could be seen as triple-scale porous media. Investigating this triple-scale flow phenomenon was beyond the

scope of the current study but could be an interesting topic for future work. Based on observations in the current study, it was reasonable to assume that the spacing between elementary flax fibres was so small that those regions were negligible in the determination of equivalent permeability.

It should be noted that it is possible that the delayed impregnation of the yarn was not visible by the naked eye and could be better detected in future studies by a technique such as that suggested by Ruiz *et al* [149]. Nonetheless, for the present study it suggested that unsaturated effects were small with a non-polar test fluid such as epoxy. However, as mentioned in Chapter 2 there has been some evidence that suggests that use of a polar test fluid can increase these unsaturated effects due to swelling of the cellulose-based fibres [91, 92, 121]. In the case of non-polar fluids, the transverse swelling has been previously shown to be minimal (<2%) for exposure periods on the scale of the infusion times witnessed in the current thesis (less than 10 minutes) [91].

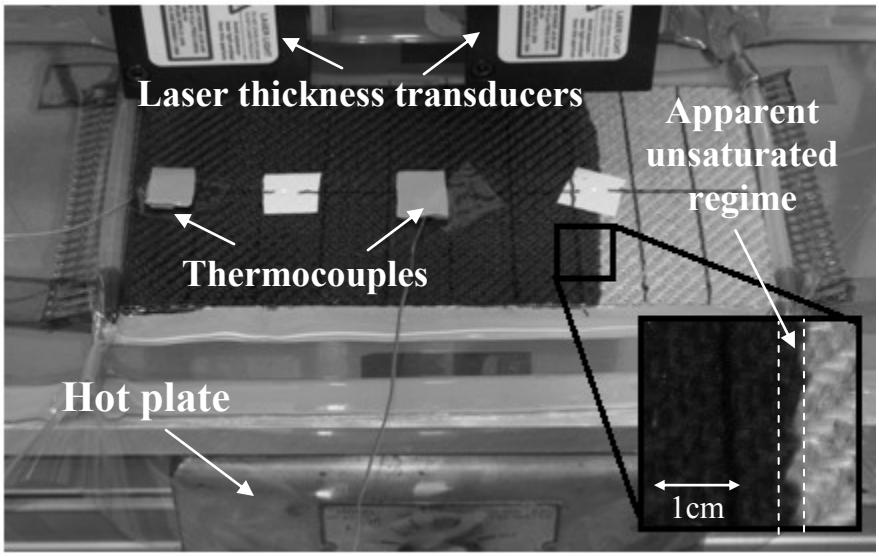

Figure 4-6: Permeability test apparatus #1 for unsaturated measurements during infusion: note that apparent unsaturated flow front was observed to be very small (about 5mm)

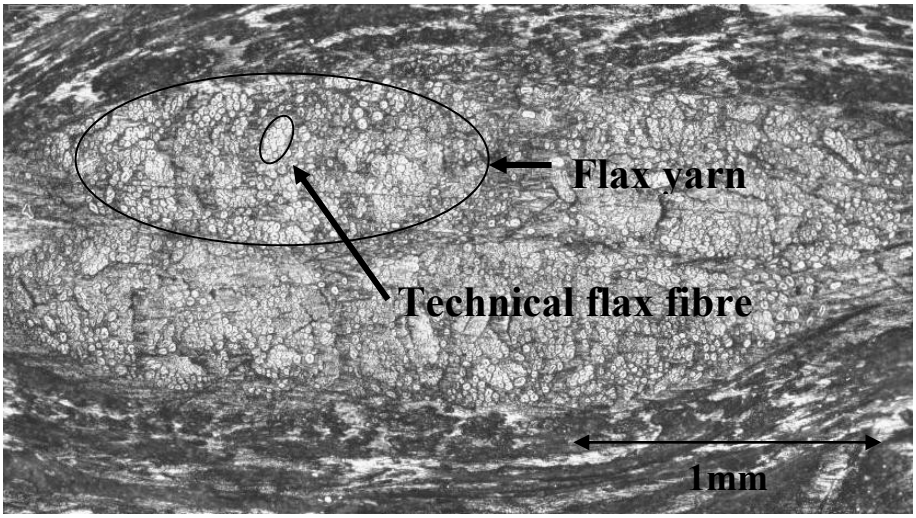

Figure 4-7: Cross-section of compacted CL015 flax fabric at 100 kPa of pressure: note similarity in inter-yarn and intra-yarn length scales

4.1.3.3 Effect of surface treatments

Using the above procedure, the treated fabrics were also tested using setup #1. The surface free energy values measured in Section 3.5 were used to determine the capillary pressures. The areal weight and fibre densities were assumed to remain constant for the treated fabrics. The results for equivalent permeability and porosity are plotted in Figure 4-8.

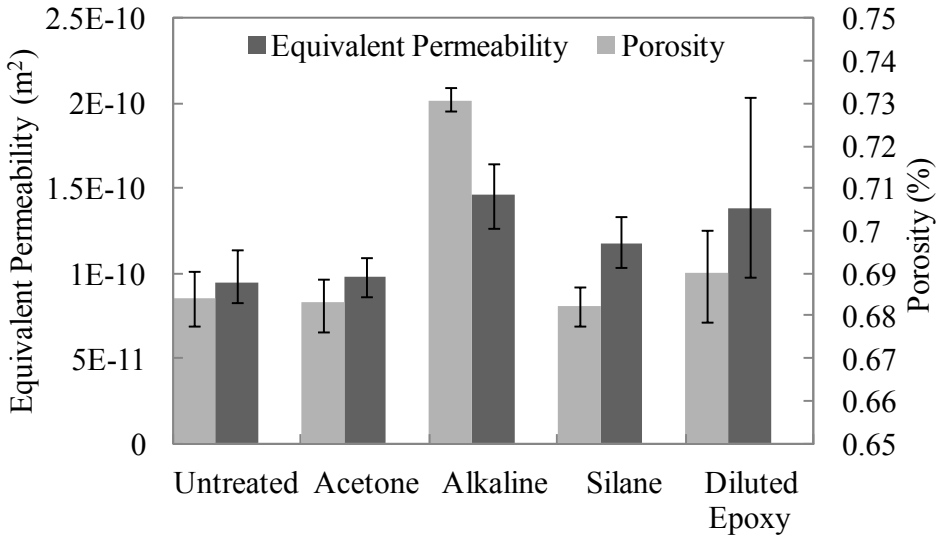

Figure 4-8: Equivalent in-plane permeability and porosity values for treated flax fabrics measured during the resin infusion process (error bars represent maximum and minimum values)

In principle, any difference in permeability due to the surface treatments would be a result of changes in porosity, fibre surface morphology and/or fabric architecture since the capillary pressure was accounted for. The results suggest that, in general, the use of chemical treatments did not result in significant changes of equivalent permeability for resin infusion. An exception was the alkaline treatment which showed a distinct increase in equivalent permeability likely due to a large increase in porosity. This was likely due to the apparent swelling which alkaline treatments induce in cellulose fibres as a result of increased fibrillation due to the removal of lignin, pectin and hemicellulose [25]. This would have caused more fibre-fibre contact points and thus would have increased the required load to attain a given fibre volume fraction. This apparent swelling effect is commonly minimized by tensioning the fabrics during treatment [54]. Thus, it can be concluded that for the purpose of composite processing, the fabric boundary condition during the alkaline treatment plays a key role.

In the case of the silane and diluted epoxy treatments, analysis-of-variance (ANOVA) revealed that the permeability values were not statistically different from the untreated or acetone cleaned fabrics. A large degree of scatter for the diluted epoxy treatment was likely a result of the non-uniformity of the applied treatment as was seen in the SEM images (Figure 3-4). Therefore, similar to the alkaline treatment, the method of treatment must be chosen appropriately in order to obtain the desired result.

4.1.4 Saturated

For the purposes of modelling, the saturated permeability was measured over a relevant range of fibre volume fractions on test setup #2. Although during the resin infusion filling stage, the fibre bed is not strictly saturated, the saturated permeability was selected for the model since unsaturated effects were observed to be small with a non-polar fluid. The experimental procedure, calculation method and results for the saturated permeability determination are described below.

4.1.4.1 Experimental procedure

The experimental procedure for the saturated permeability measurement on test setup #2 was identical to that of the unsaturated measurement with the following exceptions.

- Silicone putty (DAP® AlexPlus®) was used in place of sealant tape on the sides of the preform since there were no compatibility issues with the resin.
- The resin inlet was kept open past the saturation of the preform until the flow and pressure readings stabilized.
- The preform was 20 cm longer since the viscosity of the test fluid was lower and the infiltration times were reasonable.
- One layer of distribution media was used at the inlet (before p_1) and outlet (after p_5) so that the vacuum bag did not seal directly on the tool plate.

4.1.4.2 Permeability calculation

During the saturated regime, the flow rate and pressure gradient all remained constant. Thus, with knowledge of the compaction behaviour of the preform, the permeability was calculated based on pressure sensor measurements along the mould length by Eq. 3 from Section 2.2.1. The volumetric flow rate was determined from the mass flow rate using the density of the silicone oil (0.971 g/cm^3). The mass flow rate was taken to be the slope of remaining resin mass versus time in the saturated regime of the experiment (Figure 4-9).

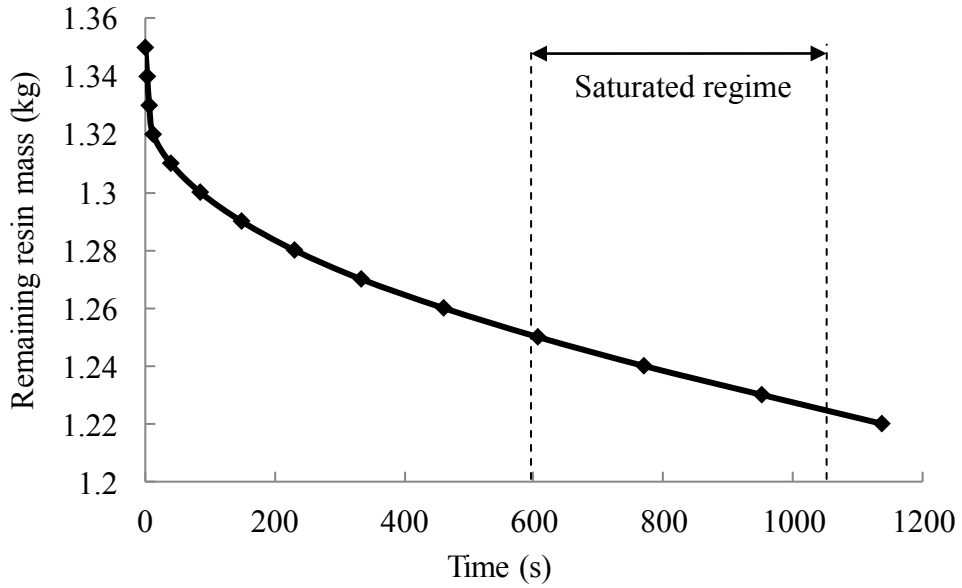

Figure 4-9: Evolution of resin mass during in-plane saturated permeability measurement

The pressure gradient during the saturated regime was recorded for calculation of the permeability values. By simultaneously characterizing the wet unloading behaviour (described in section 4.2.3), the thickness profile along the length of the preform could also be determined (Figure 4-10). The compaction pressure at the pressure sensor locations was calculated from Terzaghi's law (Eq. 4 from Section 2.2.1).

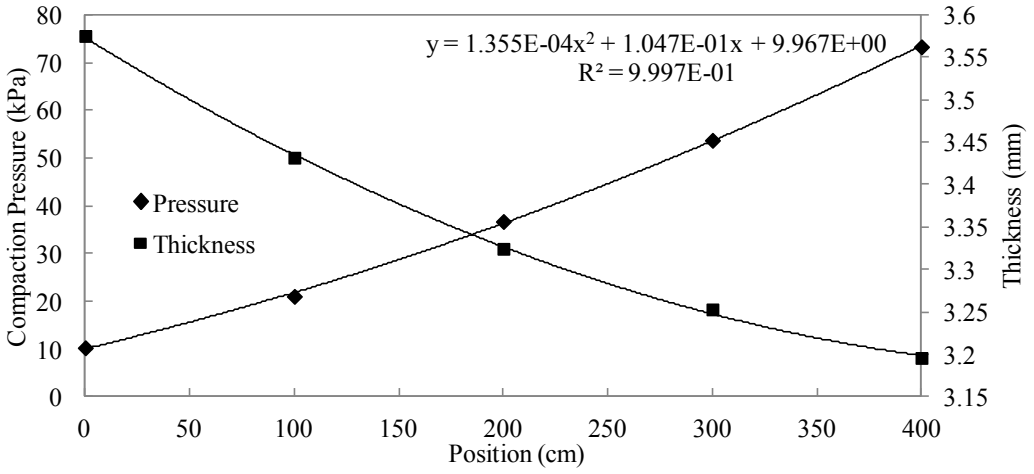

Figure 4-10: Representative spatial variation of pressure and thickness during saturated permeability measurement during saturated regime of infusion

The pressure data in Figure 4-10 was found to follow a 2nd order polynomial. Based on the derivative of this function, the saturated permeability was then computed along the length of the mould by Eq. 3 from Section 2.2.1. The parameters for the case shown in Figure 4-10 are presented in Table 8. It is apparent in Figure 4-11 that the pressure at the beginning of the preform was above atmospheric pressure and at the end of the preform was below the vacuum level (about 4.75 kPa). This is a result of the resistance to flow due to the distribution media. Although the permeability of this layer was relatively high, the vacuum bag tended to contact the tool plate directly through the distribution media and reduce the permeability. To avoid this, several layers of distribution media can be stacked. However, since the pressure was measured at the beginning and the end of the preform, this was not necessary in the current study.

Table 8: Sample parameters in computation of saturated permeability

Distance (mm)	**0**	**100**	**200**	**300**	**400**
$p_{compaction}$ (kPa)	10.3	21.0	36.7	53.8	73.4
dp/mm (kPa/mm)	1.05E-01	1.32E-01	1.59E-01	1.86E-01	2.13E-01
V_f	0.298	0.310	0.320	0.327	0.333
h (mm)	3.58	3.43	3.32	3.25	3.20
φ	0.702	0.690	0.680	0.673	0.667
u (mm/s)	0.163	0.170	0.176	0.179	0.183
K (m^2)	1.08E-10	8.74E-11	7.38E-11	6.38E-11	5.61E-11

Once the parameters from Table 8 were calculated, the saturated permeability-fibre volume fraction relationship was determined for a given sample (Figure 4-11). It can be seen in Figure 4-11 that for the limited range of porosities witnessed in the resin infusion process, a power-law model provided a good fit to the experimental data. Therefore, in the current study, the Kozeny-Carman relationship (Eq. 13) was not used due to the simplicity of the power-law model.

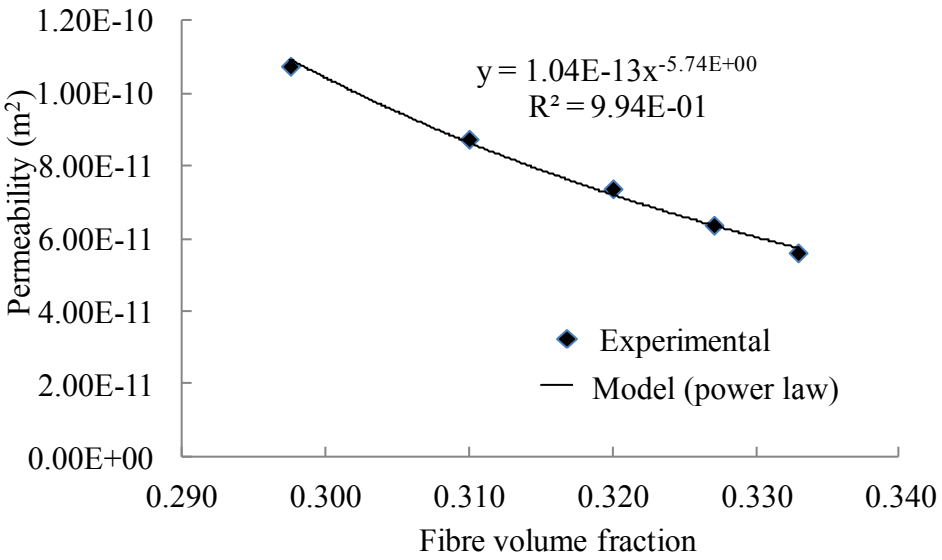

Figure 4-11: Representative permeability versus fibre volume fraction relationship for saturated permeability measurement

Using the above procedure, a total of 4 samples were tested and an average of each model was obtained for the permeability-fibre volume fraction relationship over the range of observed porosities (Figure 4-12).

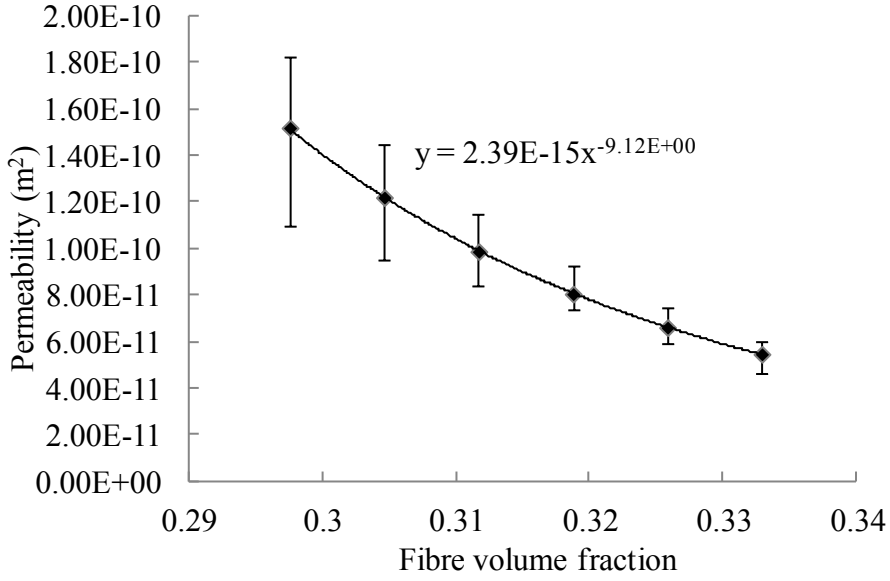

Figure 4-12: Average of models for saturated permeability versus fibre volume fraction for untreated CL015 flax fabrics (error bars represent maximum and minimum values)

After comparing the results from Figure 4-12 to data in the literature for similar E-glass systems, it was apparent that the permeability of the CL015 flax fabric was significantly lower for a given fibre volume fraction. For example, Young *et al* studied a plain weave glass fabric and for the same range of fibre volume fractions, the permeability was higher by about tenfold [150]. This was likely due to the rougher surface morphology of flax fibres as well has the disorderly nature of the CL015 fabric in comparison to typical E-glass textiles. These factors both would have led to a more tortuous path for the resin and consequently lower permeability values for a given fibre volume fraction.

4.2 Compaction

Along with permeability, another important input parameter for the process model in Chapter 5 was the compaction behaviour of the preform. To characterize this property for the studied fabrics, two different test methods were employed in this thesis. A description of these methods is presented below followed by the characterization of the three types of compaction behaviour observed during the resin infusion process; dry compaction, wet unloading and wet compaction.

4.2.1 Test methods

The first compaction test method was carried out on a fixture consisting of two nested steel plates similar to that described by Hubert *et al* [151] (Figure 4-13). This compaction fixture was installed on an MTS Insight universal testing machine with a 5kN load cell.

Figure 4-13: Test fixture used to measure the transverse compliance of fibre beds

For test method #1, the sample area was 5.5 x 5.5 cm^2. The sample length and width were measured at three positions and an average was taken to determine the exact area. The average from the three layer areas was then used to compute the stress in the preform stack. This setup was used as a tool in the prepreg case study (Chapter 6).

The second method was carried out *in-situ* during the permeability measurements described in Section 4.1 through use of the laser thickness transducers (Banner LG5A65NIQ). Since the thickness measurements were taken at two positions along the preform length, each permeability measurement resulted in two sets of compaction data. Therefore, the reported data represented an average of six compaction measurements. The thickness of the vacuum bag and release film was subtracted from the measured values (0.054 and 0.028 mm respectively). Using the corrected thickness data along with knowledge of the test fluid pressure, the load carried by the fibre bed was determined by Terzaghi's law (Eq. 4 from Section 2.2.1). Thus, with the pressure and laser sensors, the compaction stress versus fibre volume fraction relationship was obtained throughout the entire resin infusion process. This method was employed to characterize the dry compaction, wet unloading and wet compaction of the fibre bed. The second of these was used

as input in the process model developed in Chapter 5. This test method was well suited for this task due to its inherent similarity to the actual process given the same range of pressures and strain rates involved. The dry compaction was determined when the vacuum was applied during the pre-filling stage. The wet unloading was measured when the fibre bed was wet by the resin during the filling stage. The wet compaction behaviour was recorded during the post-filling stage. Sample pressure and thickness data for an infusion illustrating these stages is presented in Figure 4-14.

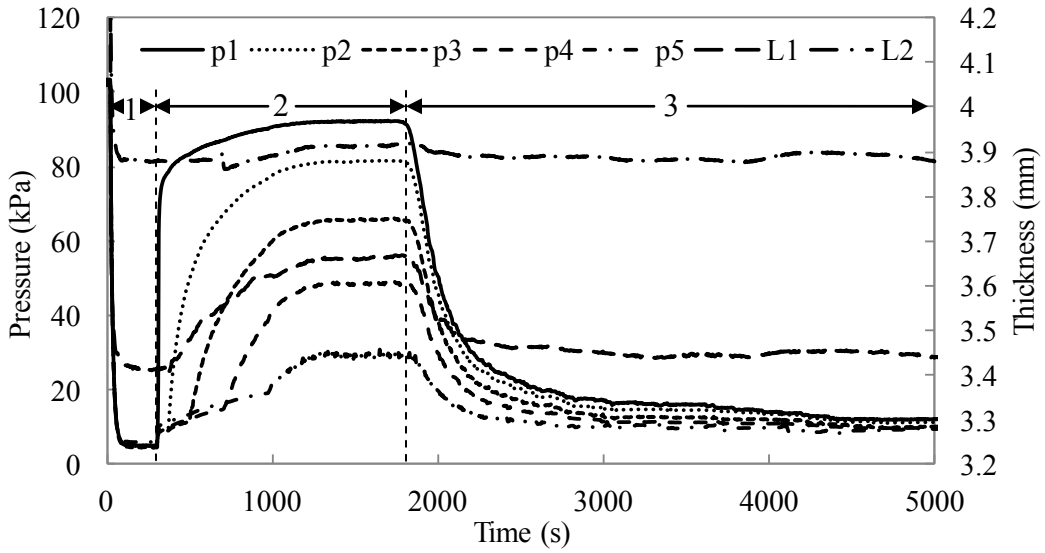

Figure 4-14: Sample acquisition data during infusion experiments; 1=pre-filling stage, 2= filling stage and 3=post-filling stage

The general behaviour of the resin infusion process can be observed in Figure 4-14. Initially there was a thickness decrease due to the application of vacuum (stage 1). During stage 2, the pressure sensor readings increased at the moment the resin reached their location. Thus, the readings rose consecutively and were spaced in time according to the pressure sensor positions in the mould. When the resin reached pressure sensors 2 and 5, the thickness in laser sensors 1 and 2 began to increase respectively due to the load sharing between the resin and fibre bed. Finally during stage 3, the inlet was clamped and excess resin was drawn off until the resin pressure and thickness approached a minimum. The infusion kinetics data for all measurements is presented in Appendix D. The compaction models derived from this data are described below.

4.2.2 Dry compaction

In determining the dry compaction behaviour, the loading rate corresponded to the starting capacity of the vacuum pump. Since a leak check was carried out prior to the test, the reported results represent the behaviour after one compaction cycle.

To model the measured compaction behaviour, the data were fit using a power-law as suggested by Robitalle *et al* [105]. The pressure range from 10 to 100 kPa was used in fitting the model, as incorporation of very low pressures (<10kPa) resulted in an inferior fit and was deemed unnecessary since such low compaction pressures only occurred in the immediate vicinity of the inlet during the resin infusion process. A representative experimental compaction curve along with the power-law curve fit is shown in Figure 4-15. The R^2 value was at least 0.95 for all the experimental data which was deemed acceptable for the purposes of this study.

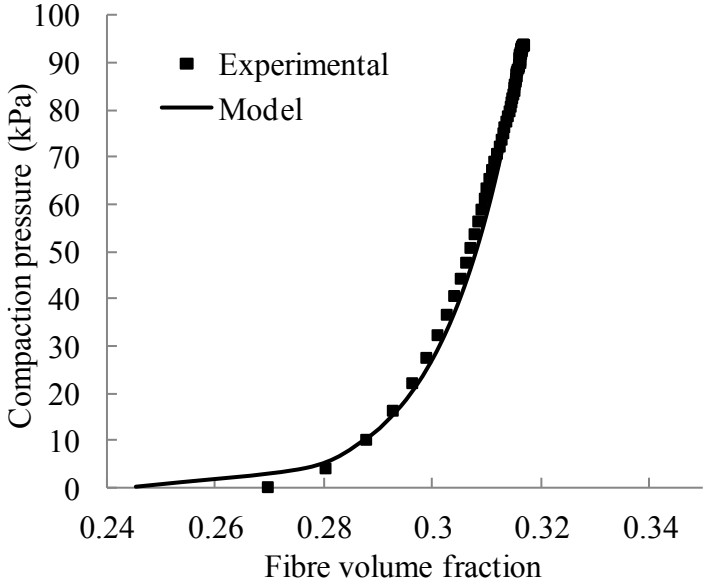

Figure 4-15: Representative compaction curve and power law model; R^2 value was a minimum of 0.95 for all experimental data

In the power-law model, *A* and *B* can be seen as constants related to the compaction behaviour of the reinforcements. Constant *A* represents the fibre volume fraction at a compaction pressure of 1 Pa and *B* represents the compaction stiffening index [105]. The power-law constants for the treated and untreated

fabrics are provided in Table 9 and average compaction curves shown in Figure 4-16. It can be seen that, similar to the equivalent permeability values, there was not a large difference in compaction curves. However, the alkaline treatment showed much lower fibre volume fractions for a given pressure due to increased fibrillation as discussed in Section 4.1.3.3. In addition, the diluted epoxy treatment showed the same trend to a much lesser extent. This was likely due to stiffening of the fabric as a result the low concentration of epoxy. This stiffening also likely caused a reduction in yarn 'nesting' (i.e. the packing of yarns from different layers) which can assist in achieving higher fibre volume fractions for multi-layered preforms [105].

Table 9: Power-law constants for dry compaction behaviour of CL015 fabric

	A (kPa^{-B})	**B**	**V_{fmax}**
Untreated	0.257	0.0442	0.316
Acetone	0.251	0.0474	0.313
Alkaline	0.234	0.0300	0.269
Silane	0.253	0.0474	0.316
Diluted epoxy	0.246	0.471	0.306

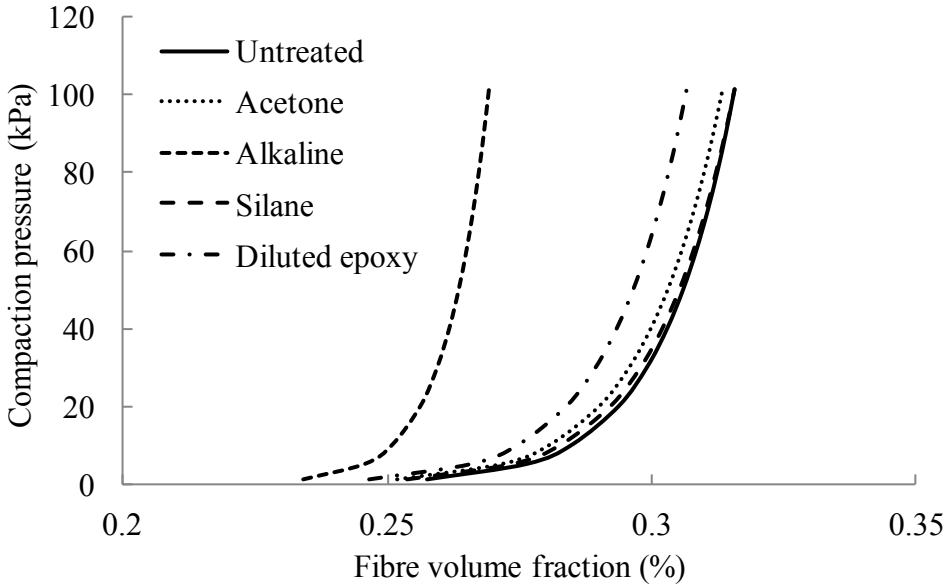

Figure 4-16: Average compaction pressure versus fibre volume fraction for dry treated CL015 flax fabric (3 layers total)

4.2.3 Wet unloading

The second type of compaction behaviour experienced during the resin infusion process is wet unloading. This behaviour was recorded during the infusion experiments by method #2 using silicone oil. Only the data recorded by the laser thickness transducer #1 was used to determine the empirical models since a larger range of fibre volume fractions was inherently experienced by this sensor. Thus, only one data set per infusion (a total of four) was used in determining the average wet unloading curve (Figure 4-17). The power law constants determined from this data were A=0.282 $kPa^{-0.0377}$ and B=0.0377.

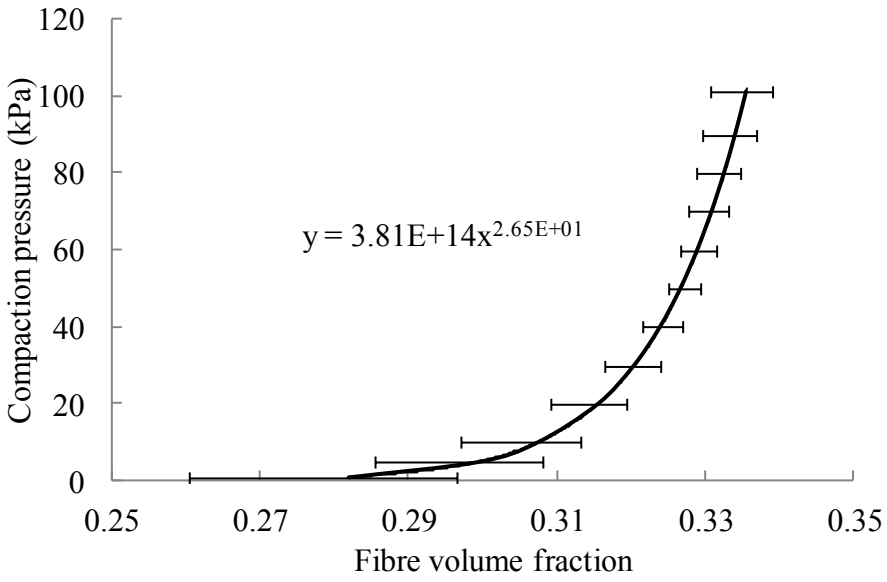

Figure 4-17: Wet unloading behaviour of untreated CL015 flax fabric (error bars represent maximum and minimum values)

4.2.4 Wet compaction

The final type of compaction behaviour experienced during the resin infusion process is wet compaction during the post-filling stage. Although this stage was not modelled in the current thesis, the compaction data still provides useful insight into the behaviour for this class of fabrics. Similar to the wet unloading, only the data from laser sensor #1 was used in computing the average compaction curve (Figure 4-18). The power law constants determined from this data were A=0.283$kPa^{-0.0342}$ and B=0.0342.

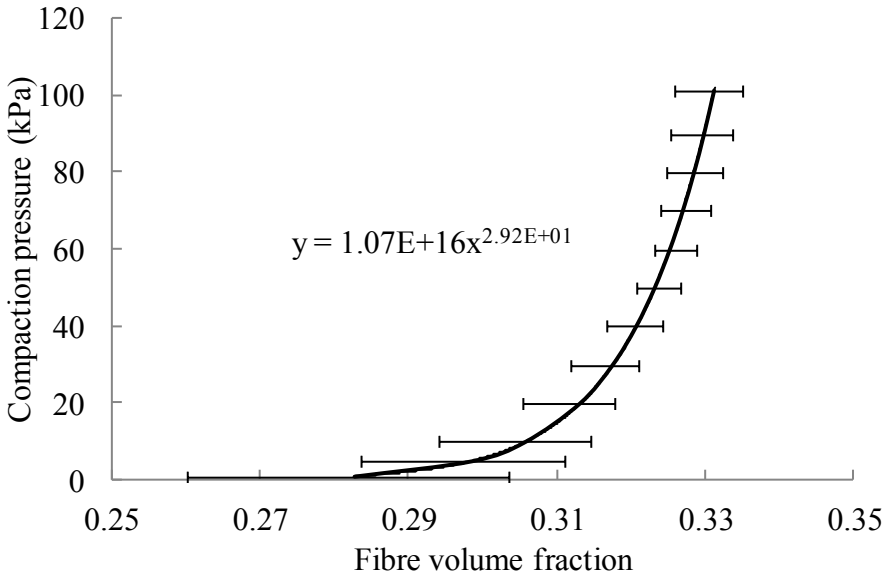

Figure 4-18: Wet compaction behaviour of CL015 flax 2/2 twill weave fabric (error bars represent maximum and minimum values)

4.2.5 Comparison of compaction stages

It is finally useful to compare the behaviour of the above three stages to understand the changes in compaction behaviour due to lubricating and hysteresis effects experienced during the resin infusion process. The average data from the above three stages is presented in Figure 4-19. It is immediately apparent that the lubricating effect is quite pronounced as seen by an increase of maximum fibre volume fraction of about 2% between the wet and dry compaction behaviour. However, this is the case for non-polar test fluids and, as will be shown in the resin infusion case study presented in Chapter 6, this effect is significantly more pronounced for a polar liquid such as water.

A second observation was that the unloading of the fibre bed occurs at higher fibre volume fractions compared to the compaction for a given pressure range. This is typical of compaction phenomena, and is due to both delayed rearrangements of the fibres as well as plastic deformation due to fibre kinking and/or breakage. It should be noted however, that the strain rates were lower in the case of unloading and could have assisted in fibre rearrangement which would

have resulted in a better packing density for a given pressure. In any case, the difference was slight in comparison to the effect of lubrication by the test fluid.

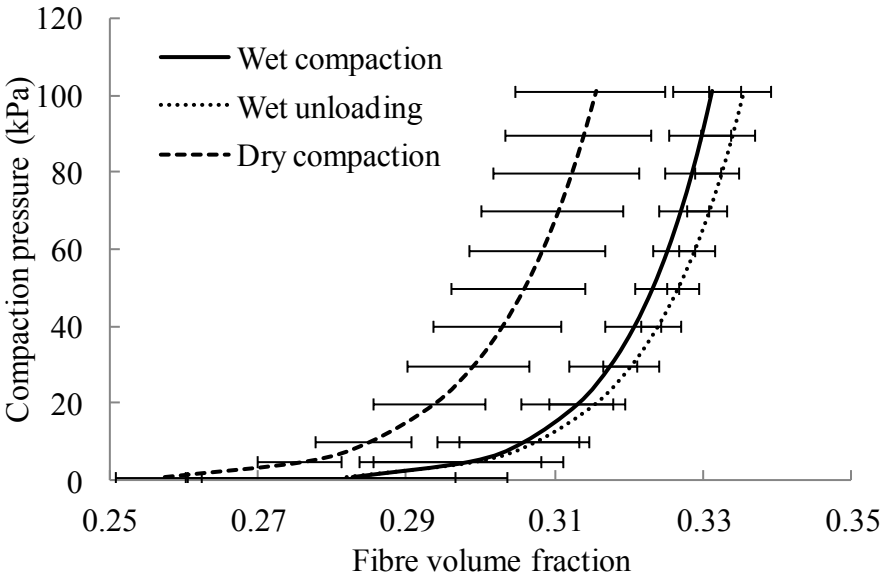

Figure 4-19: Average compaction curves for flax 2/2 twill weave fabrics during dry compaction, wet unloading and wet compaction (error bars represent maximum and minimum values)

4.3 Summary

In summary, this chapter presented a methodology for characterizing the permeability and compaction behaviour of flax fabrics for use in the resin infusion process. Unsaturated and saturated permeability values were first obtained by means of two test setups. An empirical model was fit to the saturated permeability data in the relevant range of fibre volume fractions for use in the process model developed in Chapter 5. The influence of common chemical treatments on the equivalent unsaturated permeability was also investigated. In general, the treatments did not significantly affect the equivalent unsaturated permeability except for the alkaline treatment which showed an increase due to an increase in porosity.

Similar to the permeability, the transverse elastic behaviour of the CL015 flax fabric was characterized. The elastic behaviour of the preforms was shown to

vary according to lubrication and loading scenarios. To quantify these differences, a set of empirical models were developed for the unique loading cases experienced during the resin infusion process. The experimental characterization of the flax fabric set the stage for the following chapter which describes the processing, process modelling and characterization of flax/epoxy composites manufactured by the resin infusion process.

Chapter 5

Composite processing and characterization

Following the fabric characterization, composites were manufactured and the processing data was compared with the predictions of a 1-dimensional process model. This chapter begins with a description of the composite processing followed by the development of a process model. The results from a mechanical characterization of the cured composites are finally presented.

5.1 Composite processing

Composites were manufactured during the unsaturated permeability measurements by curing the epoxy following the infusion. The resin was first mixed by hand for 5 minutes and degassed for 30 minutes prior to the infusion. Preliminary experiments revealed that the resin tended to degas under very low vent pressures. To alleviate this issue, the resin was degassed at about 0.5 kPa lower pressure than that which was set at the vent during the filling stage using a vacuum regulator. Furthermore, two additional post-fill vent pressures (25 and 50 kPa) were included in the design of experiments to produce composites of varying

void content so that the effect of voids on flexural and Charpy impact properties could be studied.

Following the infusion and a 1-hour post-fill stage, the composites were cured based on the recommended cure cycle for the resin. A cure temperature of approximately 50±5°C was selected for a curing period of 16 hours. The heating and cooling rate resulting from the hot plate was approximately 0.7±0.1 °C/min. Sample data from a thermocouple during the curing stage is shown in Figure 5-1.

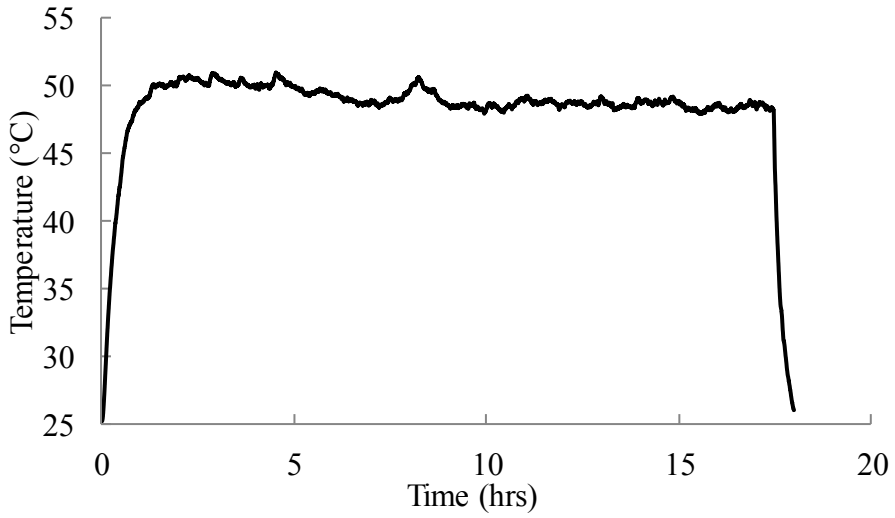

Figure 5-1: Sample thermocouple data during curing stage of flax/epoxy processing by resin infusion

5.2 Process model

The results from the composite processing were compared to the predictions of a 1-dimensional resin infusion process model. The development of the model followed by a comparison with the kinetics data from the unsaturated permeability experiments is presented below.

5.2.1 Model development

As discussed in Section 2.2.1, LCM processes such as resin infusion, are typically modelled by Darcy's law given by Eq. 1, given here in one-dimensional form for the longitudinal direction of flow:

$$u = -\frac{K}{\mu}\frac{\partial p}{\partial x} \tag{18}$$

The continuity for liquid composite moulding process, assuming the resin to be incompressible and neglecting saturation effects, is given by:

$$-\frac{\partial (hu)}{\partial x} = \frac{\partial h}{\partial t} \tag{19}$$

Combining Eq. 18 and Eq, 19 results in general governing 1-dimensional equation for the resin infusion process given by:

$$\frac{\partial}{\partial x}\left(\frac{Kh}{\mu}\frac{\partial p}{\partial x}\right) = \frac{\partial h}{\partial t} \tag{20}$$

As discussed in Section 2.2.1, this is same governing equation derived by other authors [83, 84, 86]. To simplify the solution of Eq. 20, a quasi-static assumption will be made (i.e. *h* has a chance to stabilize at every instant in time) which results in the final governing equation for the model in this thesis:

$$\frac{\partial}{\partial x}\left(\frac{Kh}{\mu}\frac{\partial p}{\partial x}\right) = 0 \tag{21}$$

Eq. 21 is the same governing equation derived by Hammami *et al* [84]. In the current thesis, the model differed in terms of the boundary conditions. Instead of neglecting capillary pressure at the flow front, the following boundary conditions were imposed:

- at x=0; p = p_{atm}
- at x= x_f (flow front); p = p_v - p_c

where p_{atm}, p_v and p_c are the atmospheric, vacuum and capillary pressure respectively. The last of these pressures is given by Eq.8 and depends on the preform porosity. However, since the porosity is constant at the flow front (as dictated by the wet compaction behaviour of the preform), the capillary pressure can be expressed as [103]:

$$p_c = \frac{F}{D}\cdot\frac{(1-\varphi_0)}{\varphi_0}\cdot\gamma_r\cdot\cos\theta \tag{22}$$

where φ_0 is the initial porosity of the preform prior to wetting as calculated from the empirical model for the wet compaction of the preform.

In the current thesis, Eq. 21 was solved using a finite difference scheme over the interval from x=0 to x=x_f. The number of nodes (N) was set to 10. Given that *K* and *h* are functions of the resin pressure, discretization of Eq. 21 yields:

$$-G(p_{i+1})p_{i+1} + (G(p_{i+1}) + G(p_i))p_i - G(p_i)p_{i-1} = 0 \qquad (23)$$

where,

$$G(p_k) = K(p_k)h(p_k) \qquad (24)$$

It is interesting to note that due to the quasi-static assumption, Eq. 23 does not depend on the viscosity of the test fluid. However, this equation simply solves for the pressure field for a given flow length. To determine the velocity at the flow front, Darcy's law was solved at the last two nodes of the discretized pressure field to determine the interstitial velocity (i.e. the velocity experienced by the fluid in the pores) given by:

$$v = -\frac{K}{\mu\phi}\frac{P_N - P_{N-1}}{dx} \qquad (25)$$

The new flow front position was then determined using a time step of 1s and the velocity at the flow front. The above discretization was implemented in a MatLAB® code in order to solve for the pressure distribution and flow front velocities for the cases discussed below.

5.2.2 Model validation

The predictions from the above model were first compared to the results from the infusion experiments conducted in Section 4.1.3. As in Section 4.1.3, the contact angle with the resin was determined from Eq. 8 using literature values for the surface free energies of a similar epoxy [52]. The viscosity in the model was set to the average for all of the experiments. The experimental curve was also taken to be the average from all trials (Figure 5-2). As can be seen in Figure 5-2, the model predictions were reasonably close to the observed flow front evolutions. It

should be noted however, that due to the high variability of the material, there was a relatively large range of error for the time to reach a given flow front position. Comparing the average flow front position, it can be seen that early on in the process, the model tended to over predict the flow front position while later on it tended to under predict this position. This suggests that fibre swelling was not significant for the studied scenario since swelling would have resulted in lower permeability later on in the process and consequently a slower flow front evolution. In any case, the effect of capillary pressure predicted by the model was slight, due to the low ranges of porosity for the studied fabric system in the given pressure range. However, capillary pressure could have been non-negligible (exceeding 10 kPa) if lower ranges of porosity had been achieved as demonstrated in Figure 5-3.

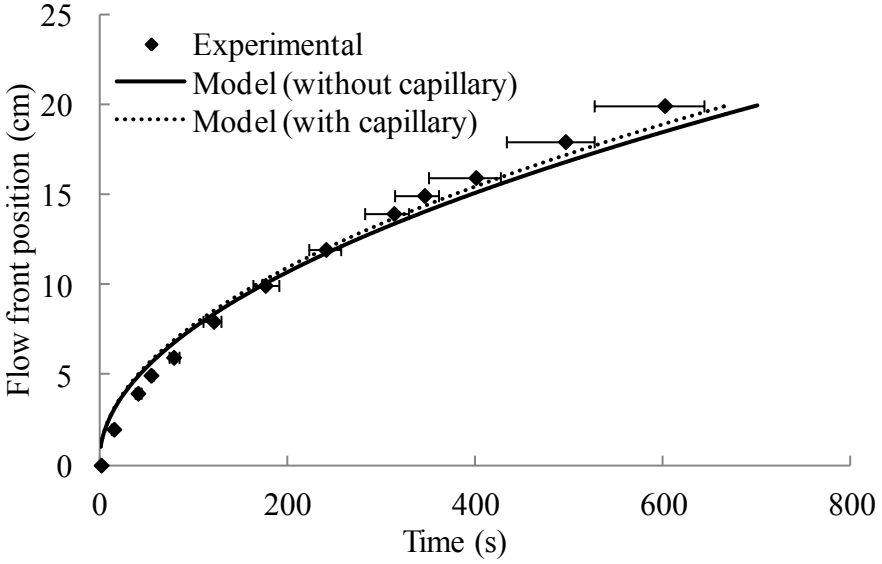

Figure 5-2: Comparison of model predictions and experimental results for flow front evolution of epoxy through untreated CL015 flax fabric (error bars represent maximum and minimum values)

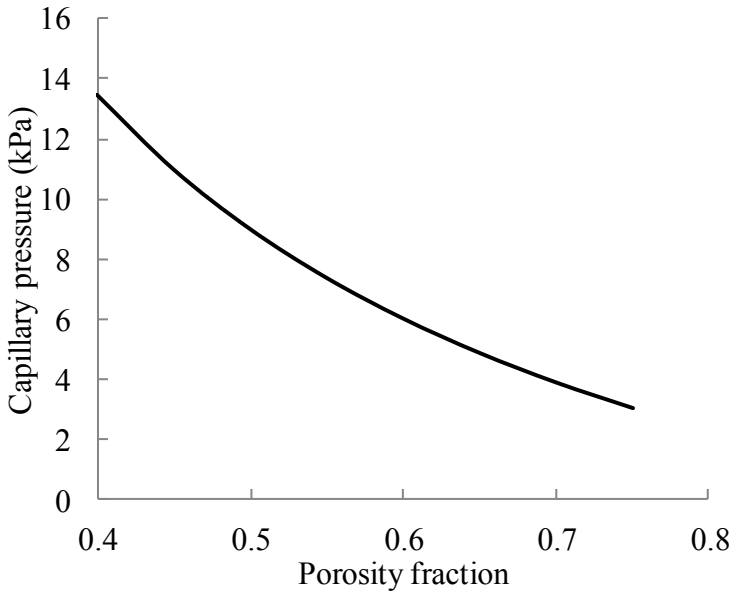

Figure 5-3: Capillary pressure versus fabric porosity as calculated from Eq. 4 for untreated fabric

Similar to the evolution of flow front, the pressure distribution during the infusion was found to vary slightly as a result of the capillary effects (Figure 5-4). It is interesting to note, that due to the coupled nature of the resin infusion process, the capillary pressure at the flow front boundary resulted in a change in thickness profile during the unsaturated regime.

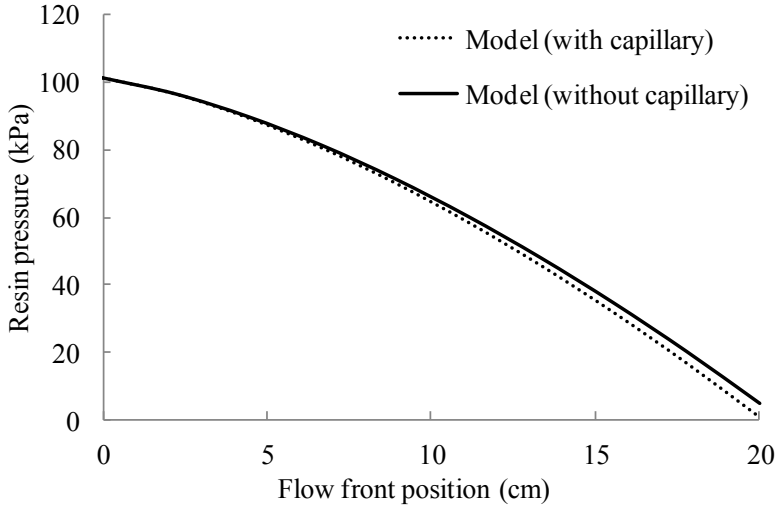

Figure 5-4: Predicted pressure distribution along CL015 flax fabric preform length during resin infusion for untreated fabric

Based on the measured surface free energy values reported in Section 3.5, the effect of fibre surface free energy on the flow front evolution was investigated (Figure 5-5). As expected, due to the high range of porosity for the fabric system investigated there was a negligible difference in flow kinetics for the various treatments.

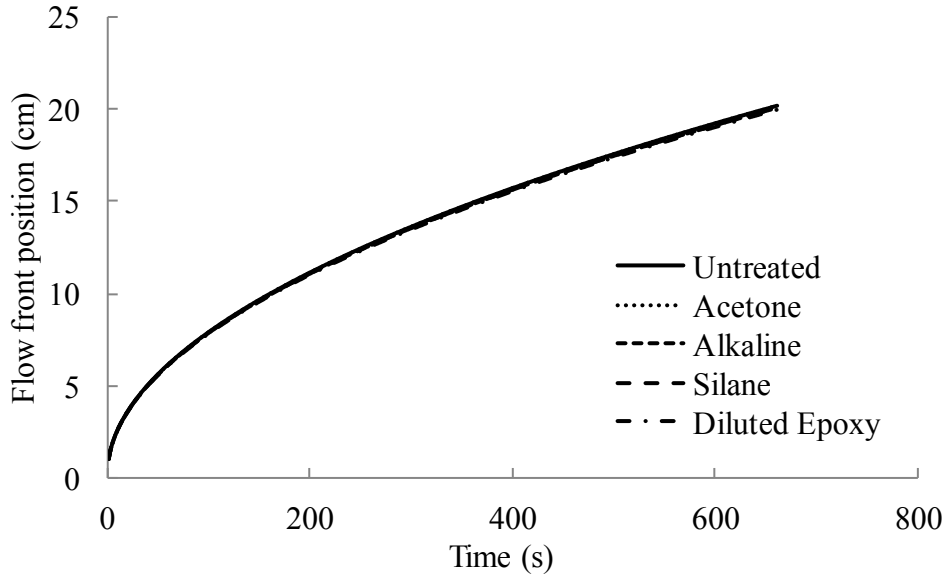

Figure 5-5: Model predictions for flow front evolution during resin infusion of treated flax fabrics

During the analysis, the wet unloading behaviour of the treated fabrics was assumed to be the same as the untreated fabrics. Therefore, the predictions in Figure 5-5 do not take into account other changes that result from the chemical treatments such as increases in fibrillation and consequently fabric porosity. The results from the unsaturated permeability measurements indicate that these factors are significant for some treatments (e.g. alkaline). In LCM processes such as RTM, where the cavity thickness is held constant, these changes may go unnoticed. However, due to the unique coupled flow and compaction behaviour of the resin infusion process, these treatments resulted in changes in the equivalent permeability as discussed in Section 4.1.3. Therefore, simply looking at the capillary pressure to understand changes in process kinetics does not

provide the complete story. To accurately model the effect of these changes, the differences in fibre and fabric morphology must be taken into account.

5.3 Mechanical characterization

As a last step after processing, the cured composites were subjected to a mechanical characterization. The following tests were carried out and the results are presented below; void analysis, flexural and Charpy impact.

5.3.1 Void analysis

In the current thesis, the percentage of voids in laminates was used as an indicator of the quality of the composite. Thus, in establishing the link between composite processing and the quality of the final parts, void analysis was essential. Void analysis was carried out by optical microscopy and image analysis due to the inappropriateness of the commonly used resin-burn off technique (ASTM D2734) for composites reinforced with cellulose-based fibres. A 5 cm long polished cross section from the center of each laminate was used for the analysis. Due to the limited field of view of the microscope, a minimum of 60 images were necessary for each sample which were then assembled in a freeware image editing software, ImageJ. Upon examination of the images, it was noted that the contrast of the voids with the rest of the composite was very low. To better distinguish them, they were highlighted manually and filled in with black pixels. The images were then converted to 8-bit greyscale and a threshold function was applied to isolate the filled in regions whose area was finally measured by the software. A sample cross-section and summary of the measured void contents are given in Figure 5-6 and Figure 5-7 respectively. Cross-sections of all tested samples are shown in Appendix E. The results confirmed that with increasing pressure at the outlet, the degassing effect was minimized and the overall void content tended to decrease.

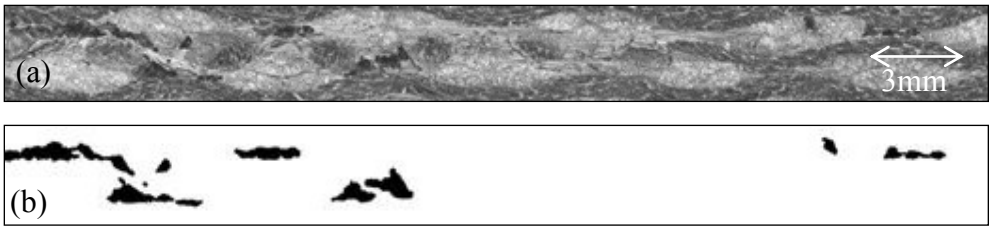

Figure 5-6: Example cross-section of untreated flax/epoxy for void analysis after 25 kPa post-fill vent pressure a) before thresholding and b) after thresholding

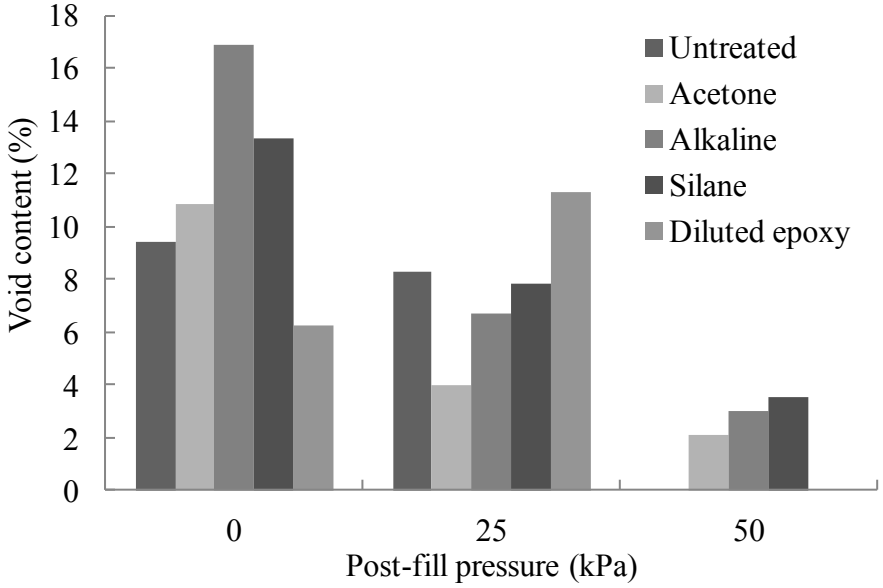

Figure 5-7: Void content versus post-fill pressure for flax CL015 fabric/epoxy composites; note that lower post-fill pressures resulted in degassing of resin and an increase in voids in the final laminates

5.3.2 Flexural behaviour

Flexural testing was carried out in accordance with ASTM D790 on an MTS Insight load testing machine with a 5 kN load cell. A sample area of 12.7 x 80 mm^2, span of 64mm and loading rate of 2 mm/min were selected. The results are summarized in Figure 5-8 and Figure 5-9.

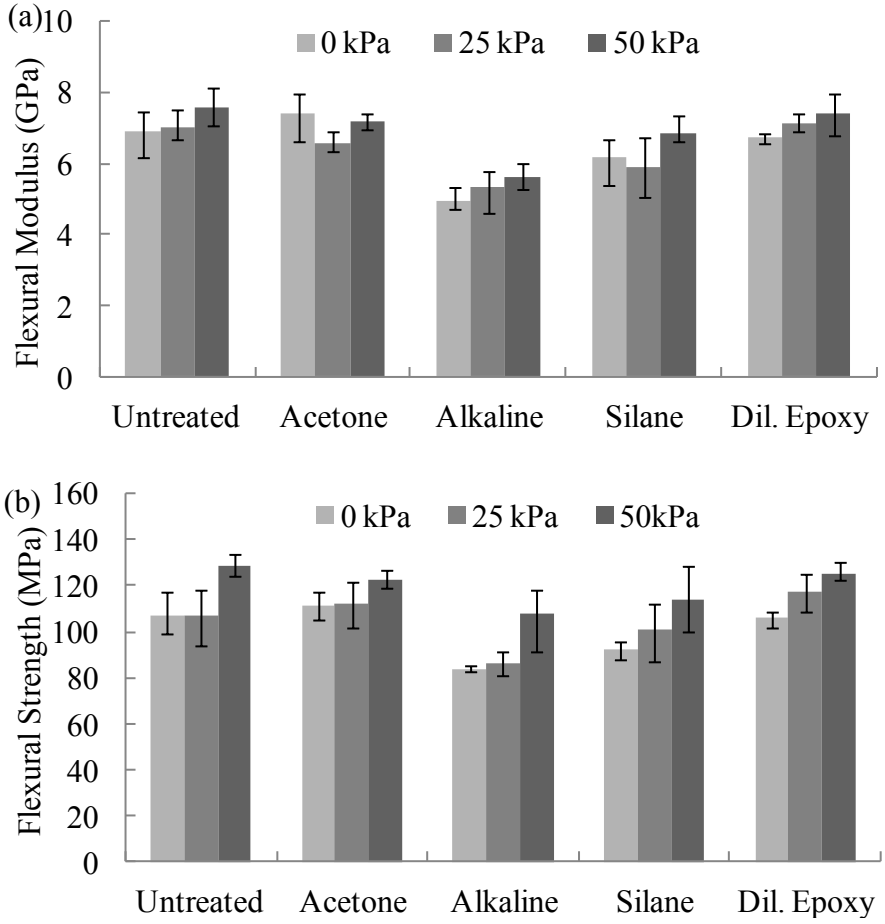

Figure 5-8: Flexural properties of flax/epoxy composites manufactured by resin infusion at different post-fill pressures using common chemical treatments: a) modulus and b) strength (error bars represent maximum and minimum values)

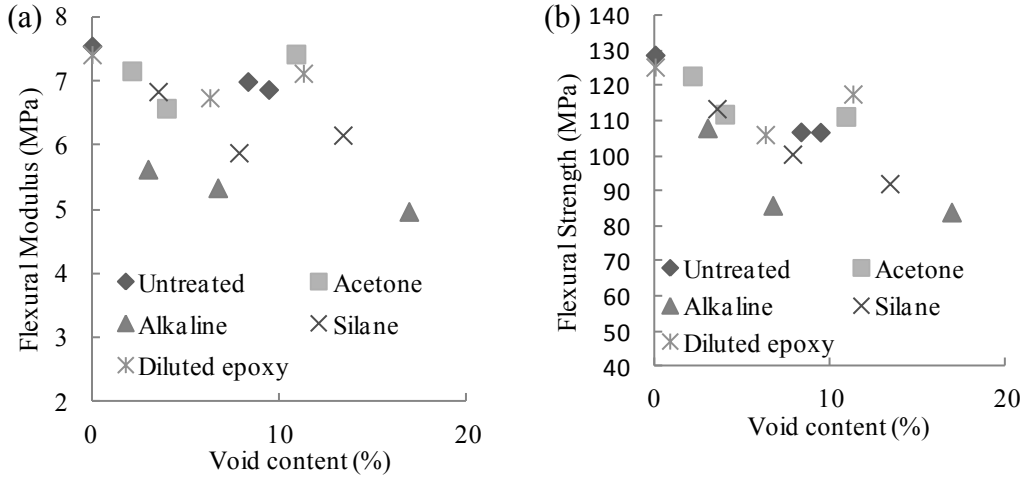

Figure 5-9: Flexural properties versus void content of flax/epoxy composites manufactured by resin infusion at different post-fill pressures using common chemical treatments: a) modulus and b) strength

Two key findings were revealed by the flexural testing. First, among the studied treatments, the untreated fabrics resulted in the best flexural properties (albeit marginally) as verified by ANOVA. On the other hand, the lowest properties were exhibited by the alkaline treatment, likely due to a lower fibre volume fraction. The second finding was that with increasing void content the flexural properties of the composites decreased. This is consistent with the findings of other studies for conventional composites [34, 135]. The samples that experienced the 50 kPa post-fill pressure showed the most pronounced increase in mechanical properties due to lower void content.

5.3.3 Charpy impact behaviour

Charpy impact testing was carried out in accordance with ISO 179 in an edgewise parallel configuration. A sample area of 12.7 x 80 mm^2 was selected with a span of 60 mm. The frictional loss induced by the setup was measured prior to the tests and taken into account. The results are shown in Figure 5-10.

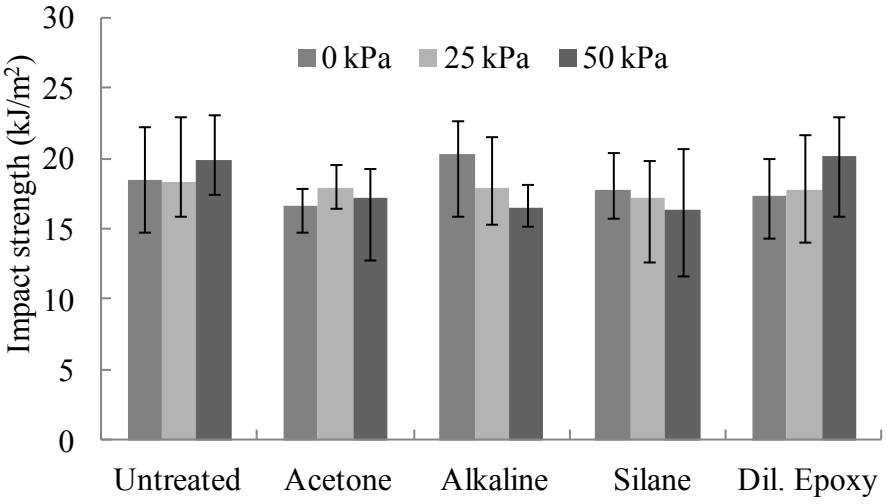

Figure 5-10: Charpy impact properties of flax/epoxy composites manufactured by resin infusion at different post-fill pressures using common chemical treatments (error bars represent maximum and minimum values)

Figure 5-10 suggests that there was no clear trend between the various treatments and the measured Charpy impact strengths. The same was indicated for the effect of voids on the Charpy impact properties. However, the large coefficient of

variance (~ 15%) indicates that a more suitable impact test configuration may be required for this type of material.

5.4 Summary

In summary, the current chapter addressed the processing and mechanical characterization of flax/epoxy composites manufactured by resin infusion. A 1-dimensional process model was developed and the model predictions were shown to be in reasonably good agreement with the experimental results for flow front evolution. The predicted difference in capillary pressure for the chemical treatments was shown to be small in the observed range of porosities. This suggested that for some of the chemical treatments (e.g. alkaline and diluted epoxy), changes in fibre surface morphology and fabric porosity played a much more significant role in terms of the kinetics of the resin infusion process. A mechanical characterization was finally presented and the studied chemical treatments were shown to not significantly change the flexural and Charpy impact properties. However, the properties obtained from the flexural test were shown to be highly void sensitive.

Chapter 6

Case studies

An important part of this thesis was dedicated to the application of the studied tools with the intent of improving the current state-of-the-art for this class of materials. As an attempt to improve the properties of this class of materials, two scenarios were investigated; incorporation of nanocellulose (NC) into the resin infusion process and the autoclave processing of flax/epoxy prepregs. The latter case study was selected since prepregs are generally used as a benchmark for comparison with composites produced by processes such as resin infusion.

6.1 Multi-scale composites by resin infusion

In parallel with the development of flax-based composites, there have been significant advancements in the understanding of nano-modified resin systems. This includes use of bio-based nano-modifiers such as NC which is promising due to its abundance, low cost and excellent mechanical properties [152]. Advancement in these two areas raises the possibility of producing novel multi-scale biocomposites which could mimic the hierarchical structure of highly efficient materials found in nature. Some studies have already shown noticeable

increases in mechanical properties by making use of hierarchical structures in biocomposites using conventional manufacturing processes [153]. However, it is clear that these conventional composite manufacturing processes fall short in producing biocomposites of similar complexity to those found in nature and therefore must be adapted.

As a step in this direction, the first case study considers the resin infusion process as a base in producing multi-scale biocomposites from flax and nanocellulose. The aim was to produce a hierarchical biocomposite with markedly improved impact and interlaminar shear properties over the single-scale composite. This case study begins with a description of the fabric treatment process followed by the manufacturing of multi-scale plates by the resin infusion process. The results from void analysis, drop-weight impact testing and short beam testing are then presented.

6.1.1 Fabric treatment

Chemical treatment of the fabrics was carried out in order to improve both the compatibility with the selected resin system as well as to increase the affinity for the NC. The same silane treatment described in Section 3.3.2 was applied to the fabrics in the first case study. The only difference was that, for one of the methods, the NC was incorporated directly in the silane solution bath to explore the possibility of 'grafting' the NC directly on the flax fibres. The NC used in this study was synthesized at the University of Toronto as described by Alemdar and Sain [134].

6.1.2 Laminate manufacturing

For the laminate manufacturing, the same tool plate setup that was used during the unsaturated permeability measurements was employed. However, in this case study a conventional bagging arrangement was selected (Figure 6-1). A distribution media (AirTech® Resinflow 60) was incorporated in the layup that was cut two centimeters short of the preform end to avoid race tracking. The

distribution media was incorporated to encourage through-thickness flow of the resin and consequently better distribution of the NC in the laminate.

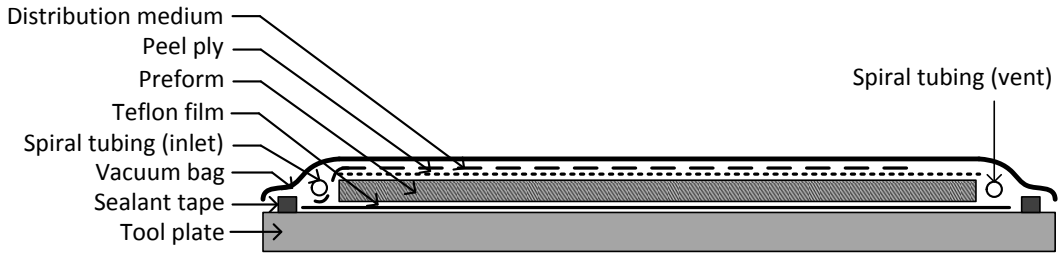

Figure 6-1: Bagging arrangement for resin infusion laminate manufacturing

Two methods were developed that incorporated the NC into the multi-scale composite. The first involved grafting the NC directly onto the flax fibre surface during the treatment process (labelled MS (Grafted) in Table 10). This method involved consolidating the fibre bed in a dry state during the resin infusion pre-filling stage. This method was accomplished by adding an aqueous NC solution to the silane solution during the treatment process. . The mass ratio of NC to flax fibre was selected as 10%. To better distribute the NC in the silane bath, spacers made up of glass fibre screen were placed in between the flax fabrics during the treatment process. The silane bath was then allowed to evaporate at room temperature until the fabrics were dry (about 48 hours). Following this treatment process, it was noted that the NC tended to agglomerate on the surface of the fabrics and agglomerations could be observed on the cured laminates (Figure 6-2).

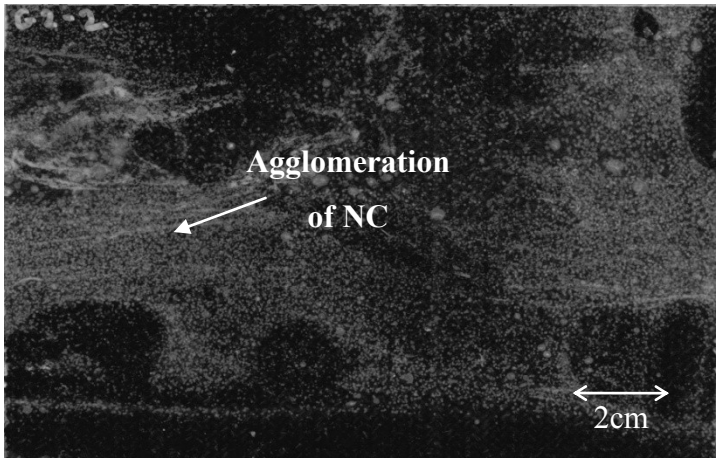

Figure 6-2: Scanned surface of cured laminate using grafting technique; note agglomerations of nanocellulose are clearly visible

The second method involved modifying the standard resin infusion procedure so that the aqueous NC solution could be incorporated directly in the ply stack by wet layup prior to bagging (labelled MS (Wet-layup) in Table 10). The stack was then heated to 80 °C for one hour to evaporate the bulk of the water. During the pre-filling stage some moisture remained which resulted in softening and lubrication during the compaction of the preform. Following this procedure, the consumables were placed and a vacuum hold was applied for 24 hours in order to eliminate the residual moisture. The mass ratio of NC to flax fibre for this method was selected as 7%. This ratio was lower than for the grafting method as it was the maximum amount of aqueous NC solution that could be feasibly spread on the dry fabrics.

Following the above preparations, the epoxy resin (Araldite LY1564/Aradur 3486) was mixed by hand with the hardener for 5 minutes. This was followed by a 45 min debulk at 4.5 kPa of pressure. The resin was then infused with a fill and post-fill outlet vacuum pressure of 50 kPa as controlled by a vacuum regulator. This high outlet pressure was selected based on the results of Section 5.3.1 to avoid degassing of the resin during processing. The inlet was clamped at the point the resin reached the end of the preform. The tool plate heating was commenced after 15 minutes elapsed during the post-fill stage. During the filling stage, the flow front position squared versus time was approximately linear up until the point where the distribution media ended (Figure 6-3). This was due to the ability of the distribution media to decrease the filling time during the resin infusion process.

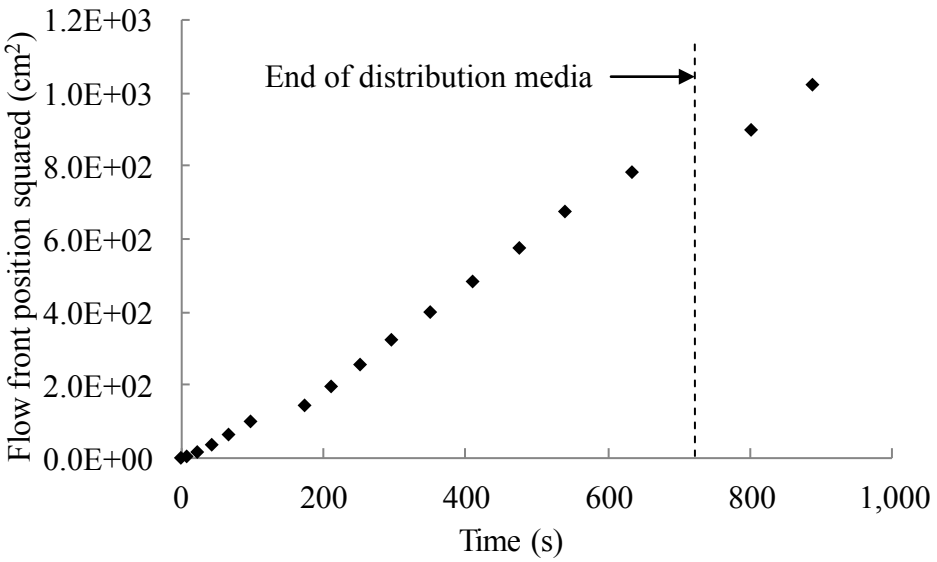

Figure 6-3: Flow front position squared versus time for single-scale composite manufactured from initially wet preform: note deviation from linearity due to end of distribution media

To investigate the influence of the NC on mechanical properties, three panels measuring 150 x 330 mm^2 were manufactured by each of the above two methods. An additional six panels that did not incorporate NC were also manufactured for comparison. For three of these panels, the preforms were saturated with tap water and subjected to the same 80 °C one hour drying and 24-hour debulk as the NC wet-layup technique (labelled SS (Wet) in Table 10). This was done to achieve the same lubricating and softening effect of the water so that a better comparison could be made with the multi-scale composite manufactured by the wet-layup technique where an aqueous NC solution was spread on the fabrics. The other three panels were compacted in a dry state (labelled SS (Dry) in Table 10).

Table 10: Test matrix for laminate manufacturing for nanocellulose experiments

Panel	m_{NC}/m_{flax} (%)*	Method
SS(Dry)	0	Dry flax preform
MS(Grafted)	10	Grafted NC onto flax preform
SS(Wet)	0	Wet flax preform
MS(Wet-layup)	7	Wet NC layup onto flax preform

* mass ratio of NC to flax fibre

During the infiltration of the panels, there were clear differences in the flow behaviour for the different preparation methods. Most striking was the difference in infusion time. For the SS (Wet) composite, the infusion took approximately 15 minutes whereas for the MS (Wet-Layup) technique the infusion time took about 20 minutes for approximately the same porosity and ambient temperature. In addition, the flow front pattern was much more erratic for the processes that incorporated NC (Figure 6-4). For the MS (Grafted) method, there was not even a clear flow front and large pockets of dry spots remained unfilled when the resin reached the end of the preform. These areas gradually filled radially until the preform was completely saturated.

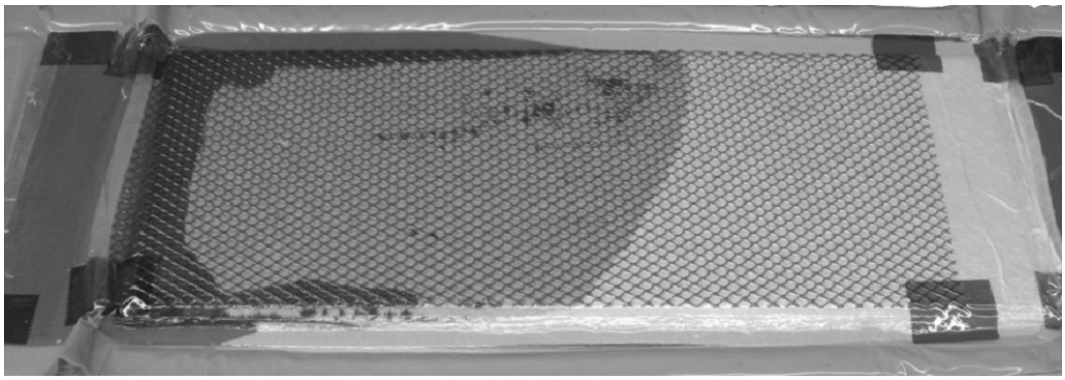

Figure 6-4: Infusion of flax fabric after MS (Wet-layup) preparation; note the rapidly advancing flow front in the distribution medium indicating low in-plane and through-thickness permeability of the modified fabric

In addition to differences during processing the final laminates showed distinct differences. Most apparent was variations in thickness and consequently fibre volume fraction (Figure 6-5).

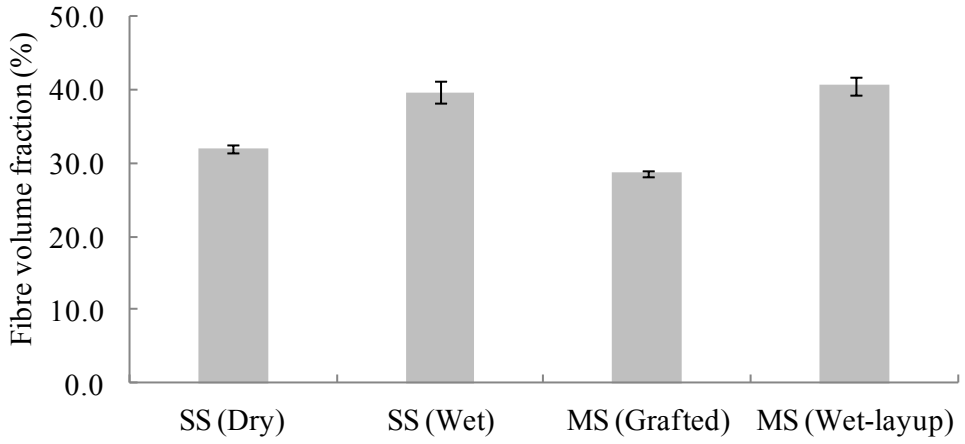

Figure 6-5: Fibre volume fraction for single- and multi-scale nanocellulose, flax and epoxy composites manufactured by the resin infusion process (error bars represent maximum and minimum values)

It is evident from Figure 6-5 that the processes that begun with wetting of the preform with water reached significantly higher fibre volume fractions than those that were dry upon initial compaction for the same consolidation pressure. The single- and multi-scale composite made from an initially wet preform reached fibre volume fractions of 40.6±0.8 and 39.7±1.1% respectively. In contrast, the single- and multi-scale composite manufactured without initially wetting the preform reached fibre volume fractions of merely 31.9±0.4 and 28.7±0.4% respectively. The reason for the lower fibre volume fraction achieved by the MS (Grafted) technique compared to the SS (Dry) technique was likely due to the agglomeration of NC at the fabric surface and the resultant resistance to yarn nesting during compaction.

For the purposes of comparing mechanical properties, the SS (Dry) properties were used as reference for the MS (Grafted) composites and the SS (Wet) case was used as reference for the MS (Wet-layup) composites due to the similarity of fibre volume fraction.

6.1.3 Mechanical characterization

Subsequent to the laminate manufacturing, they were subjected to a mechanical characterization. Nano-modifiers such as NC can improve the interlaminar

properties since they provide reinforcement in a region of the composite which would otherwise be devoid of fibres [153-156]. For this reason, the following properties were investigated; void content, interlaminar strength and drop-weight impact resistance.

6.1.3.1 Void analysis

The void analysis was carried out by the same procedure as that described in Section 5.3.1. Samples with a length of 2 cm were cut with a tile saw 1 cm from the outlet where the highest void content was thought to occur due to the low resin pressures that occur near the outlet. The results are summarized in Figure 6-6. The sample cross-sections are given in Appendix E.

	Sample cross-section	Void percent
SS (Dry)		0.7±0.6
SS (Wet)	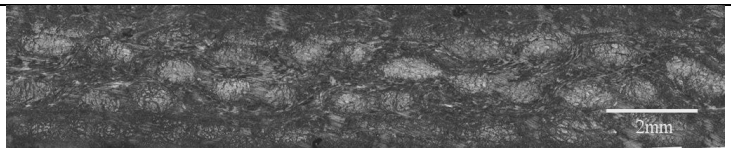	0.3±0.3
MS (Grafted)	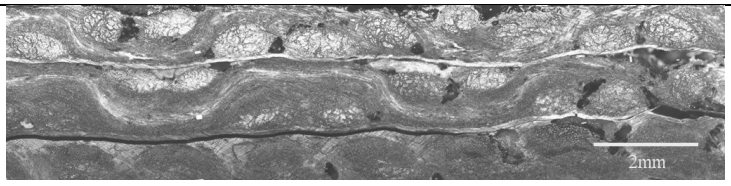	11.3±2.7
MS (Wet-layup)	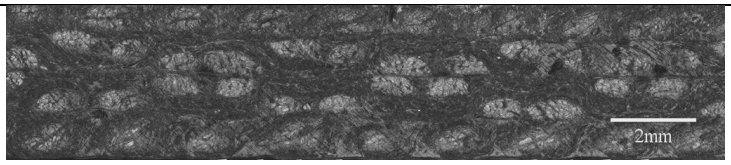	1.0±0.5

Figure 6-6: Cross-sections of single- and multi-scale composites consisting of flax, nanocellulose and epoxy manufactured by resin infusion (± standard deviation)

The microscopy results provided valuable insight about the consequences of the two methods explored to incorporate the NC. Most obvious was the difference in

overall void content. The grafting technique resulted in significantly higher void content. As can be seen in Figure 6-6, the voids for this technique were both large inter-yarn voids and smaller elongated inter-ply voids. The latter void morphology was deemed most critical since the NC was primarily intended to improve interlaminar properties. It should be noted that, during the void analysis, microscale voids were neglected. Regions of micro-porosity were likely contained within the yarns and fibres themselves. However, the primary goal of the void analysis was to investigate the morphology of the interlaminar regions.

The multi-scale composites produced by the wet-layup technique, showed much more reasonable void contents as well as a better fibre volume fraction as shown in Figure 6-5. Thus, the multi-scale composites produced by this technique were expected to result in superior mechanical properties compared to the grafted technique simply based on the quality of the composites.

6.1.3.2 Interlaminar strength

One of the most often studied properties that is known to be void sensitive is interlaminar shear strength [34, 157-160]. Interlaminar shear strength (ILSS) was obtained by the short beam test carried out in accordance with ASTM D2344 on a MTS Insight load testing machine with a 5kN load cell. Although this is a controversial method to obtain ILSS (due to the complex stress state involved) it was deemed appropriate for comparative purposes. A loading rate of 0.5 mm/min was applied and the span to depth ratio was set to 4. The sample geometries are given in Table 11. The samples were cut on a diamond tile saw and the edges were sanded using 240 grit sand paper.

Table 11: Measured sample geometries for short beam strength specimens (± standard deviation)

Samples	Thickness (mm)	Width (mm)	Length (mm)
SS (Dry)	4.51±0.06	8.79±0.28	28.5±0.1
MS (Grafted)	5.01±0.07	9.99±0.11	30.5±0.2
SS (Wet)	3.54±0.07	7.38±0.32	22.1±0.1
MS (Wet-layup)	3.62±0.1	8.28±0.10	22.9±0.1

This configuration resulted in a mode of failure of interlaminar shear for both systems as observed under a microscope. The interlaminar shear strength was calculated from:

$$ILSS = 0.75 \cdot \frac{P}{h \cdot w} \qquad (26)$$

where P is the maximum observed load during the test, h is the specimen thickness at centre span and w is the specimen width at centre span. The calculated ILSS values are summarized in Figure 6-7.

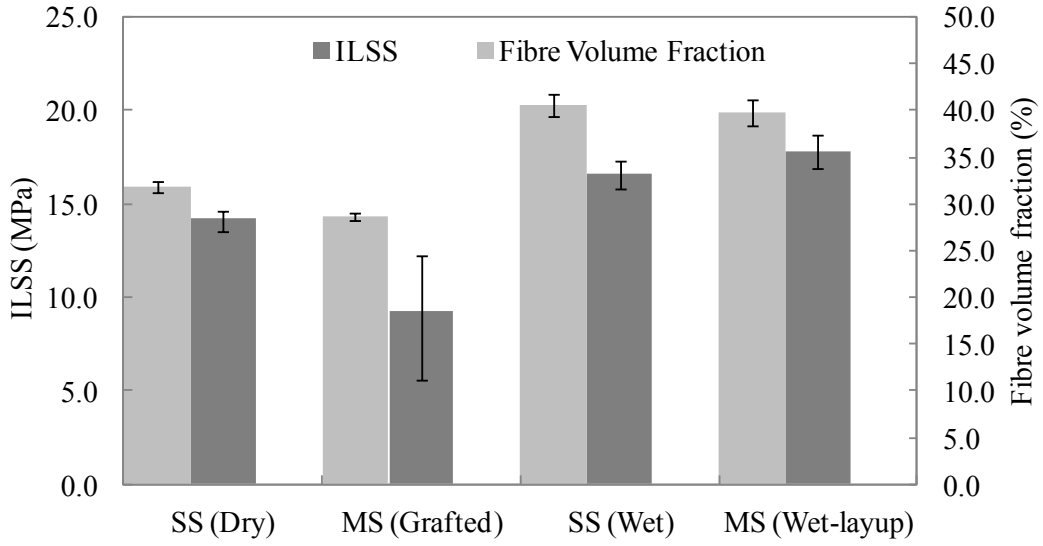

Figure 6-7: Interlaminar shear strength for single- and multi-scale composite manufactured by resin infusion; incorporation of nanocellulose fibres did not lead to an increase in interlaminar shear strength (error bars represent maximum and minimum values)

The results indicated that the incorporation of the NC did not lead to an increase in interlaminar shear strength. In the case of the grafted technique, it led to a 35% decrease in ILSS. However, there was also a 10% decrease in fibre volume fraction so part of this decrease was likely due to this fact. Nonetheless, the microscopy results indicated a large presence of interlaminar voids for this processing technique which is in agreement with this large decrease in interlaminar sterngth. Thus, the processing method led directly to voids and consequently a reduction in interlaminar properties. Therefore, even if the NC

fibre led to an increase in ILSS, the importance of proper incorporation of these nano-modifiers to produce high quality composite parts cannot be underestimated. For the case of the single- and multi-scale cases that began with a wet preform, there was not a significant difference in ILSS.

6.1.3.3 Drop-weight impact

As discussed in Chapter 1, automotive applications have been sighted as a major market for bio-based composites due to their low cost and relatively good mechanical properties. Consequently, impact properties are of importance. The influence of NC on the impact properties was investigated in accordance with ASTM 7136. Five samples were tested with a ply sequence of $[(45/-45)/(0/90)]_S$ and dimensions of 4.5 x 100 x 150 mm^3. The same sample cutting procedure was used as for the short beam samples presented in the preceding section. The impact energy was selected as 7J based on initial trials with spare specimens. This corresponded to a height of 11.6cm for the 1.6cm diameter hemispherical impacting head. The total weight of the impact head and test frame crosshead was 6.143 kg. The velocity at the point of impact was measured with an Instron optical gate and the force was monitored by a 22kN-capacity Instron® force transducer. The specimens were installed in the fixture outlined in ASTM D7136 and were impacted on the tool side. Representative force histories for the various samples are presented in Figure 6-8a. The velocity, displacement and energy histories were then determined as outlined in ASTM D7136 (based on the integration of the force history) and are presented in Figure 6-8. A complete set of the force history data for all specimens is provided in Appendix F.

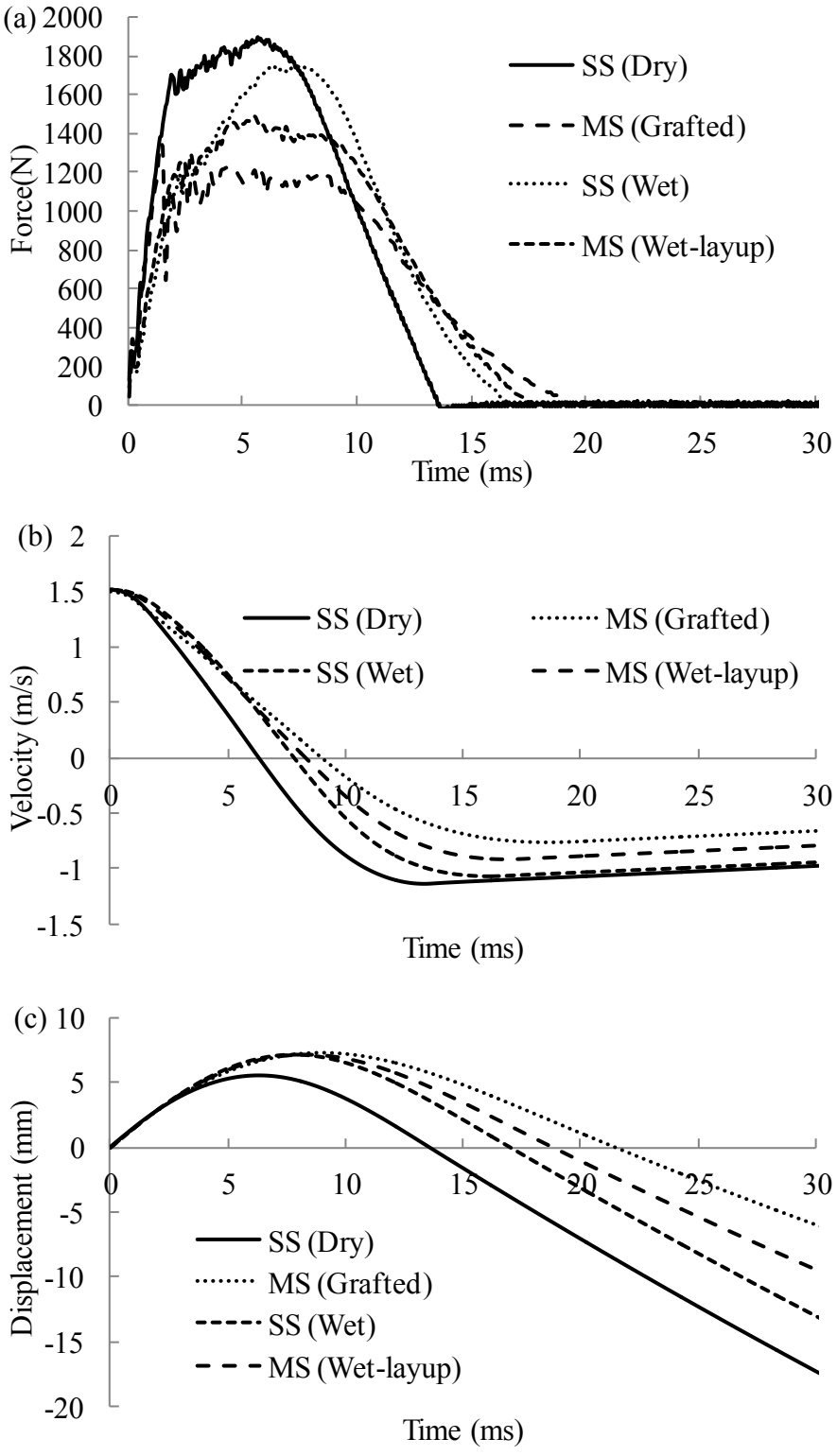
(a)
Force(N)
Time (ms)
SS (Dry)
MS (Grafted)
SS (Wet)
MS (Wet-layup)
(b)
Velocity (m/s)
Time (ms)
SS (Dry)
MS (Grafted)
SS (Wet)
MS (Wet-layup)
(c)
Displacement (mm)
Time (ms)
SS (Dry)
MS (Grafted)
SS (Wet)
MS (Wet-layup)

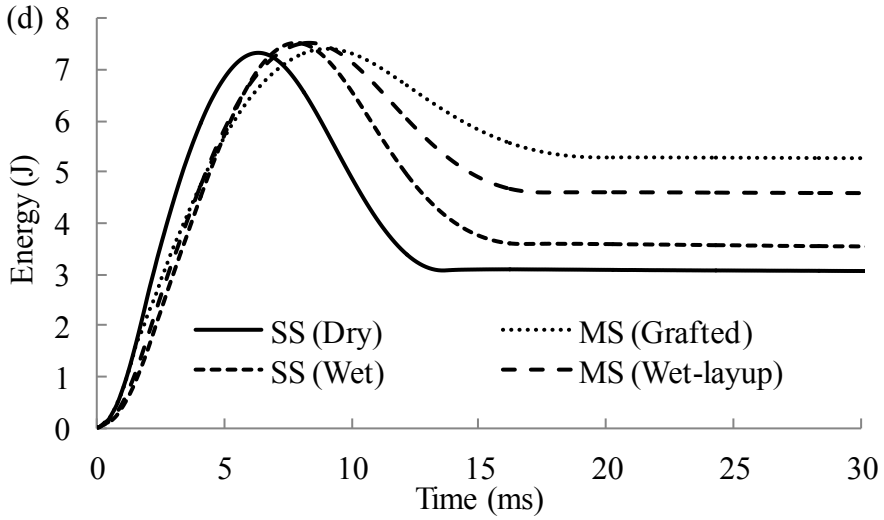

Figure 6-8: Representative histories for drop-weight impact testing for single- and multi-scale composites manufactured from flax, epoxy and nanocellulose by resin infusion (a) force, (b) velocity, (c) displacement and (d) energy

Figure 6-8 provides much insight into the extent of damage induced in the single- and multi-scale composite manufactured by the various techniques. The force histories revealed that the single-scale composites were able to carry more load before experiencing damage in comparison to the multi-scale composites. The SS (Dry) and SS (Wet) laminates reached maximum loads of 1932±53N and 1761±35N respectively. The reason for the higher load for the dry case was likely due to its larger thickness. In contrast, the MS (Grafted) and MS (Wet-layup) reached loads of only 1450±145N and 1507±64N. The high amount of error for the MS (Grafted) technique was likely due to the non-uniformity of NC as illustrated in Figure 6-2.

The velocity data indicated that more elastic recovery occurred for the single-scale composites and consequently a higher velocity was achieved on the rebound of the impacting head. The maximum velocity after the rebound was over 30% higher for the SS (Dry) case compared to the MS (Grafted) case. Similarly, the maximum velocity was over 10% higher for the SS (Wet) case compared to the MS (Wet-layup) case. This higher rebound velocity led to a greater increase in displacement of the impacting head as indicated in Figure 6-8c.

Finally, the energy absorption history indicated a lower amount of recovered energy (i.e. the difference between the peak and final energy) for the multi-scale composites. As can be seen in Figure 6-8d, after the impact event the recovered energy was almost 50% higher for the SS (Dry) case compared to the MS (Grafted) case. Similarly, a decrease of 20% was recorded for the MS (Wet-layup) case compared to the SS (Wet) case. This decrease in energy recovery was presumably due to a greater dissipation of energy in damaging the multi-scale composites. These results imply that between the two methods explored for incorporating the NC, the wet-layup technique led to superior impact properties.

Following the testing of the samples, the extent of damage was evaluated by measuring the impact dent depth and the maximum damage diameter (Figure 6-9).

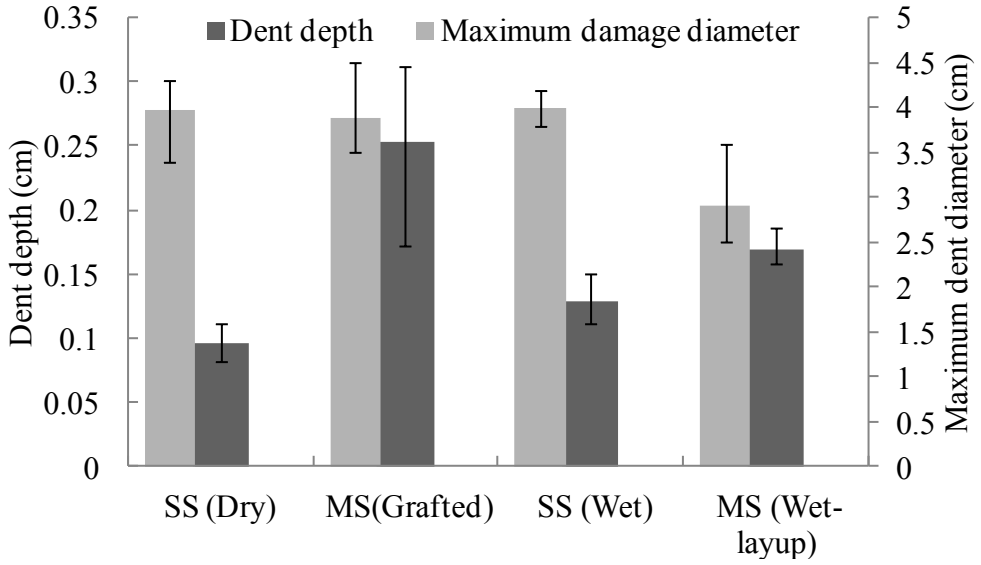

Figure 6-9: Dent depth and maximum dent diameters of single-scale and multi-scale flax, nanocellulose and epoxy composites after being impacted by 1.6cm diameter hemispherical striker head with 7J of impact energy (error bars represent maximum and minimum values)

It can be seen from Figure 6-9, that the extent of the damage was generally greater in the case of the multi-scale composites as was suggested by Figure 6-8. For roughly the same fibre volume fraction, the depth of the dent was over twice as large for the multi-scale composite manufactured by the grafting technique. This was likely due to the significant amount of interlaminar voids as observed in

Section 6.1.3.1. Similarly, a distinct increase in dent depth was noted for the multi-scale composite manufactured by the wet-layup method suggesting that the addition of the NC did not contribute to an improvement in interlaminar properties. Representative damage areas for all types of samples are shown in Figure 6-10.

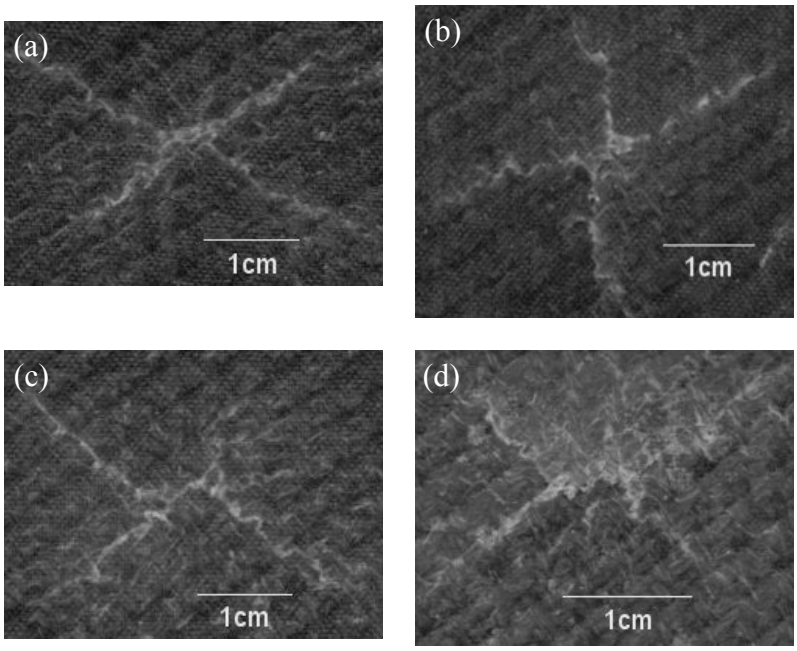

Figure 6-10: Representative bag-side damage areas after drop-weight impact testing for single- and multi-scale composites manufactured from flax, nanocellulose and epoxy by resin infusion; (a) SS (Dry), (b) MS (Grafted), (c) SS (Wet) and (d) MS (Wet-layup)

In terms of damage modes, cracks were observed on the bag-side of all samples. However, in the case of the multi-scale composite, there were dramatic signs of delamination as well (especially in the case of those manufactured by the grafting technique). This further suggests that the NC incorporated by both methods led to a decrease in interlaminar properties.

6.2 Flax/epoxy prepregs

The second case study pertained to the understanding of the nature and processing requirements of prepregs based on flax/epoxy. Although, this case study did not directly relate to the resin infusion process, prepregs represent the upper end in performance for composites and understanding their processing can increase the

state-of-the-art for flax-based composites. Up to date, there have only been a few studies on the processing and mechanical properties of flax/epoxy prepreg systems. Van De Weyenberg *et al* investigated a drum-wound prepreg and determined that pre-treating the fibres in an NaOH solution improved the mechanical properties of the composite [20]. Phillips *et al* made use of unidirectional flax/epoxy hot melt prepregs in a balsa core sandwich structure to achieve similar bending properties to wood species commonly used in the top plates of string musical instruments [161]. In a study by Baets *et al* on flax yarn twist angle, it was shown that an automated prepregger allows for the use of untwisted yarns that make full use of the mechanical properties of flax fibres [66].

Although the above studies have shown the potential of these materials, little is known on the relationships between uncured prepreg properties, processing parameters and part quality. The current case study aimed to use the tools and methodology proposed in this thesis to improve the understanding and current state-of-the-art for the processing of this class of prepregs. In achieving this, the results from thermal gravimetric analysis and compaction experiments on two uncured prepreg systems will first be presented. This is followed by a description of the manufacturing of cured laminates at autoclave pressures of 1, 3 and 5 bars. Finally, results from tensile, interlaminar shear and moisture absorption tests are presented and some insight is given into how this class of prepreg systems can be improved.

6.2.1 Materials

The two fabrics described in Section 3.1 were used in two hot-melt flax prepregs (denoted BL200 and BL550 for the CL001 and CL015 fabrics respectively). The prepregs were kindly supplied by Lineo NV. Both systems employed the same epoxy resin system (Huntsman LY5150) and the fabrics were treated by a patented sizing (Patent No. US8080288). The resin mass fraction, ε_r, for the BL200 and BL550 systems were 52.1±1.8% and 46.8±2.0% respectively as determined from:

$$\varepsilon_r = 1 - \frac{\alpha_d}{\alpha_p \cdot \varepsilon_m} \qquad (27)$$

where α_p is the areal weight of the supplied prepreg, α_d is the dry areal weight of the fabrics (as described in Section 3.1) and ε_m is the fraction of the prepreg that does not contain moisture as determined by thermal gravimetric analysis (TGA) as described below.

6.2.2 Uncured prepreg characterization

In order to better understand the behaviour of the prepregs during processing, the compaction response of the reinforcement textiles and moisture content of the prepregs was measured. The experimental methods used to obtain this information are described in the subsequent sections.

6.2.2.1 Thermal gravimetric analysis

It is generally accepted that the diffusion of moisture and volatiles as well as air entrapment are dominant void formation mechanisms in the curing of prepregs [162]. The moisture content of prepregs can be a critical variable in the formation of voids during curing [35]. Thermal gravimetric analysis (TGA) was carried out on a TA Q500 in order to obtain the overall moisture content of the supplied materials. A ramp cycle was run with 5°C/min up to 100 °C followed by 10 °C/min up to 500°C. Nitrogen was selected as a purge gas. Typical results in the range of interest (below 150°C) for the supplied prepregs and neat resin are plotted in Figure 6-11.

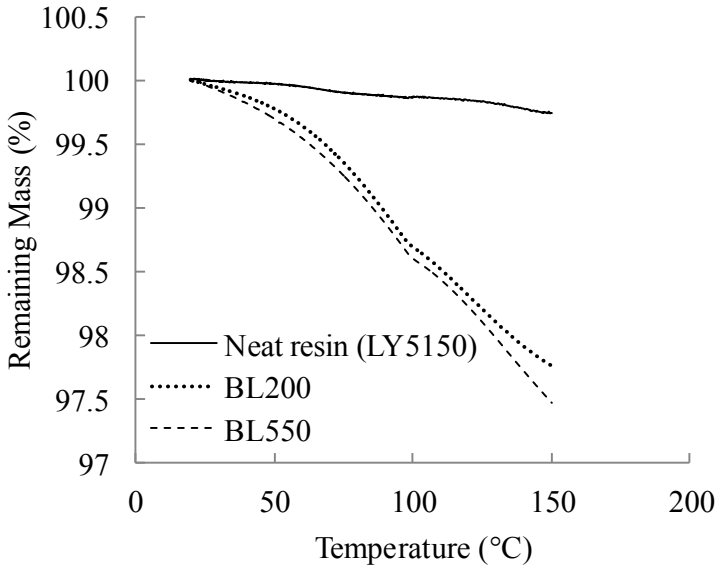

Figure 6-11: Typical mass loss curves obtained by thermal gravimetric analysis for BL200 prepreg, BL550 prepreg and LY5150 epoxy

The results indicated a decrease in mass of approximately 2.5% at 150 °C for both prepreg systems. The neat resin system showed a very minor mass loss of about 0.25% for the same temperature. This suggests that the majority of the weight loss in the prepreg was due to the flax fibre which likely lost moisture.

To better determine the exact moisture content, the results were compared with that obtained by drying 10 x 10 cm^2 sections of the prepregs in a desiccant chamber. The mass loss measured by this method corresponded to a temperature of 146±2 °C for the given TGA ramp cycle. Taking this as the calibration temperature, the constituent moisture contents were determined to be 4.33±0.06% and 0.263±0.004% for the fibre and resin respectively for the BL200 system. For the BL500 system, these values were similar (4.16±0.17% and 0.25±0.21 respectively).

Although the above moisture percentages may not seem significant, it has been shown previously that much lower moisture contents can lead to significant void percentages due to the relatively low molecular weight of water [35]. Therefore, it was expected that without sufficient autoclave pressure the diffusion of

moisture would likely be a major source of voids in this type of composite. This is a clear issue that needs to be addressed in future studies, especially with the growing trend of vacuum-bag only cure where the high consolidation pressures provided by the autoclave are not available.

6.2.2.2 Compaction

Along with the moisture content of the prepregs, the compaction behaviour of the fibre bed also plays a key role in the formation of voids. Not only does it define the required fibre/resin mass ratio to avoid resin starvation but it also affects the resin pressure, which is known to be an important parameter in diffusion-controlled void growth due to moisture and air entrapment [35].

To understand the behaviour of a fibre bed during processing, the actual processing conditions must be simulated as closely as possible due to high dependency of compaction behaviour on factors such as strain rate, lubrication and number of layers [105]. The test fixture described in Section 4.2.1 was employed for this portion of the case study. Layers of the sized fabrics were soaked in silicone oil for five minutes prior to testing to simulate the lubrication effect of the epoxy. The same number of layers was selected as the laminates manufactured in the autoclave experiments in Section 6.2.3 (3 and 6 for the BL550 and BL200 respectively). Furthermore, the tests were carried out at 130°C to eliminate any discrepancies due to temperature dependence.

The test consisted of five sequential 0.5 mm/min ramps and holds at 1, 3, 5, 7 and 9 bars. At the crosshead positions corresponding to these pressures, the system was held for 15 minutes which allowed the test fluid to flow and the fibre bed to relax sufficiently. The compliance of the test fixture was measured prior to testing and taken into account by linear interpolation. Fibre volume fraction was calculated from Eq. 16. However, instead of using the areal weight of the fabrics, the samples were weighed and the mass of fibre was taken to be:

$$m_f = m_s \cdot \varepsilon_m \cdot \varepsilon_s \quad (28)$$

where m_f, m_s, ε_m and ε_s are the dry fibre mass, sample mass, moisture weight fraction and sizing weight fraction respectively. The moisture weight fraction was taken to be that which was measured at ambient conditions by TGA as described by the procedure discussed in Section 6.2.2.1. The volume of fibre was then determined using the density determined in Section 3.4. For each fabric type, five samples were tested. Representative compaction curves are given in Figure 6-12.

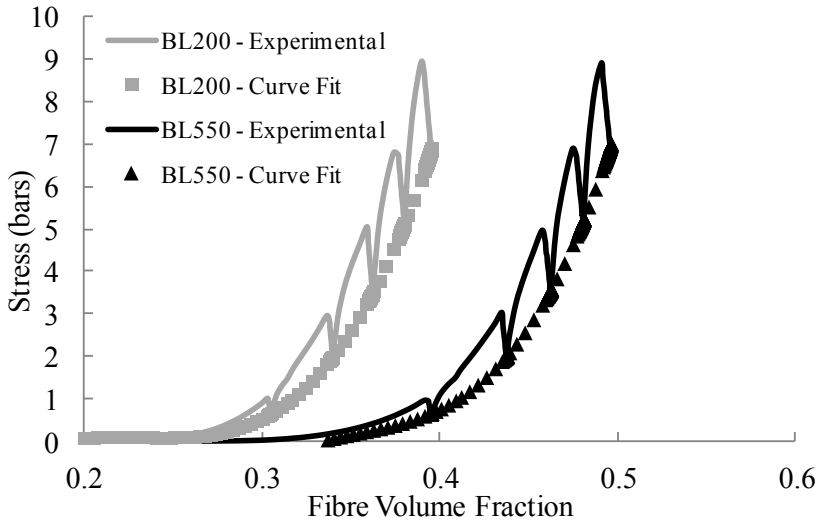

Figure 6-12: Representative compaction curves for 2x2 twill weave fabrics used in BL200 and BL550 flax/epoxy prepregs with holds applied at 1, 3, 5, 7 and 9 bars (3rd order polynomial curve fit represents relaxed fibre bed)

The resulting compaction curves provide much information including the minimum amount of resin required to minimize the void content for a given pressure. Based on the measured resin mass percentages (from Section 6.2.1) and using a constant fibre and resin density of 1.51 g/cm^3 and 1.22 g/cm^2 respectively, the minimum required pressure to achieve a void-free part for the BL550 system was determined to be 4.7±1.1 bars. For the BL200 system, the required pressure was beyond the capacity of the installed load cell (5kN) and the autoclave (8 bars).

The above calculation assumes a best case scenario whereby the fibre bed is able to relax fully and achieve a maximum volume fraction for a given pressure. If

this relaxation process is inhibited for reasons such as resin gelation, the actual void content due to resin starvation would likely be higher. Furthermore, the calculation assumes that the difference in fibre bed load history between the experiment and a typical processing cycle, results in a negligible difference in the final state of the relaxed fibre bed.

6.2.3 Cured prepreg characterization

The above characterization of the uncured prepregs provided valuable insight into the likely void sources during the processing of the studied flax/epoxy prepreg systems. To confirm these hypotheses and to determine mechanical properties, laminates were manufactured in an autoclave at varying pressures and subjected to void analysis and mechanical testing. The results of these efforts are presented below.

6.2.3.1 Sample preparation

Laminates were first manufactured in an autoclave at pressures of 1, 3 and 5 bars. The cure cycle was selected based on the resin specifications (Figure 6-13). A 60 minute debulk at 50 °C and a pressure of -0.7 bars was added at the beginning of the cure cycle to encourage air and moisture evacuation. This same level of vacuum was applied throughout the entire process. A conventional vacuum bagging arrangement incorporating 'edge breather' [163] was employed (Figure 6-14). Plates were manufactured with dimensions of 30 x 30 cm^2. The number of layers was selected to comply with thickness requirements stated by ASTM D3039 and ASTM2344 (3 and 6 for the BL550 and BL200 respectively). In the case of the BL550, two layers were placed in the warp direction and one in the weft direction. For the BL200, the difference in warp and weft properties was neglected since the difference in crimp and fibre content was slight for the CL001 fabric (see Table 5). Sample data obtained from the thermocouples is provided in Figure 6-13 along with the evolution of the resin storage and loss moduli as determined by parallel plate rheometry on the neat resin. The gel time was taken to be the point which G' and G'' cross in a 25 mm parallel plate oscillation

experiment [164]. These experiments were carried out at a frequency of 1 Hz and strain of 0.1% on a TA AR2000 rheometer.

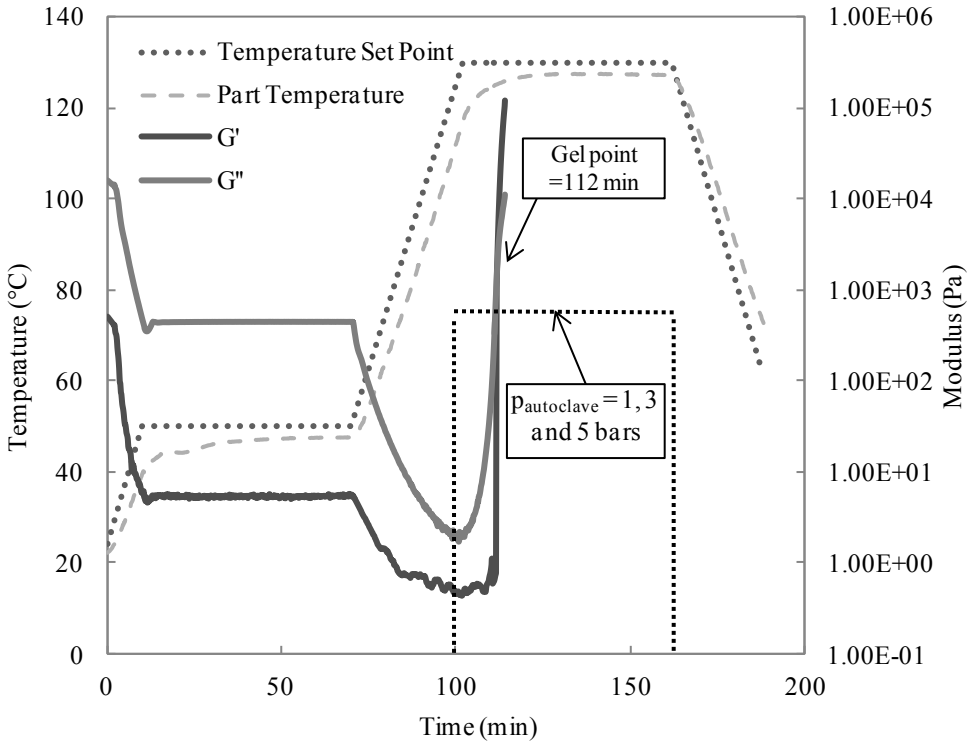

Figure 6-13: Processing cycle applied during manufacturing of studied flax/epoxy prepregs in an autoclave

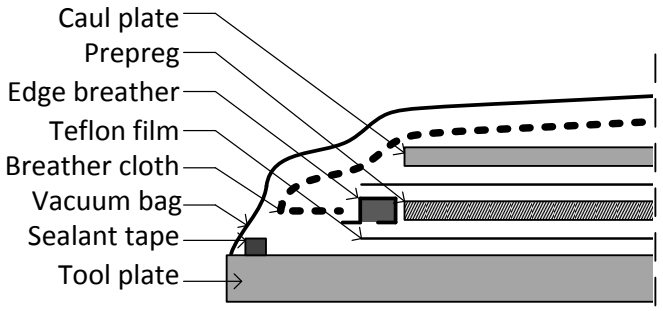

Figure 6-14: Vacuum bag arrangement used in prepreg case study

6.2.3.2 Void analysis

Optical microscopy was selected to measure the void content as in Sections 5.3.1 and 6.1.3.1. Samples of 45 mm in length were cut by water jet from the center of

the laminates and the cross-sections were polished. The same image analysis procedure as described in Section 5.3.1 was employed. A summary of the results along with the sample cross-sections is shown in Figure 6-15. A complete collection of all cross-sections is provided in Appendix E.

	P (bar)	Polished cross-section	Image analysis	Void percent
BL200	1	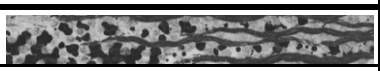	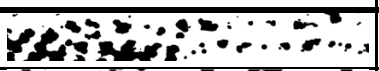	21.4±4.4
	3	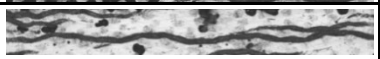	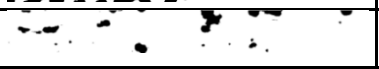	3.7±1.1
	5	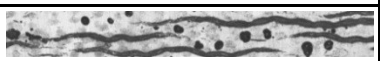		4.5±0.9
BL550	1	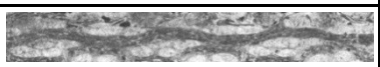		3.5±2.1
	3		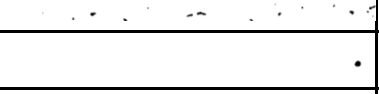	0.2±0.1
	5			0.03±0.02

Figure 6-15: Representative cross-sections of flax/epoxy prepregs processed at varying pressure and void contents as determined by image analysis (± standard deviation).

The image analysis results revealed that, due to the difference in applied pressure, composites of void content ranging from below 1% to over 20% were produced. The relationship between void content and autoclave pressure was non-linear (Figure 6-16) likely due to the non-linear stress-strain behaviour of the fibre bed. As discussed in Section 2.2.2, the latter has been shown to follow closely a power law function [105] which also describes the former well.

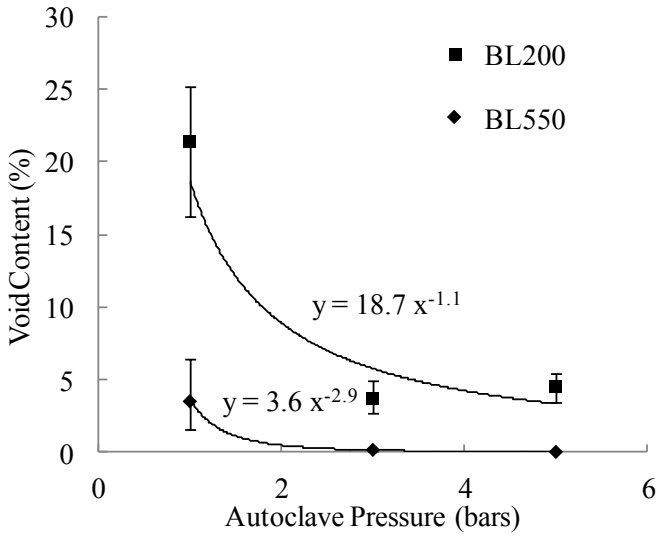

Figure 6-16: Void content versus applied autoclave pressure for cured BL200 and BL550 prepregs (error bars represent maximum and minimum values)

Based on the spherical void morphology, they were deemed to result from a combination of moisture diffusion, entrapped air and resin starvation. The transient behaviour of the former two can be described well by a diffusion-based growth model proposed by Kardos *et al* [35]. This model was not applied in this case due to the difficulty in determining experimentally the initial dimensions of entrapped air. Furthermore, a representative unit volume is necessary to determine the void content as a percentage [165] which further limits the uniqueness of the solution. However, based on the results of the compaction tests, the dominant void formation mechanism was likely resin starvation. The point at which the void content in BL550 becomes close to zero agrees well with this scenario. Therefore, the results suggest that the selected autoclave pressure suppressed the moisture diffusion well.

It should be noted, that the analysis of voids was limited to inter-yarn voids. In the case of bast fibre reinforced composites, voids can not only occur in the resin but also within the yarns and even the fibres themselves [166]. Therefore, the actual void content is likely higher. The influence of these intra-yarn and intra-fibre voids was beyond the scope of the current study.

6.2.3.3 Static tension

Tension tests were carried out in accordance with ASTM D3039 on an Instron servo-hydraulic testing machine with a 100kN load cell and 50 mm extensometer. A specimen area of 25 x 250 mm^2 was selected. Samples were cut by a water jet cutter and E-glass epoxy tabs were bonded to them. A loading rate of 2 mm/min was applied during the tests. The portion of the stress/strain curve up to 0.2% strain was used to calculate the Young's modulus. The results are summarized in Table 12 with representative stress/strain curves in Figure 6-17. A complete set of the stress-strain data for all specimens is provided in Appendix G.

Table 12: Summary of tensile testing results for cured BL200 and BL550 flax/epoxy prepregs (± standard deviation)

	Autoclave Pressure (bars)	**V_f (%)**	**Young's Modulus (GPa)**	**Strength (MPa)**	**Elongation (%)**
BL200	1	31.4±0.2	8.8±0.4	95±7	1.77±0.15
BL200	3	34.3±0.4	9.7±0.4	102±4	1.74±0.05
BL200	5	35.8±0.4	10.0±0.2	104±3	1.68±0.06
BL550	1	40.6±0.7	9.5±0.2	88±3	1.79±0.05
BL550	3	42.3±0.3	11.1±0.2	101±2	1.68±0.08
BL550	5	44.7±0.6	11.2±0.6	94±2	1.39±0.06
Epoxy[a]	-	-	3.52-3.62	68-78	2.0-3.0

[a]From manufacturers specifications for Huntsman LY5150/XB3471

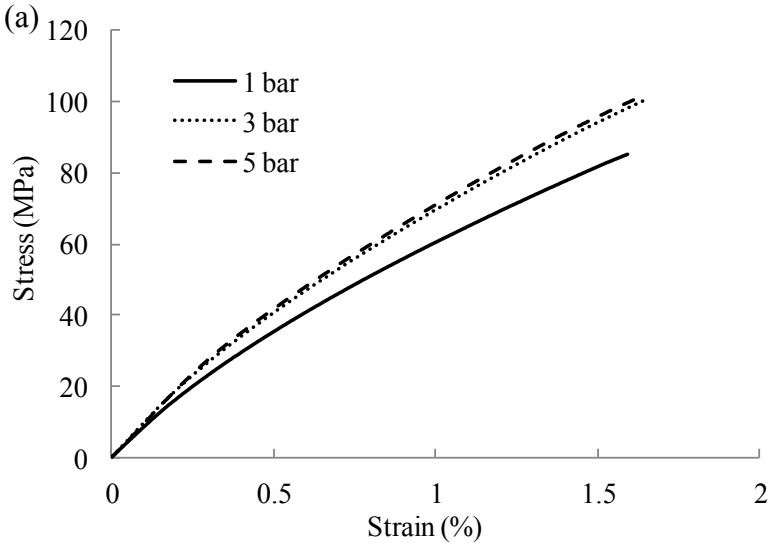

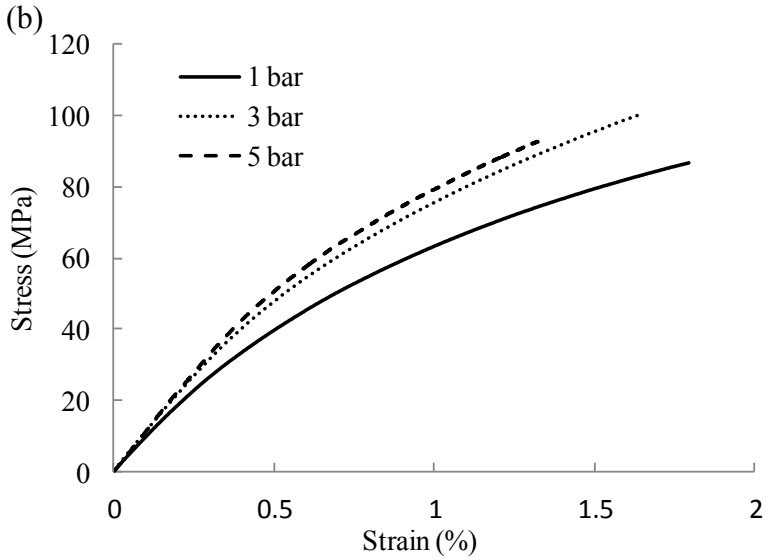

Figure 6-17: Representative stress/strain curves for balanced twill weave flax/epoxy prepregs (a) BL200 and (b) BL550

From the above results, it first appears that the voids have a relatively large influence on the tensile properties. However, due to the resin starvation the increase in pressure also resulted in an increase in fibre volume fraction. Therefore, the effects of voids on tensile properties are not entirely clear in this study. Nonetheless, the effective tensile properties for the studied material systems were increased with increasing autoclave pressure.

One aspect of the prepregs that was found to highly affect the tensile properties was the crimp percentage. In a separate set of experiments, panels were manufactured with varying numbering of layers in the warp and weft direction for the BL550 system. The crimp percentages in both fibre directions were determined by image analysis and the results are given in Table 5. The results of tensile testing are shown in Figure 6-18.

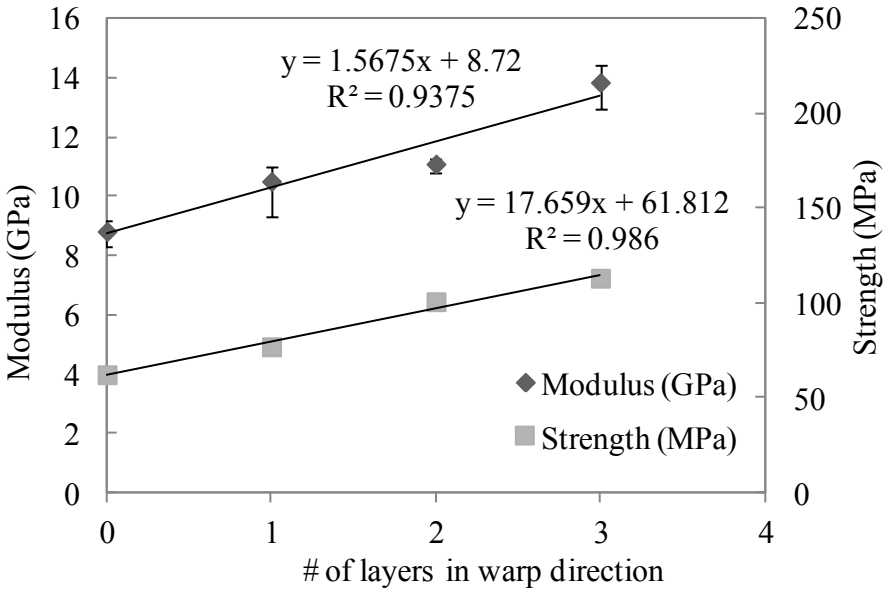

Figure 6-18: Tensile modulus and strength versus number of layers in the warp direction (error bars represent maximum and minimum values)

Figure 6-18 reveals that the difference in warp and weft direction properties is quite significant. The weft direction showed a 36% and 51% reduction in tensile stiffness and strength respectively. The exact reasons for this surprising decrease in properties will be a topic for future work but is presumably due to the difference in warp and weft crimp as shown in Table 5.

6.2.3.4 Interlaminar strength

As in Section 6.1.3.2, interlaminar shear strength (ILSS) was obtained by the short beam test carried out in accordance with ASTM D2344 on an MTS Insight load testing machine with a 5kN load cell. A sample area of 50 x 150 mm^3 was selected and a load rate of 0.5 mm/min was applied. The span to depth ratio was set to 4. This configuration resulted in a mode of failure of interlaminar shear for both systems as observed under a microscope. Unpolished cross-sections of selected fracture surfaces are shown in Figure 6-19 along with a plot of interlaminar shear strength versus void content.

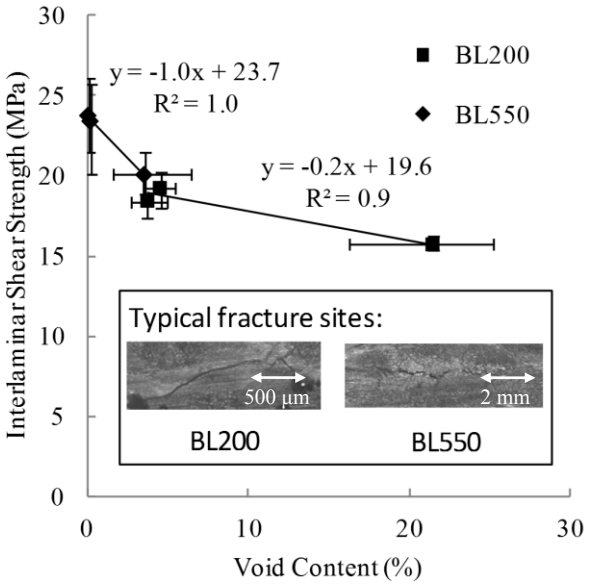

Figure 6-19: Void content versus interlaminar shear strength for BL200 and BL550 flax/epoxy prepregs processed a 1, 3 and 5 bars (error bars represent maximum and minimum values)

Contrary to the tensile properties, the ILSS exhibited a consistent decrease in properties with increasing void content. For the BL550 system, the strength decreased 11% with a 3.5% increase in void content. The rate of decrease was less pronounced in higher ranges of void content which is typical of observations made by other authors for unidirectional carbon fibre/epoxy composites [167].

6.2.3.5 Water absorption

On top of a reduction in interlaminar shear strength, the resistance to moisture absorption [168, 169] has also been shown to be compromised by voids. A saturated moisture absorption test was carried out in accordance with ASTM D570 and a sample area of 25x45 mm^2 was selected. To minimize in-plane absorption, the sides of the samples were sealed with a silicone sealer. The weight of the silicone was determined based on the difference in dry sample weight before and after the application of the silicone. The drying process consisted of heating in a convection oven for 24 hours at 50 °C followed by cooling in a desiccant chamber.

The specimens were weighed after submersion in distilled water at 2 and 24 hours. Prior to weighing, they were dabbed with a lint free cloth in order to remove excess liquid. The amount of water absorbed under these conditions and a plot of void content versus effective water equilibrium after 24 hours are given in Table 13 and Figure 6-20 respectively.

Table 13: Mass gain after 2 and 24 hours submersion in water of cured flax/epoxy prepreg samples processed at varying pressure (± standard deviation)

	Processing Pressure (bars)	Mass gain after 2 hours (%)	Mass gain after 24 hours (%)
BL200	1	5.1±0.6	12.5±1.5
	3	4.7±0.4	9.4±1.3
	5	3.5±0.2	6.4±0.4
BL550	1	2.9±0.3	6.5±0.5
	3	2.3±0.2	4.9±0.4
	5	2.7±0.3	5.3±0.4

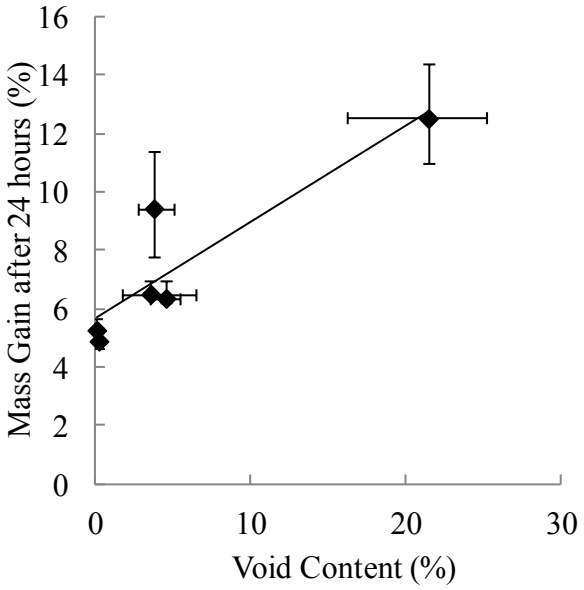

Figure 6-20: Void content versus mass gain after 24 hours in water absorption test (error bars represent maximum and minimum values)

The results indicate a large dependence of water absorption rate on the level of voids. The effective moisture equilibrium after 24 hours increased 33% with only a 3.5% increase in void content. Furthermore, the amount of scatter was generally higher for higher void contents. From Figure 6-20, it can also be seen that the

relationship between the effective moisture equilibrium after 24 hours and void content was in general linear. The outlying point indicated that the level of voids was not well distributed throughout the manufactured plates. It suggested that the void content in the moisture absorption samples was higher than in those used for image analysis for the BL200 system processed at 3 bars.

The results of the water absorption tests are deemed to be most critical of all mechanical properties investigated in this thesis. This is due to the fact that water absorption has been previously shown to in turn lead to a reduction in mechanical properties in some cellulose-based fibre-reinforced plastics [170-173]. However, it should be noted that coatings are available that greatly reduce the moisture absorption rate for this class of materials [174].

6.3 Summary

This chapter addressed two important case studies with the aim of improving the state-of-the-art for flax-reinforced epoxy composite materials. The first investigated the incorporation of nanocellulose (NC) in the resin infusion process to produce multi-scale composites consisting of flax, NC and epoxy. Two different methods were explored to incorporate the NC directly in the resin infusion process to eliminate the need to modify the resin. The first involved grafting the fibres directly on the flax yarn during a silane-based chemical treatment process and the second involved directly adding the NC during the layup stage by wet-layup of an aqueous NC solution. The incorporation of the NC led to both changes in the processing behaviour as well as interlaminar mechanical properties. Void analysis revealed the grafting technique to induce large interlaminar voids whereas the wet-layup technique produced composites of very low void content (< 2%). However, through drop-weight impact testing, the impact properties of both multi-scale composites were shown to degrade from the single-scale composite. Thus, for the resin infusion methods investigated, the incorporation of the NC was not justified. These results epitomized the link between processing methods, part quality and mechanical performance for this

class of materials and highlighted the effect of nano-modifiers on composite part quality.

The second case study pertained to state-of-the-art prepregs based on flax yarns. To understand the primary source of voids during curing of these systems, thermal gravimetric analysis and compaction experiments were carried out. The former test revealed a high amount of moisture in the supplied materials stressing the need to evacuate moisture from these prepregs during cure. The latter test revealed a shortage of resin in the prepregs leading the resin starvation at insufficient compaction pressures. A series of panels manufactured at varying autoclave pressures, agreed well with the resin starvation scenario based on the results of void analysis. The presence of voids was finally shown to degrade interlaminar shear as well as moisture absorption properties.

Chapter 7

Conclusions and future work

This thesis pertained to the characterization of flax fibres for application in the resin infusion process and included two case studies that aimed to improve the state-of-the-art for this class of materials. Untreated and treated flax fibres were first characterized at the fibre level through advancing contact angle analysis, scanning electron microscopy (SEM) and helium pycnometry. The results from advancing contact analysis revealed a reduction in the polar component of surface energy for a silane and diluted epoxy treatment. A 2% alkaline treatment did not result in a significant change in surface free energy due to the relatively low concentration.

The fibres were then characterized at the fabric level by compaction and permeability experiments for the purpose of quantifying this behaviour for process modelling. The dry compaction behaviour of the alkaline treated fabrics was shown to vary significantly from that of the untreated fabrics. A higher amount of compaction stress was required for a given fibre volume fraction for the alkaline treated fabrics. This was attributed to an increase in fibrillation in the

fibres and consequently an increase in fibre-fibre contact points resulting in more resistance from the fibre bed for a given pressure. The equivalent permeability was also measured for the treated fabrics and a significant difference was generally not observed for the different treatments. However, due to the increase in fibrillation for the alkaline-treated fibres there was a 50% increase in equivalent permeability for the compaction pressure involved in the pre-filling stage of the resin infusion process. This result stressed the coupled nature of this process and how changes in the compaction response of a fibrous reinforcement can lead to changes in the equivalent permeability.

Flax/epoxy panels were then manufactured from the treated fabrics and the processing behaviour was compared with that predicted by a 1D resin infusion process model. The evolution in flow front was shown to be in reasonably good agreement with the model predictions. In addition, the model was used to predict the theoretical effect of the observed changes in surface energy on the infiltration times. Due to the relatively high range of measured porosities, the effect of the treatments due to changes in capillary pressure was shown to be negligible. However, this demonstrated that other outcomes of the chemical treatments (e.g. increase in fibrillation) played a much larger role in the processing kinetics of resin infusion. This was further emphasized in the results from a mechanical characterization. The alkaline treatment showed a large reduction in flexural properties due to a reduced fibre volume fraction compared to the untreated flax-reinforced composite. Thus, simply looking at the adhesion strength between individual flax fibres and the resin does not provide a complete picture for the case of the resin infusion process. The fibre, processing and composite characteristics are intimately linked and all aspects must be considered.

The final component of this thesis aimed to improve the state-of-the-art for the studied class of materials by considering two case studies. The first case study considered novel methods of incorporating nanocellulose (NC) in the resin infusion process to reinforce the interlaminar regions of flax/epoxy composite to

produce a multi-scale composite. The NC was shown to increase the amount of damage suffered after subjection to a drop-weight impact event. The type of damage included delamination which suggested that the NC did not result in the intended increase in interlaminar properties. However, use of an aqueous NC solution during the layup resulted in an increase in final fibre volume fraction due to the softening and lubricating effect caused by the water. A 10% increase in fibre volume fraction was measured for the composite manufactured with the wetted preform prior to the debulk stage. This led to an increase in interlaminar properties as measured by a short beam shear test.

The second case study investigated the primary source of voids in commercially available flax prepregs. TGA and compaction experiments were first carried out and the primary sources were shown to be moisture contained within the prepregs as well as a starvation of resin due to insufficient resin in the supplied materials. Part of the problem in calculating the required amount of resin in the prepregs lied in the difficulty in accurately measuring the areal weight of flax fabrics due to the relatively high amount of possible moisture uptake (up to 30%). This stresses the need for a standard addressing the measurement of the areal weight of cellulose-based fabrics. A series of panels were then manufactured at autoclave pressures of 1, 3 and 5 bars. The interlaminar properties were shown to degrade with increasing void content. Similarly, moisture sorption increased for the composite with increasing void content.

7.1 Contributions

From the characterization of the flax fibres, flax fabrics, flax/epoxy composites and case studies the most significant contributions were deemed as follows:

- Methodology for characterization of cellulose-based fabrics for application in the resin infusion process
- Better understanding of implications of chemical treatments on the processing kinetics and mechanical properties of flax/epoxy composites manufactured by resin infusion

- Quantification of permeability and compaction behaviour of a commercially available flax fabric
- Measurement of surface free energies for selected chemical treatments of flax fibres
- Development of novel method to incorporate nano-modifiers and concurrently increase the final fibre volume fraction of flax/epoxy composites manufactured by the resin infusion process
- Identification of key processing issues in flax/epoxy prepregs that relate to the improvement of this class of prepregs

These contributions led to the publication of one peer reviewed journal article [175], one submitted article [176] and one article which was under preparation at the time of this writing [177]. In addition, two conference papers were published as part of this study [178, 179] and one was submitted at the time of this writing [180].

7.2 Future work

Based on the conclusions of this thesis, one area was deemed most critical for future work. The poor compaction behaviour of flax and other cellulose-based fibre reinforcements needs to be addressed. A major limiting factor in the mechanical performance was shown to be a consequence of the poor process-ability of flax-based reinforcements due primarily to poor compaction behaviour. Since this factor was shown to be affected by some chemical treatments (e.g. alkaline) as well as lubricating effects, future work should address these issues in more depth. In addition, other processes might be developed that employ higher compaction forces combined with more advanced forms of flax-reinforcements composed of yarns that have minimal twist and crimp.

References

[1] Bledzki AK, Faruk O, Sperber VE. Cars from Bio-Fibres. Macromolecular Materials and Engineering. 2006;291(5):449-57.
[2] Holbery J, Houston D. Natural-fiber-reinforced polymer composites in automotive applications. Journal of the Minerals, Metals and Materials Society. 2006;58(11):80-6.
[3] Pandey JK, Ahn SH, Lee CS, Mohanty AK, Misra M. Recent Advances in the Application of Natural Fiber Based Composites. Macromolecular Materials and Engineering. 2010;295(11):975-89.
[4] Lewin M. Handbook of fiber chemistry. Boca Raton :: CRC/Taylor & Francis; 2007.
[5] http://www.flaxcouncil.ca/. Flax Council of Canada. Winnipeg, MB, 2013. (accessed February 2013)
[6] Summerscales J, Dissanayake NPJ, Virk AS, Hall W. A review of bast fibres and their composites. Part 1 - Fibres as reinforcements. Composites Part A: Applied Science and Manufacturing. 2010;41(10):1329-35.
[7] Vanfleteren F. Flax-epoxy prepregs leading the race. JEC Composites Magazine. Paris: JEC; 2007. p. 44-5.
[8] Muir AD, Westcott ND. Flax : the genus linum. London ; New York :: Routledge; 2003.
[9] Foulk JA, Fuqua MA, Ulven CA, Alcock MM. Flax fibre quality and influence on interfacial properties of composites. International Journal of Sustainable Engineering. 2010;3(1):17-24.
[10] Pritchard G. Reinforced plastics durability. Boca Raton : Cambridge :: CRC Press ; Woodhead Pub.; 1999.
[11] Ebnesajjad S. Handbook of adhesives and surface preparation technology, applications and manufacturing. Kidlington, Oxford, U.K. ; Burlington, Mass. :: William Andrew; 2011.
[12] Reux F. A flax-composite boat for transatlantic races. JEC Composites Magazine. Paris: JEC; 2011. p. 33-4.
[13] Charlet K, Baley C, Morvan C, Jernot JP, Gomina M, Bréard J. Characteristics of Hermès flax fibres as a function of their location in the stem and properties of the derived unidirectional composites. Composites Part A: Applied Science and Manufacturing. 2007;38(8):1912-21.
[14] Gassan J, Mildner I, Bledzki A. Influence of fiber structure modification on the mechanical properties of flax fiber-epoxy composites. Mechanics of composite materials. 1999;35(5):435-40.
[15] Gning P, Liang S, Guillaumat L, Pui W. Influence of process and test parameters on the mechanical properties of flax/epoxy composites using response surface methodology. Journal of Materials Science. 2011;46(21):6801-11.
[16] Lamy B, Pomel C. Influence of fiber defects on the stiffness properties of flax fibers-epoxy composite materials. Journal of materials science letters. 2002;21(15):1211-3.

[17] Liu Q, Hughes M. The fracture behaviour and toughness of woven flax fibre reinforced epoxy composites. Composites Part A: Applied Science and Manufacturing. 2008;39(10):1644-52.
[18] Oksman K. High quality flax fibre composites manufactured by the resin transfer moulding process. Journal of Reinforced Plastics and Composites. 2001;20(7):621-7.
[19] Scida D, Assarar M, Poilâne C, Ayad R. Influence of hygrothermal ageing on the damage mechanisms of flax-fibre reinforced epoxy composite. Composites Part B: Engineering. 2013;48(0):51-8.
[20] Van de Weyenberg I, Chi Truong T, Vangrimde B, Verpoest I. Improving the properties of UD flax fibre reinforced composites by applying an alkaline fibre treatment. Composites Part A: Applied Science and Manufacturing. 2006;37(9):1368-76.
[21] Mohanty AK, Misra M, Drzal LT. Natural fibers, biopolymers, and biocomposites. Boca Raton, FL :: Taylor & Francis; 2005.
[22] Strong AB. Fundamentals of composites manufacturing : materials, methods and applications. Dearborn, Mich. :: Society of Manufacturing Engineers; 2008.
[23] Michaud V, Mortensen A. Infiltration processing of fibre reinforced composites: governing phenomena. Composites Part A: Applied Science and Manufacturing. 2001;32(8):981-96.
[24] Seemann W. 1990, U. S. Patent Office, Pat No. 4902215.
[25] Bledzki AK, Gassan J. Composites reinforced with cellulose based fibres. Progress in Polymer Science. 1999;24(2):221-74.
[26] Karbhari V, Palmese G. Sizing related kinetic and flow considerations in the resin infusion of composites. Journal of Materials Science. 1997;32(21):5761-74.
[27] Rodriguez ES, Stefani PM, Vazquez A. Effects of Fibers' Alkali Treatment on the Resin Transfer Molding Processing and Mechanical Properties of Jute—Vinylester Composites. Journal of Composite Materials. 2007;41(14):1729-41.
[28] Waśko J, Mańkowski T. Applicability of flax and hemp as raw materials for production of cotton-like fibres and blended yarns in Poland. Fibres & Textiles in Eastern Europe. 2004;12(3):47.
[29] Baley C. Analysis of the flax fibres tensile behaviour and analysis of the tensile stiffness increase. Composites Part A: Applied Science and Manufacturing. 2002;33(7):939-48.
[30] Francucci G, Vázquez A, Rodríguez ES. Key differences on the compaction response of natural and glass fiber preforms in liquid composite molding. Textile Research Journal. 2012;82(17):1774-85.
[31] Rong MZ, Zhang MQ, Liu Y, Yang GC, Zeng HM. The effect of fiber treatment on the mechanical properties of unidirectional sisal-reinforced epoxy composites. Composites Science and Technology. 2001;61(10):1437-47.
[32] Bos HL, Müssig J, van den Oever MJA. Mechanical properties of short-flax-fibre reinforced compounds. Composites Part A: Applied Science and Manufacturing. 2006;37(10):1591-604.
[33] Jones RM. Mechanics of composite materials. Philadelphia, PA :: Taylor & Francis; 1999.
[34] Judd NCW, Wright WW. Voids and their effects on the mechanical properties of composites- an appraisal. Sampe Journal. 1978;14:10-4.

[35] Kardos J, Duduković M, Dave R. Void growth and resin transport during processing of thermosetting matrix composites. Advances in Polymer Science. 1986;80:101-23.
[36] Truong M, Zhong W, Boyko S, Alcock M. A comparative study on natural fibre density measurement. Journal of the Textile Institute. 2009;100(6):525 - 9.
[37] Kabir MM, Wang H, Lau KT, Cardona F. Chemical treatments on plant-based natural fibre reinforced polymer composites: An overview. Composites Part B: Engineering. 2012;43(7):2883-92.
[38] Aranberri-Askargorta I, Lampke T, Bismarck A. Wetting behavior of flax fibers as reinforcement for polypropylene. Journal of Colloid and Interface Science. 2003;263(2):580-9.
[39] Kornev KG, Neimark AV. Spontaneous penetration of liquids into capillaries and porous membranes revisited. Journal of Colloid and Interface Science. 2001;235(1):101-13.
[40] Barnes G, Gentle I. Interfacial science : an introduction. Oxford :: Oxford University Press; 2011.
[41] Bismarck A, Aranberri-Askargorta I, Springer J, Lampke T, Wielage B, Stamboulis A, et al. Surface characterization of flax, hemp and cellulose fibers; Surface properties and the water uptake behavior. Polymer Composites. 2002;23(5):872-94.
[42] Holmberg K, Shah DO, Schwuger MJ. Handbook of applied surface and colloid chemistry. Chichester, England ; New York :: Wiley; 2002.
[43] Oura K. Surface science : an introduction. Berlin ; New York :: Springer; 2003.
[44] Fowkes FM. Attractive forces at interfaces. Industrial & Engineering Chemistry. 1964;56(12):40-52.
[45] Owens DK, Wendt RC. Estimation of the surface free energy of polymers. Journal of Applied Polymer Science. 1969;13(8):1741-7.
[46] Van Oss C, Good R, Chaudhury M. Additive and nonadditive surface tension components and the interpretation of contact angles. Langmuir. 1988;4(4):884-91.
[47] Zisman WA. Relation of the equilibrium contact angle to liquid and solid constitution. Advances in Chemistry Series. 1964;43(1):51.
[48] Arbelaiz A, Cantero G, Fernández B, Mondragon I, Gañán P, Kenny JM. Flax fiber surface modifications: Effects on fiber physico mechanical and flax/polypropylene interface properties. Polymer Composites. 2005;26(3):324-32.
[49] Baley C, Busnel F, Grohens Y, Sire O. Influence of chemical treatments on surface properties and adhesion of flax fibre–polyester resin. Composites Part A: Applied Science and Manufacturing. 2006;37(10):1626-37.
[50] Van De Velde K, Kiekens P. Influence of Fiber Surface Characteristics on the Flax/Polypropylene Interface. Journal of Thermoplastic Composite Materials. 2001;14(3):244-60.
[51] Paiva MC, Bernardo CA, Nardin M. Mechanical, surface and interfacial characterisation of pitch and PAN-based carbon fibres. Carbon. 2000;38(9):1323-37.
[52] Comyn J. Theories of adhesion. Handbook of Adhesives and Sealants. 2006;2:1-50.

[53] Steenkamer D, McKnight S, Wilkins D, Karbhari V. Experimental characterization of permeability and fibre wetting for liquid moulding. Journal of Materials Science. 1995;30(12):3207-15.
[54] Karmakar SR. Chemical technology in the pre-treatment processes of textiles. Amsterdam:: Elsevier; 1999.
[55] Van de Weyenberg I, Ivens J, De Coster A, Kino B, Baetens E, Verpoest I. Influence of processing and chemical treatment of flax fibres on their composites. Composites Science and Technology. 2003;63(9):1241-6.
[56] George J, Sreekala MS, Thomas S. A review on interface modification and characterization of natural fiber reinforced plastic composites. Polymer Engineering & Science. 2001;41(9):1471-85.
[57] Mishra S, Mohanty A, Drzal L, Misra M, Parija S, Nayak S, et al. Studies on mechanical performance of biofibre/glass reinforced polyester hybrid composites. Composites Science and Technology. 2003;63(10):1377-85.
[58] Mittal KL. Silanes and other coupling agents: CRC Press; 2009.
[59] Li X, Tabil LG, Panigrahi S. Chemical treatments of natural fiber for use in natural fiber-reinforced composites: A review. Journal of Polymers and the Environment. 2007;15(1):25-33.
[60] George J, Verpoest JII. Mechanical properties of flax fibre reinforced epoxy composites. Die Angewandte Makromolekulare Chemie. 1999;272(1):41-5.
[61] Kalia S, Kaith BS, Kaur I. Pretreatments of natural fibers and their application as reinforcing material in polymer composites-a review. Polymer Engineering and Science. 2009;49(Compendex):1253-72.
[62] Goutianos S, Peijs T. The optimisation of flax fibre yarns for the development of high-performance natural fibre composites. Advanced Composites Letters. 2003;12(6):237-41.
[63] Shah DU, Schubel PJ, Clifford MJ. Modelling the effect of yarn twist on the tensile strength of unidirectional plant fibre yarn composites. Journal of Composite Materials. 2013;47(4):425-36.
[64] Baley C, Perrot Y, Busnel F, Guezenoc H, Davies P. Transverse tensile behaviour of unidirectional plies reinforced with flax fibres. Materials Letters. 2006;60(24):2984-7.
[65] Bos H, Van Den Oever MJA, Peters OCJJ. Tensile and compressive properties of flax fibres for natural fibre reinforced composites. Journal of Materials Science. 2002;37(8):1683-92.
[66] Baets J, Plastria D, Ivens J, Verpoest I. Determination of the optimal flax fibre preparation for use in UD flax-epoxy composites. In: Proceedings of 14th International Conference on Sustainable Materials, Polymers and Composites. Birmingham, UK, 2011.
[67] Goutianos S, Peijs T, Nystrom B, Skrifvars M. Development of flax fibre based textile reinforcements for composite applications. Applied Composite Materials. 2006;13:199-215.
[68] Advani SG, Sozer EM. Process modeling in composites manufacturing. Boca Raton, FL :: CRC Press; 2011.
[69] Hubert P, Poursartip A. Review of flow and compaction modelling relevant to thermoset matrix laminate processing. Journal of Reinforced Plastics and Composites. 1998;17(4):286-318.

[70] Liu B, Bickerton S, Advani SG. Modelling and simulation of resin transfer moulding (RTM)—gate control, venting and dry spot prediction. Composites Part A: Applied Science and Manufacturing. 1996;27(2):135-41.
[71] Coulter JP, Guceri SI. Resin impregnation during the manufacturing of composite materials subject to prescribed injection rate. Journal of Reinforced Plastics and Composites. 1988;7(3):200-19.
[72] Gauvin R, Trochu F, Lemenn Y, Diallo L. Permeability measurement and flow simulation through fiber reinforcement. Polymer Composites. 2004;17(1):34-42.
[73] Adams KL, Miller B, Rebenfeld L. Forced in-plane flow of an epoxy resin in fibrous networks. Polymer Engineering & Science. 1986;26(20):1434-41.
[74] Cai Z. Analysis of mold filling in RTM process. Journal of Composite Materials. 1992;26(9):1310-38.
[75] Shojaei A, Ghaffarian S, Karimian S. Numerical simulation of three-dimensional mold filling process in resin transfer molding using quasi-steady state and partial saturation formulations. Composites Science and Technology. 2002;62(6):861-79.
[76] Lin M, Thomas Hahn H, Huh H. A finite element simulation of resin transfer molding based on partial nodal saturation and implicit time integration. Composites Part A: Applied Science and Manufacturing. 1998;29(5):541-50.
[77] Darcy H. Les fontaines publiques de la ville de Dijon, 1856. Dalmont, Paris.70.
[78] Terzaghi K. 1943, Theoretical Soil Mechanics, John Wiley & Sons, New York.
[79] Bruschke M, Advani S. Flow of generalized Newtonian fluids across a periodic array of cylinders. Journal of Rheology. 1993;37(3):479-98.
[80] Carman P. Fluid flow through granular beds. Transactions-Institution of Chemical Engineeres. 1937;15:150-66.
[81] Gebart R. Permeability of unidirectional reinforcements for RTM. Journal of Composite Materials. 1992;26(8):1100-33.
[82] Westhuizen J, Du Plessis JP. Quantification of unidirectional fiber bed permeability. Journal of Composite Materials. 1994;28(7):619-37.
[83] Correia NC, Robitaille F, Long AC, Rudd CD, Šimáček P, Advani SG. Analysis of the vacuum infusion moulding process: I. Analytical formulation. Composites Part A: Applied Science and Manufacturing. 2005;36(12):1645-56.
[84] Hammami A, Gebart R. Analysis of the vacuum infusion molding process. Polymer Composites. 2000;21(1):28-40.
[85] Kang M, Lee W, Hahn H. Analysis of vacuum bag resin transfer molding process. Composites Part A: Applied Science and Manufacturing. 2001;32(11):1553-60.
[86] Govignon Q, Bickerton S, Kelly PA. Simulation of the reinforcement compaction and resin flow during the complete resin infusion process. Composites Part A: Applied Science and Manufacturing. 2010;41(1):45-57.
[87] Grimsley BW, Hubert P, Song X, Cano RJ, Loos AC, Pipes RB. Flow and compaction during the vacuum assisted resin transfer molding process. In: Proceedings of International SAMPE Technical Conference, 2001. p. 140-53.

[88] Mathur R, Advani S, Heider D, Hoffmann C, Gillespie Jr J, Fink B. Flow front measurements and model validation in the vacuum assisted resin transfer molding process. Polymer Composites. 2001;22(4):477-90.
[89] Sun X, Li S, Lee LJ. Mold filling analysis in vacuum-assisted resin transfer molding. Part I: SCRIMP based on a high-permeable medium. Polymer Composites. 1998;19(6):807-17.
[90] Han K, Jiang S, Zhang C, Wang B. Flow modeling and simulation of SCRIMP for composites manufacturing. Composites Part A: Applied Science and Manufacturing. 2000;31(1):79-86.
[91] Francucci G, Rodríguez ES, Vázquez A. Study of saturated and unsaturated permeability in natural fiber fabrics. Composites Part A: Applied Science and Manufacturing. 2010;41(1):16-21.
[92] Masoodi R, Pillai KM. Modeling the Processing of Natural Fiber Composites Made Using Liquid Composite Molding. Handbook of Bioplastics and Biocomposites Engineering Applications. Hoboken: John Wiley & Sons; 2011. p. 43-73.
[93] Bréard J, Henzel Y, Trochu F, Gauvin R. Analysis of dynamic flows through porous media. Part I: Comparison between saturated and unsaturated flows in fibrous reinforcements. Polymer Composites. 2003;24(3):391-408.
[94] Simacek P, Advani SG. A numerical model to predict fiber tow saturation during liquid composite molding. Composites Science and Technology. 2003;63(12):1725-36.
[95] Pillai KM, Advani SG. A Model for Unsaturated Flow in Woven Fiber Preforms during Mold Filling in Resin Transfer Molding. Journal of Composite Materials. 1998;32(19):1753-83.
[96] Pillai KM. Modeling the unsaturated flow in liquid composite molding processes: A review and some thoughts. Journal of Composite Materials. 2004;38(23):2097-118.
[97] Lawrence JM, Neacsu V, Advani SG. Modeling the impact of capillary pressure and air entrapment on fiber tow saturation during resin infusion in LCM. Composites Part A: Applied Science and Manufacturing. 2009;40(8):1053-64.
[98] Pillai KM, Advani SG. Wicking across a fiber-bank. Journal of Colloid and Interface Science. 1996;183(1):100-10.
[99] Acheson JA, Simacek P, Advani SG. The implications of fiber compaction and saturation on fully coupled VARTM simulation. Composites Part A: Applied Science and Manufacturing. 2004;35(2):159-69.
[100] Bayldon JM, Daniel IM. Flow modeling of the VARTM process including progressive saturation effects. Composites Part A: Applied Science and Manufacturing. 2009;40(8):1044-52.
[101] Li M, Wang S, Gu Y, Zhang Z, Li Y, Potter K. Dynamic capillary impact on longitudinal micro-flow in vacuum assisted impregnation and the unsaturated permeability of inner fiber tows. Composites Science and Technology. 2010;70(11):1628-36.
[102] Francucci G, Vázquez A, Ruiz E, Rodríguez ES. Capillary effects in vacuum-assisted resin transfer molding with natural fibers. Polymer Composites. 2012;33(9):1593-602.

[103] Ahn KJ, Seferis JC, Berg JC. Simultaneous measurements of permeability and capillary pressure of thermosetting matrices in woven fabric reinforcements. Polymer Composites. 1991;12(3):146-52.
[104] Verrey J, Michaud V, Månson JAE. Dynamic capillary effects in liquid composite moulding with non-crimp fabrics. Composites Part A: Applied Science and Manufacturing. 2006;37(1):92-102.
[105] Robitaille F, Gauvin R. Compaction of textile reinforcements for composites manufacturing. I: Review of experimental results. Polymer Composites. 1998;19(2):198-216.
[106] Robitaille F, Gauvin R. Compaction of textile reinforcements for composites manufacturing. II: Compaction and relaxation of dry and H2O-saturated woven reinforcements. Polymer Composites. 1998;19(Compendex):543-57.
[107] Robitaille F, Gauvin R. Compaction of textile reinforcements for composites manufacturing. III: Reorganization of the fiber network. Polymer Composites. 1999;20(Compendex):48-61.
[108] Bickerton S, Buntain MJ, Somashekar AA. The viscoelastic compression behavior of liquid composite molding preforms. Composites Part A: Applied Science and Manufacturing. 2003;34(5):431-44.
[109] Kelly PA, Umer R, Bickerton S. Viscoelastic response of dry and wet fibrous materials during infusion processes. Composites Part A: Applied Science and Manufacturing. 2006;37(6):868-73.
[110] Pearce N, Summerscales J. The compressibility of a reinforcement fabric. Composites Manufacturing. 1995;6(1):15-21.
[111] Van Wyk C. Note on the Compressibility of Wool. Journal of the Textile Institute Transactions. 1946;37(12):285-92.
[112] Gutowski TG, Morigaki T, Zhong Cai. The Consolidation of Laminate Composites. Journal of Composite Materials. 1987;21(2):172-88.
[113] Chen B, Cheng AHD, Chou TW. A nonlinear compaction model for fibrous preforms. Composites Part A: Applied Science and Manufacturing. 2001;32(5):701-7.
[114] Chen B, Chou T-W. Compaction of woven-fabric preforms in liquid composite molding processes: single-layer deformation. Composites Science and Technology. 1999;59(10):1519-26.
[115] Saunders RA, Lekakou C, Bader MG. Compression and microstructure of fibre plain woven cloths in the processing of polymer composites. Composites Part A: Applied Science and Manufacturing. 1998;29(4):443-54.
[116] Saunders RA, Lekakou C, Bader MG. Compression in the processing of polymer composites 1. A mechanical and microstructural study for different glass fabrics and resins. Composites Science and Technology. 1999;59(7):983-93.
[117] Lomov SV, Verpoest I. Compression of woven reinforcements: a mathematical model. Journal of Reinforced Plastics and Composites. 2000;19(16):1329-50.
[118] Hammami A. Effect of reinforcement structure on compaction behavior in the vacuum infusion process. Polymer Composites. 2001;22(3):337-48.

[119] Michaud V, Manson JAE. Impregnation of compressible fiber mats with a thermoplastic resin. Part I: Theory. Journal of Composite Materials. 2001;35(13):1150-73.
[120] Ouagne P, Bizet L, Baley C, Bréard J. Analysis of the Film-stacking Processing Parameters for PLLA/Flax Fiber Biocomposites. Journal of Composite Materials. 2010;44(10):1201-15.
[121] Umer R, Bickerton S, Fernyhough A. Characterising wood fibre mats as reinforcements for liquid composite moulding processes. Composites Part A: Applied Science and Manufacturing. 2007;38(2):434-48.
[122] Umer R, Bickerton S, Fernyhough A. The effect of yarn length and diameter on permeability and compaction response of flax fibre mats. Composites Part A: Applied Science and Manufacturing. 2011;42(7):723-32.
[123] Francucci G, Rodríguez ES, Vázquez A. Experimental study of the compaction response of jute fabrics in liquid composite molding processes. Journal of Composite Materials. 2012;46(2):155-67.
[124] Xue D, Miao M, Hu H. Permeability anisotropy of flax nonwoven mats in vacuum-assisted resin transfer molding. The Journal of The Textile Institute. 2011;102(7):612-20.
[125] Bear J, Bachmat Y. Introduction to modeling of transport phenomena in porous media. Dordrecht ; Boston :: Kluwer Academic Publishers; 1990.
[126] Luo Y, Verpoest I, Hoes K, Vanheule M, Sol H, Cardon A. Permeability measurement of textile reinforcements with several test fluids. Composites Part A: Applied Science and Manufacturing. 2001;32(10):1497-504.
[127] Rouison D, Couturier M, Panthapulakkal S, Sain M. Measurement of the average permeability of natural fibre mats in resin transfer moulding application. Anglais. 2006;14(3):229-38.
[128] Re C, Bizet L, Breard J. Comparison of in-plane permeability between flax and glass stitched fabrics. In: Proceedings of 10th International Conference on Flow Processes in Composite Materials (FPCM-10). Ascona, Switzerland, 2010.
[129] Rodriguez E, Giacomelli F, Vazquez A. Permeability-porosity relationship in RTM for different fiberglass and natural reinforcements. Journal of Composite Materials. 2004;38(3):259-68.
[130] Kelly A, Zweben CH. Comprehensive composite materials. Amsterdam ; New York :: Elsevier; 2000.
[131] ASTM. Standard test method for tensile properties of polymer matrix composite materials. ASTM D3039/D 3039M, 1995.
[132] Heijenrath R, Peijs T. Natural-fibre-mat-reinforced thermoplastic composites based on flax fibres and polypropylene. Advanced Composites Letters(UK). 1996;5(3):81-5.
[133] Lomov SV, Huysmans G, Luo Y, Parnas R, Prodromou A, Verpoest I, et al. Textile composites: modelling strategies. Composites Part A: Applied Science and Manufacturing. 2001;32(10):1379-94.
[134] Chung DDL. Carbon fiber composites. Boston :: Butterworth-Heinemann; 1994.
[135] Varna J, Joffe R, Berglund L, Lundström T. Effect of voids on failure mechanisms in RTM laminates. Composites Science and Technology. 1995;53(2):241-9.

[136] Yan L, Chouw N, Yuan X. Improving the mechanical properties of natural fibre fabric reinforced epoxy composites by alkali treatment. Journal of Reinforced Plastics and Composites. 2012;31(6):425-37.
[137] Rockland LB. Saturated salt solutions for static control of relative humidity between 5° and 40° C. Analytical Chemistry. 1960;32(10):1375-6.
[138] Stamboulis A, Baillie CA, Peijs T. Effects of environmental conditions on mechanical and physical properties of flax fibers. Composites Part A: Applied Science and Manufacturing. 2001;32(8):1105-15.
[139] Xue D, Miao M. Influences of moisture absorption and chemical treatments on the resin flow characteristics of natural fibre nonwoven mats. Journal of The Textile Institute. 2012;103(9):1024-30.
[140] Aziz SH, Ansell MP. The effect of alkalization and fibre alignment on the mechanical and thermal properties of kenaf and hemp bast fibre composites: Part 1 – polyester resin matrix. Composites Science and Technology. 2004;64(9):1219-30.
[141] Wong K, Yousif B, Low K. The effects of alkali treatment on the interfacial adhesion of bamboo fibres. Proceedings of the Institution of Mechanical Engineers, Part L: Journal of Materials Design and Applications. 2010;224(3):139-48.
[142] Volpe CD, Siboni S. Some reflections on acid–base solid surface free energy theories. Journal of Colloid and Interface Science. 1997;195(1):121-36.
[143] Cantero G, Arbelaiz A, Llano-Ponte R, Mondragon I. Effects of fibre treatment on wettability and mechanical behaviour of flax/polypropylene composites. Composites Science and Technology. 2003;63(9):1247-54.
[144] Croteau-Labouly B. Caractérisation combinée de la perméabilité et de la compaction des renforts fibreux dans les procédés de fabrication des composites par infusion. École polytechnique de Montréal Thesis; Montreal, QC, 2007.
[145] Chen R, Dong C, Liang Z, Zhang C, Wang B. Flow modeling and simulation for vacuum assisted resin transfer molding process with the equivalent permeability method. Polymer Composites. 2004;25(2):146-64.
[146] Lee YJ, Wu JH, Hsu Y, Chung CH. A prediction method on in-plane permeability of mat/roving fibers laminates in vacuum assisted resin transfer molding. Polymer Composites. 2006;27(6):665-70.
[147] Mohan RV, Shires DR, Tamma KK, Ngo ND. Flow channels/fiber impregnation studies for the process modeling/analysis of complex engineering structures manufactured by resin transfer molding. Polymer Composites. 1998;19(5):527-42.
[148] Amico S, Lekakou C. An experimental study of the permeability and capillary pressure in resin-transfer moulding. Composites Science and Technology. 2001;61(13):1945-59.
[149] Ruiz E, Lebel F, Trochu F. Experimental study of capillary flows, voids formation and void migration in LCM manufacturing. In: Proceedings of 11th International Conference on Flow Processing in Composite Materials. Auckland, New Zealand, 2012.
[150] Young W-B, Wu S. Permeability measurement of bidirectional woven glass fibers. Journal of Reinforced Plastics and Composites. 1995;14(10):1108-20.

[151] Hubert P, Poursartip A. A method for the direct measurement of the fibre bed compaction curve of composite prepregs. Composites Part A: Applied Science and Manufacturing. 2001;32(2):179-87.
[152] Berglund LA, Peijs T. Cellulose biocomposites—from bulk moldings to nanostructured systems. MRS bulletin. 2010;35(03):201-7.
[153] Okubo K, Fujii T, Thostenson ET. Multi-scale hybrid biocomposite: Processing and mechanical characterization of bamboo fiber reinforced PLA with microfibrillated cellulose. Composites Part A: Applied Science and Manufacturing. 2009;40(4):469-75.
[154] Lau K-T, Hui D. Effectiveness of using carbon nanotubes as nano-reinforcements for advanced composite structures. Carbon(UK). 2002;40(9):1605-6.
[155] Rachmadini Y, Tan VBC, Tay TE. Enhancement of Mechanical Properties of Composites through Incorporation of CNT in VARTM - A Review. Journal of Reinforced Plastics and Composites. 2010;29(18):2782-807.
[156] Zhu J, Imam A, Crane R, Lozano K, Khabashesku VN, Barrera EV. Processing a glass fiber reinforced vinyl ester composite with nanotube enhancement of interlaminar shear strength. Composites Science and Technology. 2007;67(7):1509-17.
[157] Bowles KJ, Frimpong S. Void Effects on the Interlaminar Shear Strength of Unidirectional Graphite-Fiber-Reinforced Composites. Journal of Composite Materials. 1992;26(10):1487-509.
[158] Costa ML, Almeida SFMd, Rezende MC. The influence of porosity on the interlaminar shear strength of carbon/epoxy and carbon/bismaleimide fabric laminates. Composites Science and Technology. 2001;61(14):2101-8.
[159] Hancox NL. The compression strength of unidirectional carbon fibre reinforced plastic. Journal of Materials Science. 1975;10(2):234-42.
[160] Liu L, Zhang B-M, Wang D-F, Wu Z-J. Effects of cure cycles on void content and mechanical properties of composite laminates. Composite Structures. 2006;73(3):303-9.
[161] Phillips S, Lessard L. Application of natural fiber composites to musical instrument top plates. Journal of Composite Materials. 2012;46(2):145-54.
[162] Campbell FC, Mallow AR, Browning CE. Porosity in carbon fiber composites an overview of causes. Journal of Advanced Materials. 1995;26(4):18-33.
[163] Repecka L, Boyd J. Vacuum-Bag-Only-Curable Prepregs That Produce Void Free Parts. International SAMPE Symposium2002.
[164] Tung C-YM, Dynes PJ. Relationship between viscoelastic properties and gelation in thermosetting systems. Journal of Applied Polymer Science. 1982;27(2):569-74.
[165] Boey FYC, Lye SW. Void reduction in autoclave processing of thermoset composites: Part 1: High pressure effects on void reduction. Composites. 1992;23(4):261-5.
[166] Summerscales J, Dissanayake N, Virk A, Hall W. A review of bast fibres and their composites. Part 2 - Composites. Composites Part A: Applied Science and Manufacturing. 2010;41(10):1336-44.

[167] Bureau MN, Denault J. Fatigue resistance of continuous glass fiber/polypropylene composites: consolidation dependence. Composites Science and Technology. 2004;64(12):1785-94.
[168] Costa ML, Rezende MC, de Almeida SFM. Effect of Void Content on the Moisture Absorption in Polymeric Composites. Polymer-Plastics Technology and Engineering. 2006;45(6):691-8.
[169] Thomason JL. The interface region in glass fibre-reinforced epoxy resin composites: 2. Water absorption, voids and the interface. Composites. 1995;26(7):477-85.
[170] Duigou AL, Davies P, Baley C. Exploring durability of interfaces in flax fibre/epoxy micro-composites. Composites Part A: Applied Science and Manufacturing, 2013. (published online before print)
[171] Gassan J, Bledzki AK. Effect of cyclic moisture absorption desorption on the mechanical properties of silanized jute-epoxy composites. Polymer Composites. 1999;20(4):604-11.
[172] Thwe MM, Liao K. Effects of environmental aging on the mechanical properties of bamboo–glass fiber reinforced polymer matrix hybrid composites. Composites Part A: Applied Science and Manufacturing. 2002;33(1):43-52.
[173] Zamri MH, Akil HM, Bakar AA, Ishak ZAM, Cheng LW. Effect of water absorption on pultruded jute/glass fiber-reinforced unsaturated polyester hybrid composites. Journal of Composite Materials. 2012;46(1):51-61.
[174] Dweib M, Hu B, O'donnell A, Shenton H, Wool R. All natural composite sandwich beams for structural applications. Composite Structures. 2004;63(2):147-57.
[175] Phillips S, Baets J, Lessard L, Hubert P, Verpoest I. Characterization of flax/epoxy prepregs before and after cure. Journal of Reinforced Plastics and Composites. 2013; 32 (11), 777-785.
[176] Phillips S, Kuo P-Y, Demaria C, Lessard L, Sain M, Hubert P. Effect of Common Chemical Treatments on the Process Kinetics and Mechanical Properties of Flax/Epoxy Composites Manufactured by Resin Infusion. Journal of Polymers and the Environment. 2013. (submitted)
[177] Phillips S, Kuo P-Y, Demaria C, Lessard L, Sain M, Hubert P. Multi-scale biocomposites based on flax, nanocellulose and epoxy. Journal of Polymers and the Environment. 2013. (under preparation)
[178] Phillips S, Baets J, Hubert P, Lessard L, Verpoest I. Experimental investigation into void content and mechanical properties of cured flax/epoxy prepregs. In: Proceedings of 15th European Conference on Composite Materials. Venice, Italy, 2012.
[179] Phillips S, Kuo P-Y, Demaria C, Lessard L, Sain M, Hubert P. Effect of Common Chemical Treatments on the Process Kinetics and Mechanical Properties of Flax/Epoxy Composites Manufactured by Resin Infusion. In: Proceedings of 11th International Conference on Flow Processing in Composite Materials. Auckland, New Zealand, 2012.
[180] Phillips S, Kuo P-Y, Demaria C, Lessard L, Sain M, Hubert P. Development of multi-scale biocomposites from flax, nanocellulose and epoxy by resin infusion. In: Proceedings of 19th International Conference on Composite Materials. Montreal, Quebec, 2013. (submitted)

Appendix A: Mechanical properties of various cellulose-based fibres

	Fibre	Density (g/cm^3)	Tensile strength (MPa)	Young's modulus (GPa)	Specific modulus ($Nm/kgx10^{-6}$)	Price (Euro/kg)
Bast fibres	Flax	1.40-1.50	343-1035	27-80	19-53	2.29-11.47
	Jute	1.30-1.50	187-773	3-55	2-37	0.12-0.35
	Ramie	1.50	400-938	44-128	29-85	1.44-2.40
	Hemp	1.40-1.50	580-1110	3-90	2-60	0.57-1.73
	Kenaf	1.22-1.40	295-930	22-53	18-38	0.53-0.61
Leaf fibres	Banana	1.30-1.35	529-914	7.7-32.0	6-24	0.7-0.9
	Abaca	1.50	980	72	48.1	0.81-0.92
	Pineapple	1.52-1.56	170-1627	6.21-82	4-53	0.36-0.72
	Henequen	1.49	430-580	10.1-16.3	7-11	0.38-0.67
	Sisal	1.30-1.50	507-855	9-28	7-19	0.70-1.02
Non natural (for comparison	E-glass	2.50-2.55	2000-3500	73	29	1.25
	Aramide	1.40-1.45	3000-3150	63-67	45-48	7.2
	Carbon	1.40-1.75	4000	230-240	164-171	12.0

adapted from [4]

Appendix B: Sensor calibration procedures

Laser sensors (Banner® LG5A65NIQ)

1) The height of the laser was first adjusted into their active range from the tool plate (4.5 cm to 6.0cm).
2) A series of Starrett® thickness gauges were then placed underneath each laser and the current levels were recorded.
3) The current versus thickness relationship was then plotted to obtain the linear calibration coefficients (Figure B-1).
4) Steps 1 to 3 were repeated before every test due to possible movement of the tool plate.

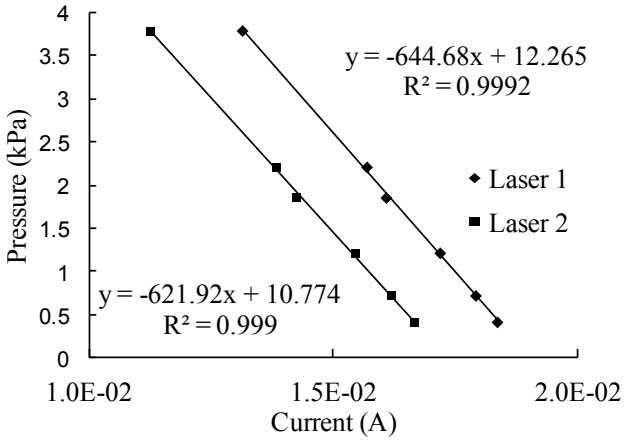

Figure B-1: Calibration relationships for Banner® LG5A65NIQ laser sensors

Wika® Eco-tronic® pressure transducer

1) The pressure sensor was installed on a sealed resin trap.
2) Vacuum was drawn and the current level was recorded.
3) The vacuum level was obtained using an Ashcroft® 733-52 pressure gauge installed on the resin trap (calibrated by the manufacturer).
4) Step 2 and 3 were repeated for five vacuum levels and the linear calibration coefficients were obtained (Figure B-2).

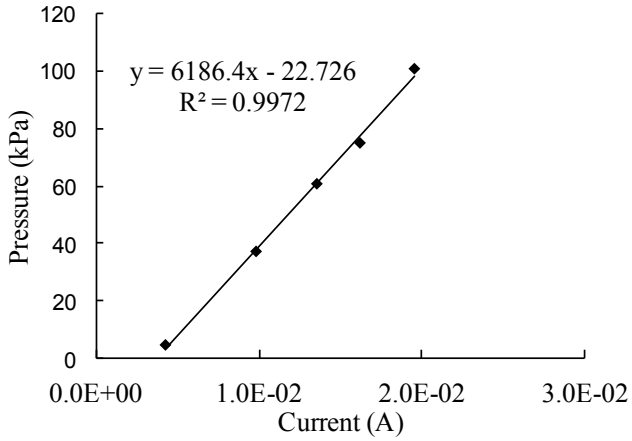

Figure B-2: Calibration relationship for Wika® Eco-tronic® pressure transducer

Omega® PX26 pressure transducers

1) A vacuum bag was placed over the pressure transducers with breather cloth and sealant tape.
2) Vacuum was pulled and the system was checked for leaks by disconnecting the vacuum line and monitoring the vacuum level on an Ashcroft® 733-52 pressure gauge (calibrated by the manufacturer) installed on the resin trap.
3) The current level was recorded for the five pressure transducers.
4) The vacuum level was read off the Ashcroft® 733-52 pressure gauge.
5) Steps 3 and 4 were repeated for five vacuum levels and the calibration curve was obtained (Figure B-3).

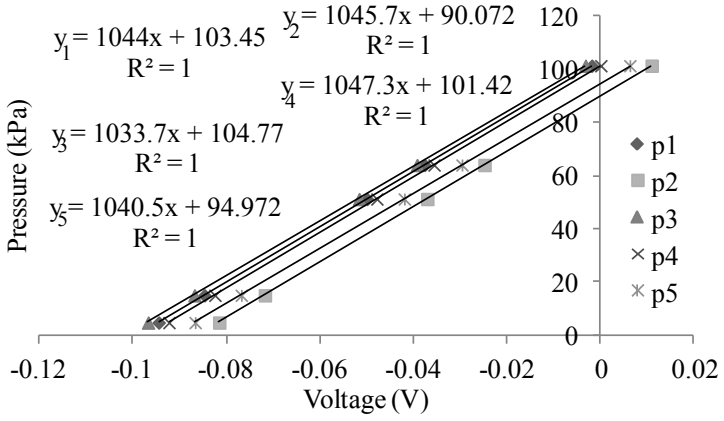

Figure B-3: Calibration relationships for Omega® PX26 pressure transducers

Appendix C: Data from unsaturated permeability measurements

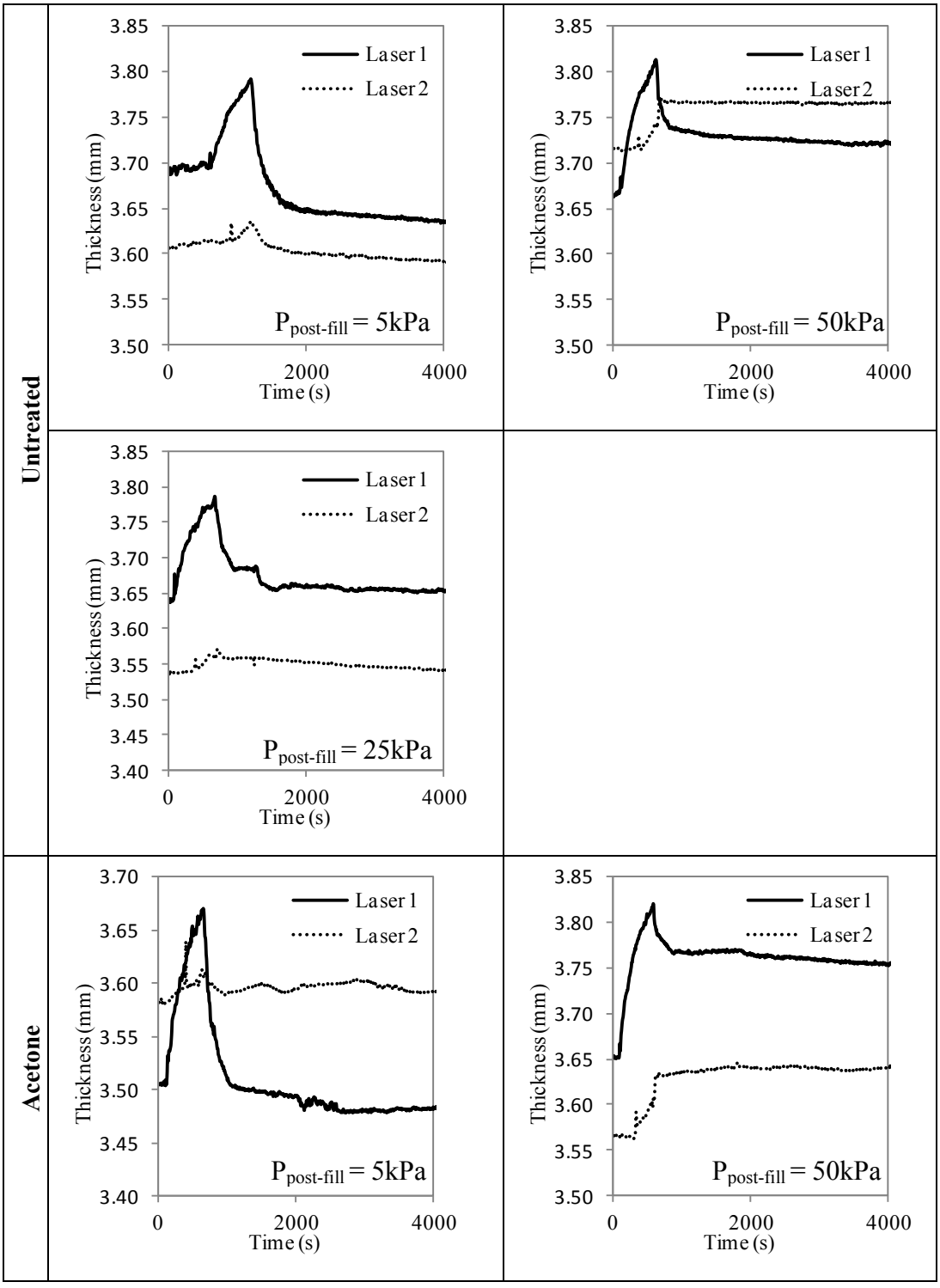

Acetone	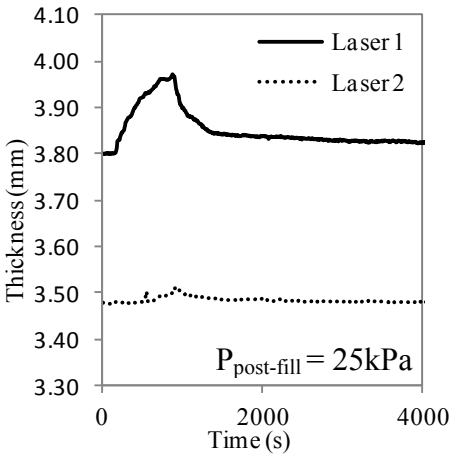	
Alkaline	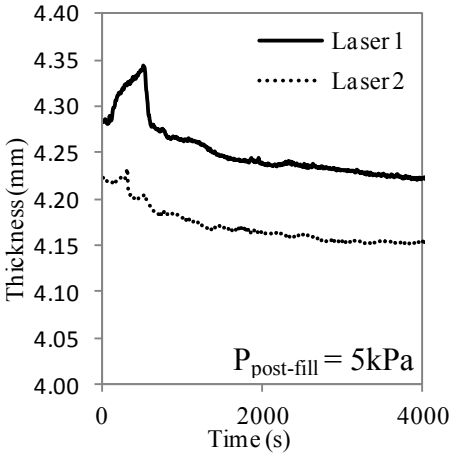	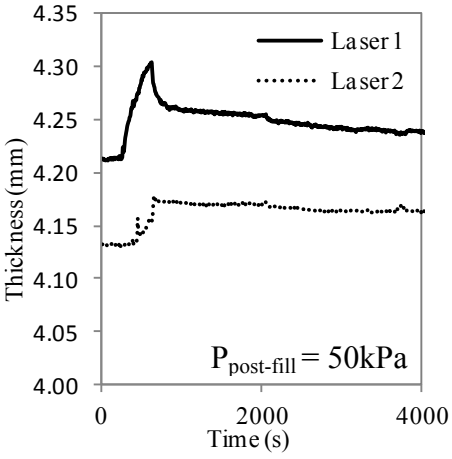
	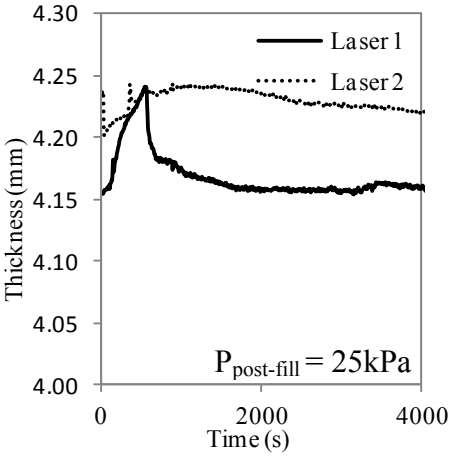	

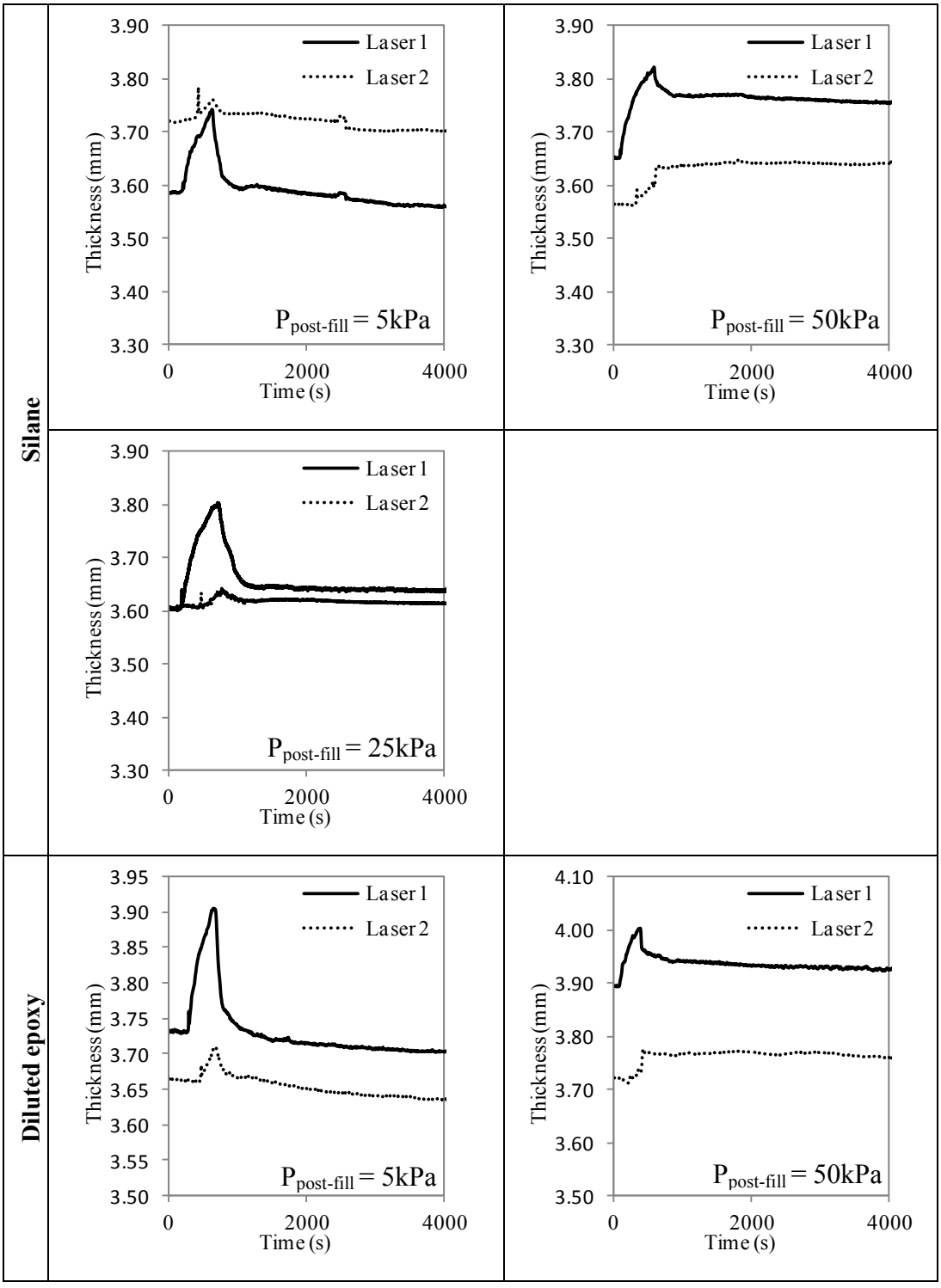
Silane
Diluted epoxy
Laser 1
Laser 2
Thickness (mm)
Time (s)
$P_{post-fill}$ = 5kPa
$P_{post-fill}$ = 25kPa
$P_{post-fill}$ = 50kPa

Diluted epoxy	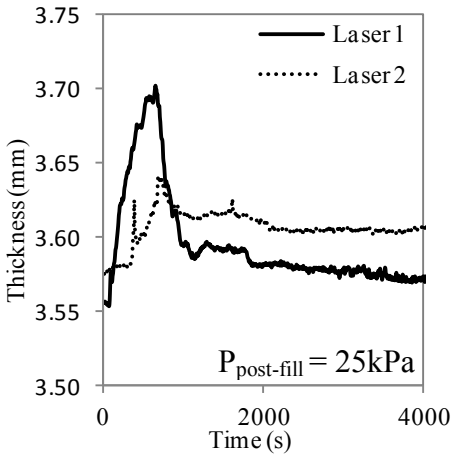	

Appendix D: Data from saturated permeability measurements

Infusion 1

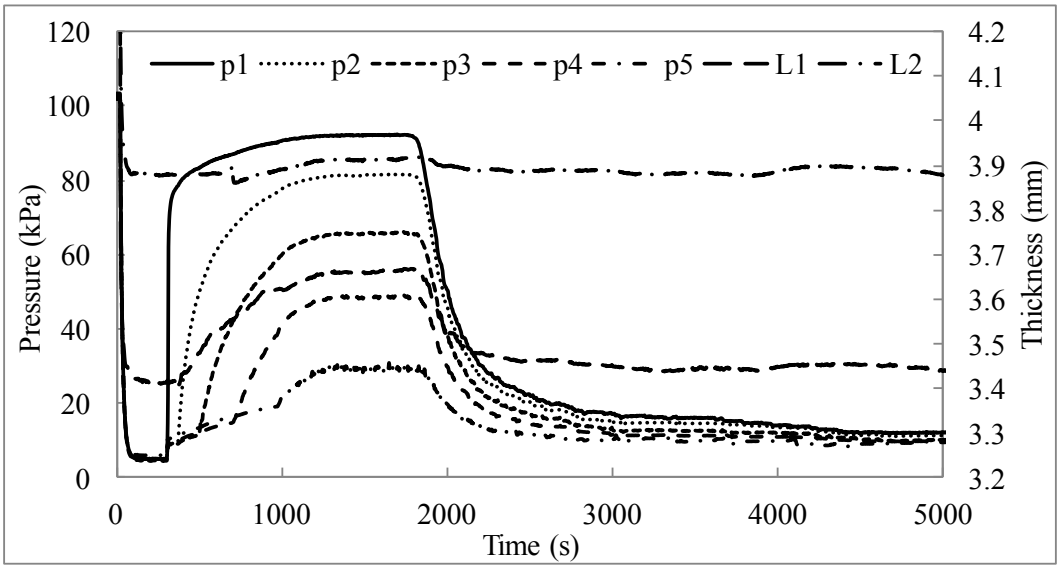

Infusion 2

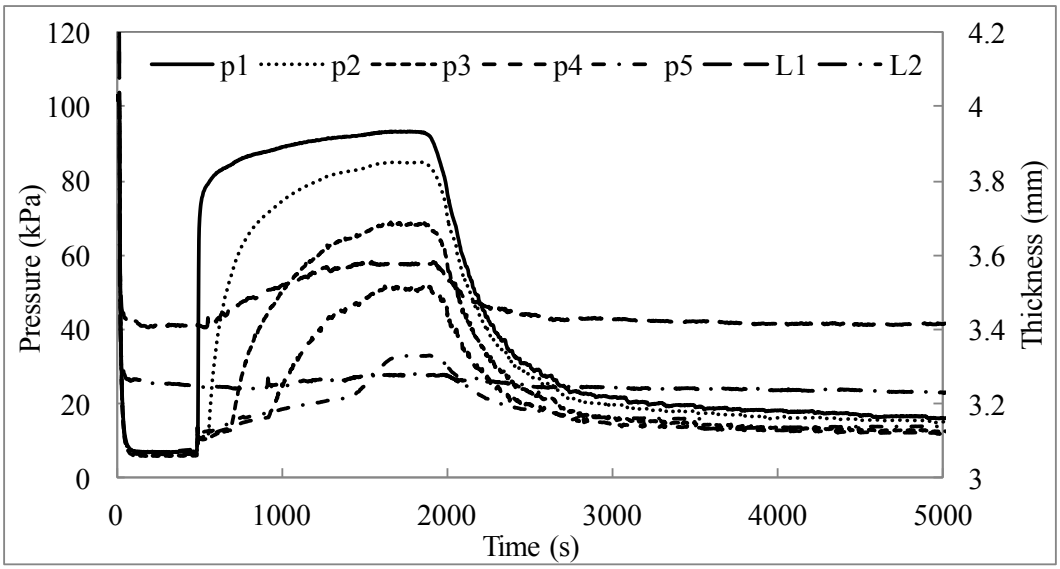

Infusion 3 (vacuum turned off during post-fill)

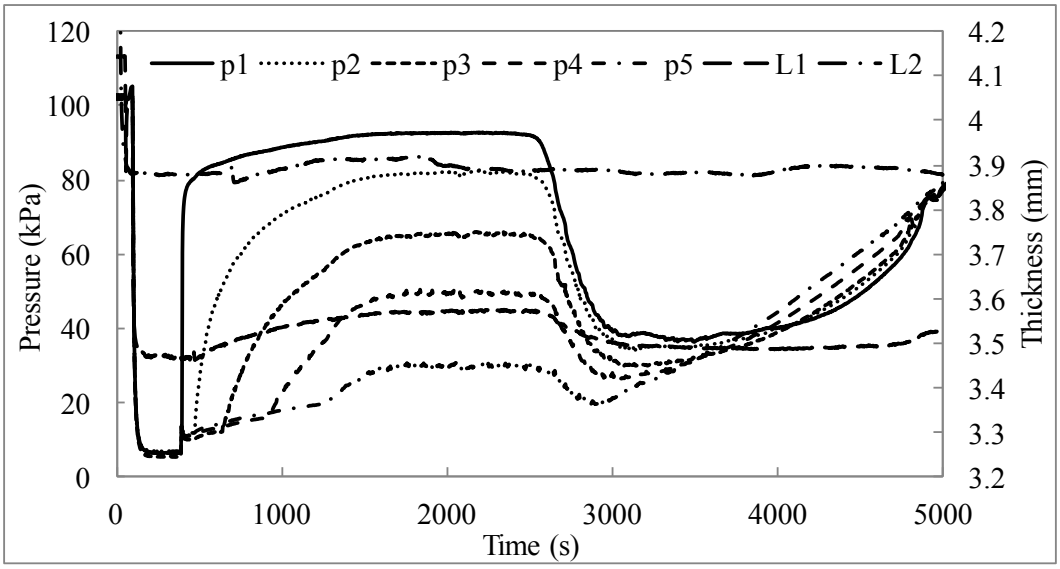

Infusion 4

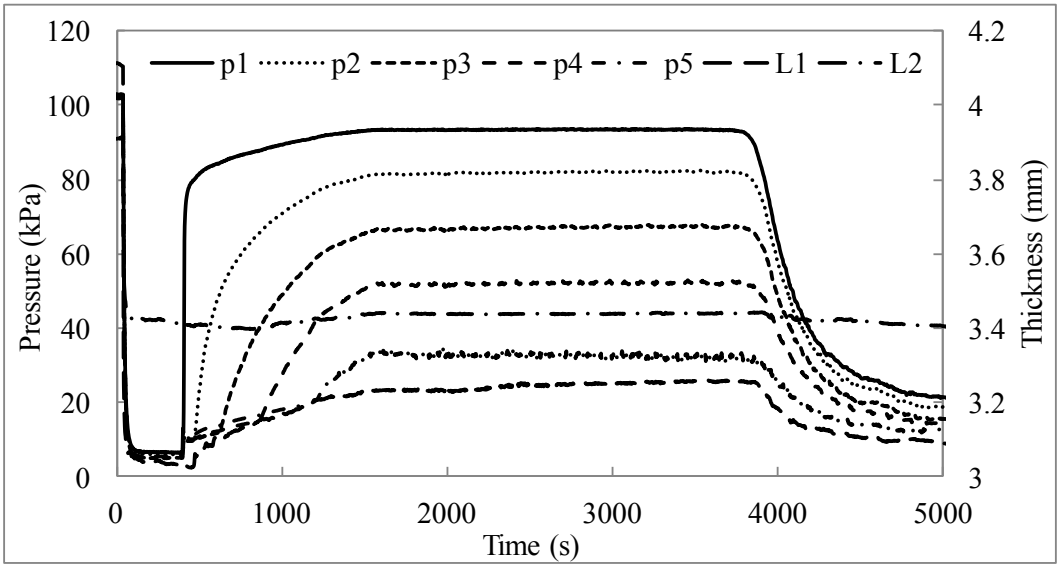

Appendix E: Sample cross-sections for void analysis

Surface treatment case study (Section 5.3.1)

Untreated

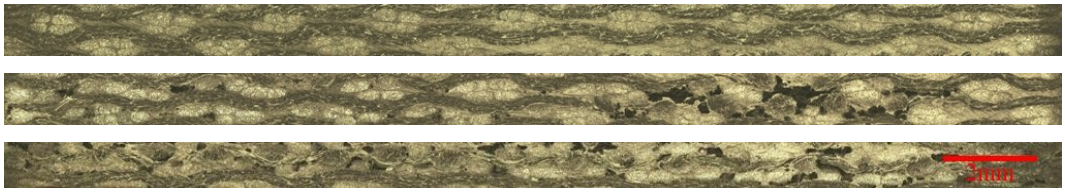

Acetone

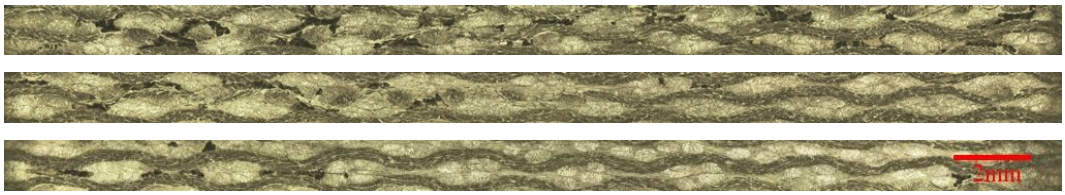

Alkaline

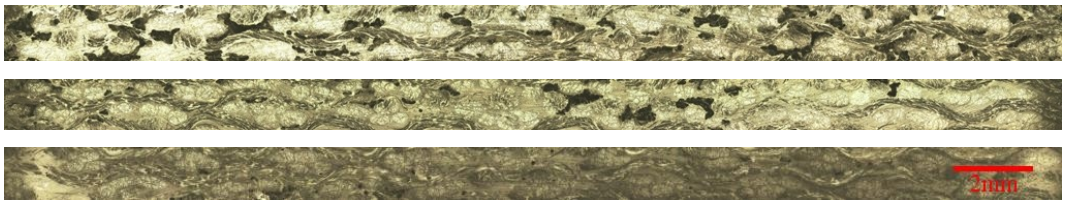

Silane

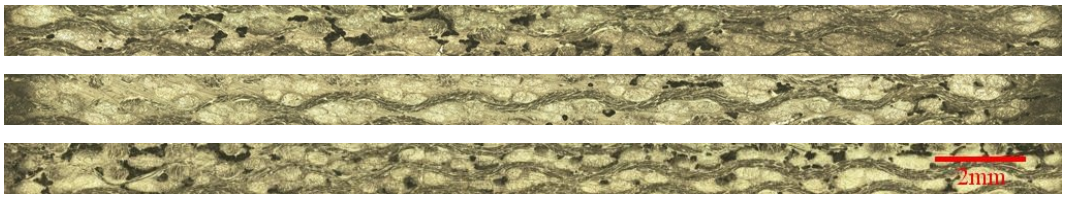

Diluted epoxy

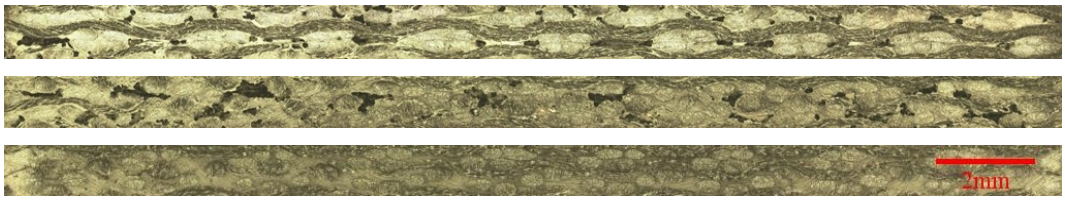

Multi-scale composites by resin infusion (Section 6.1)

SS (Dry)

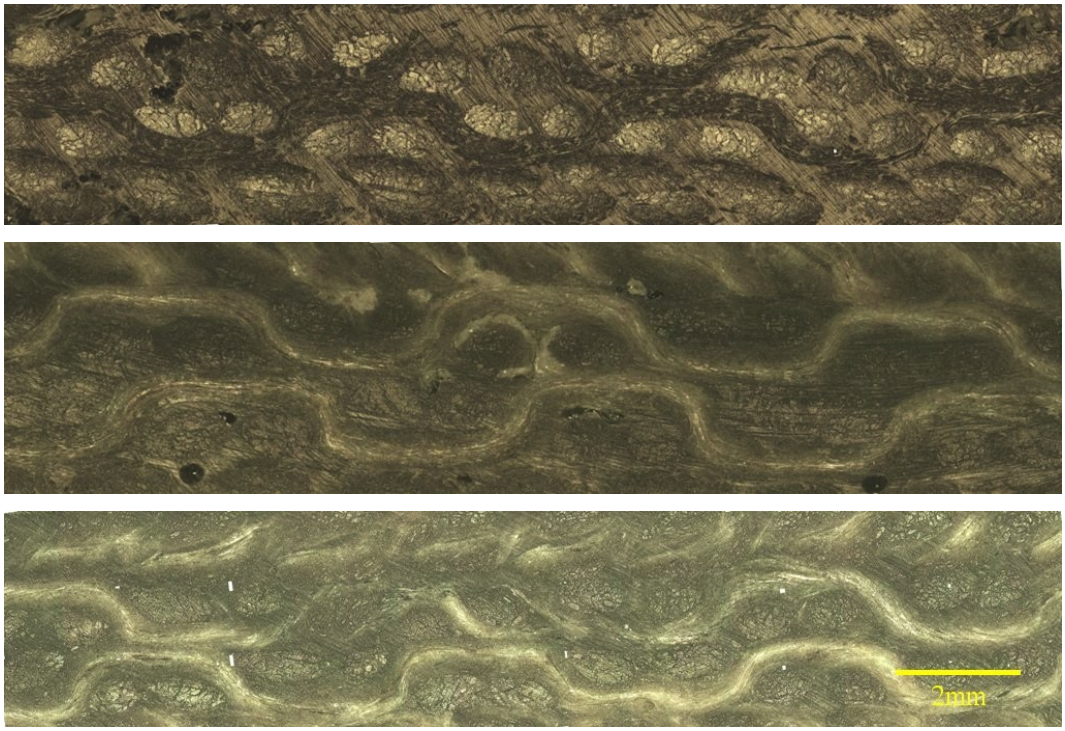

SS (Wet)

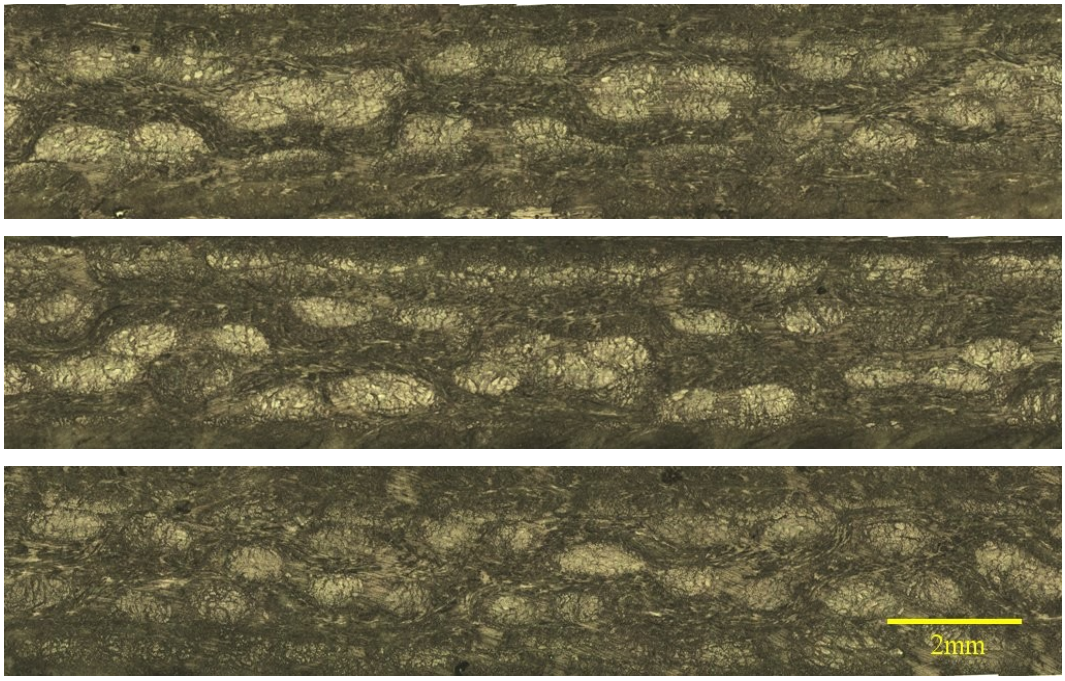

MS (Grafted)

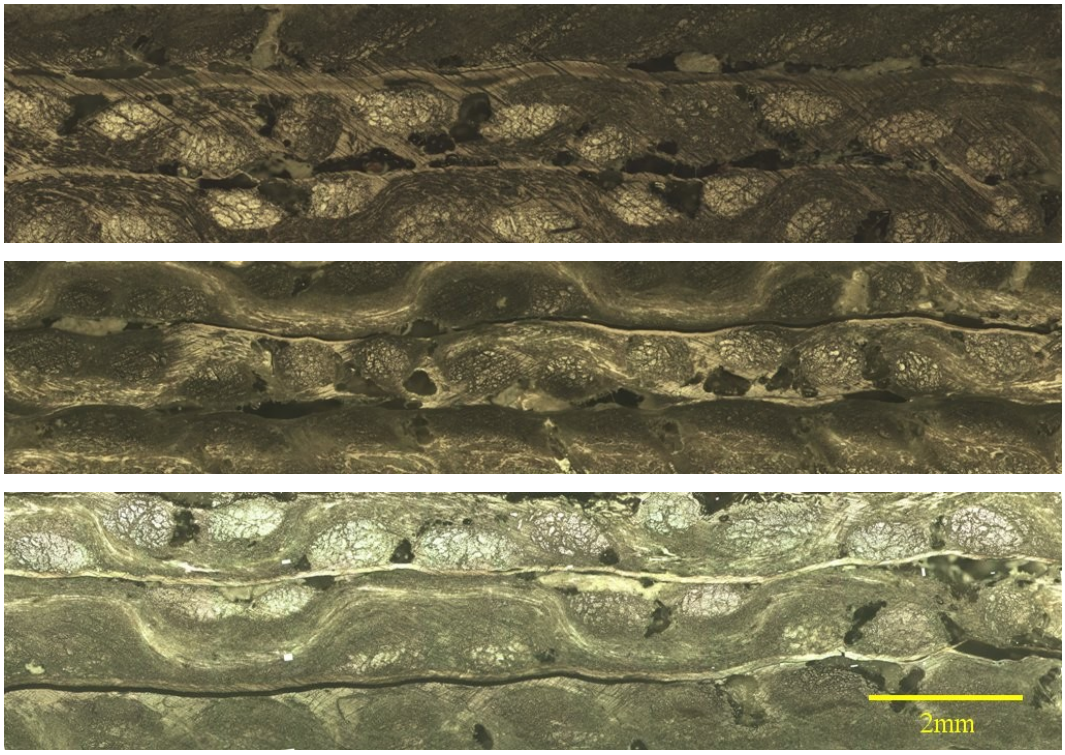

MS (Wet-layup)

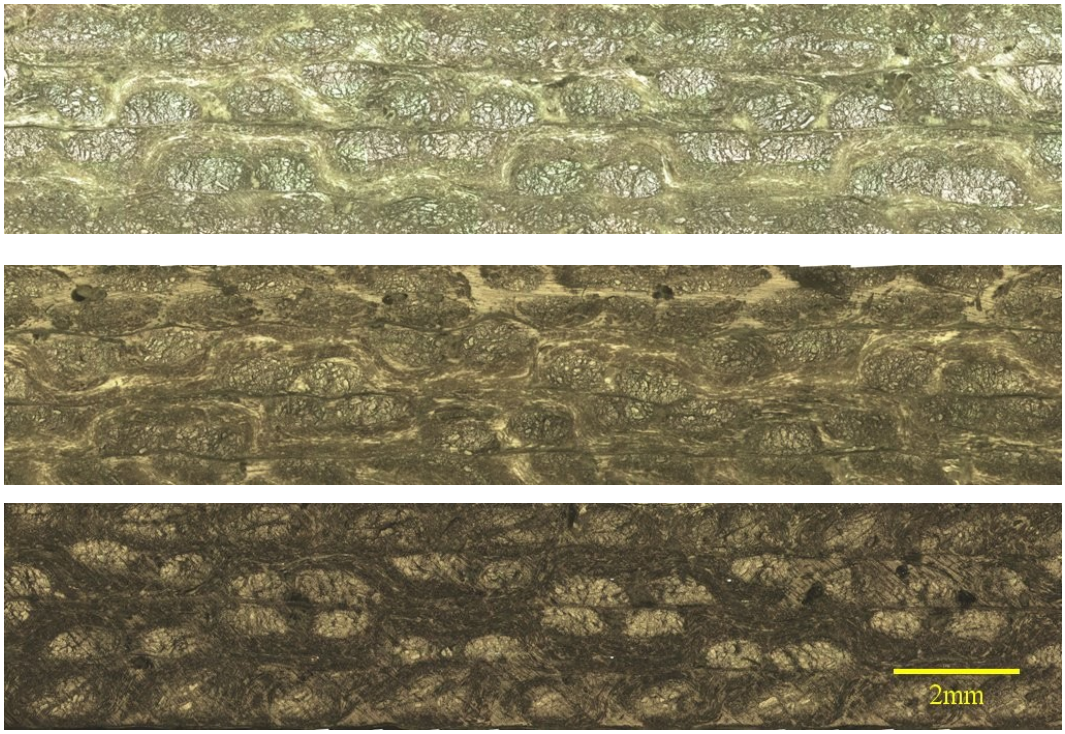

Prepreg case study (Section 6.2)

BL200

1 bar

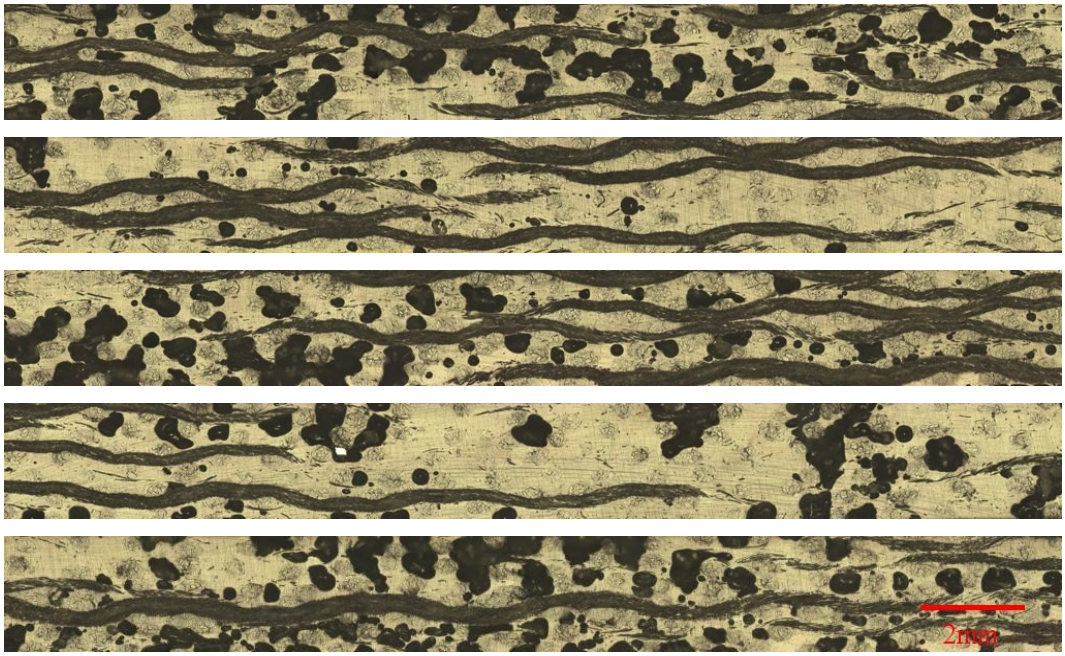

3 bar

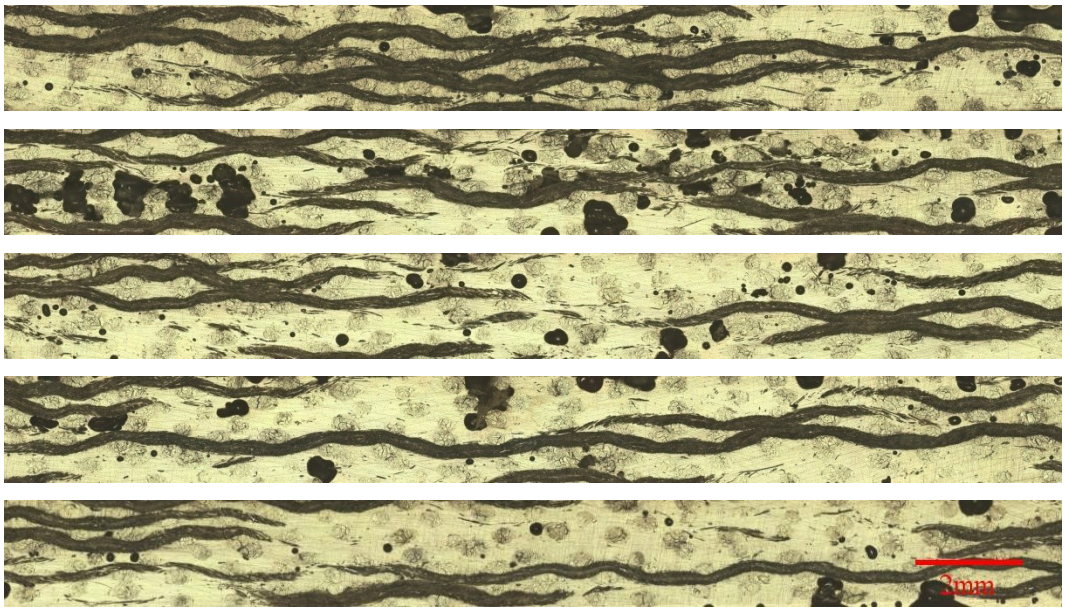

5 bar

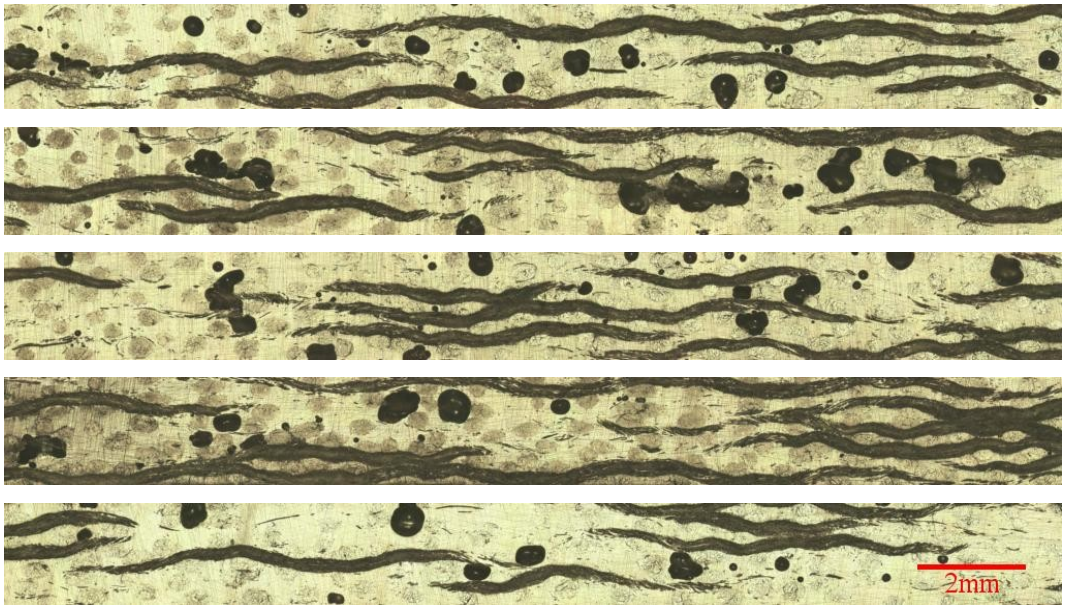

BL550

1 bar

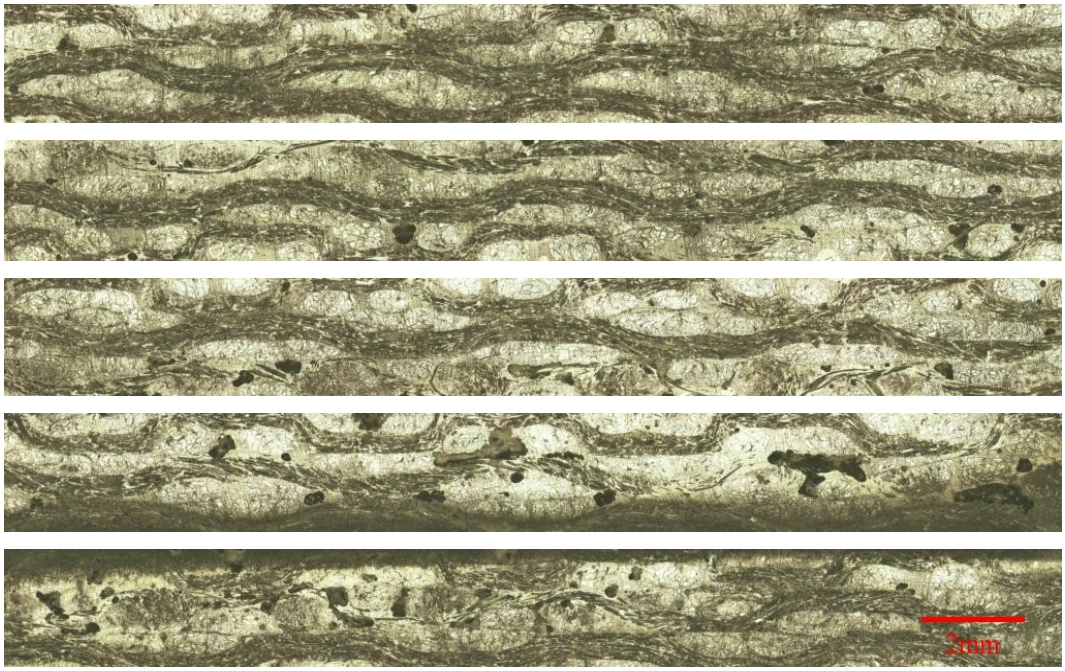

3 bar

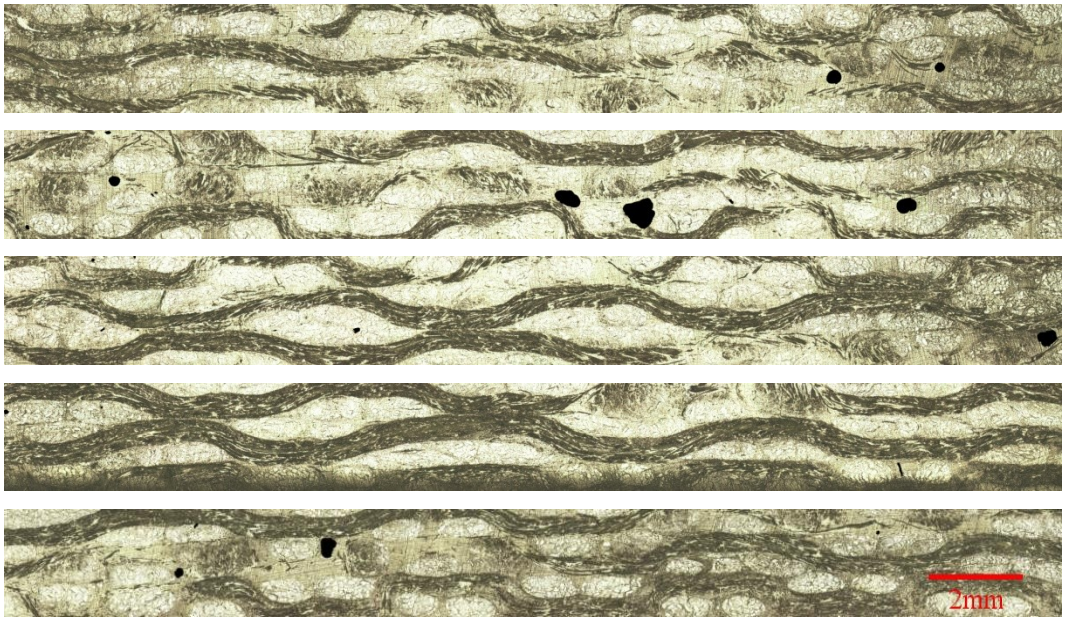

5 bar

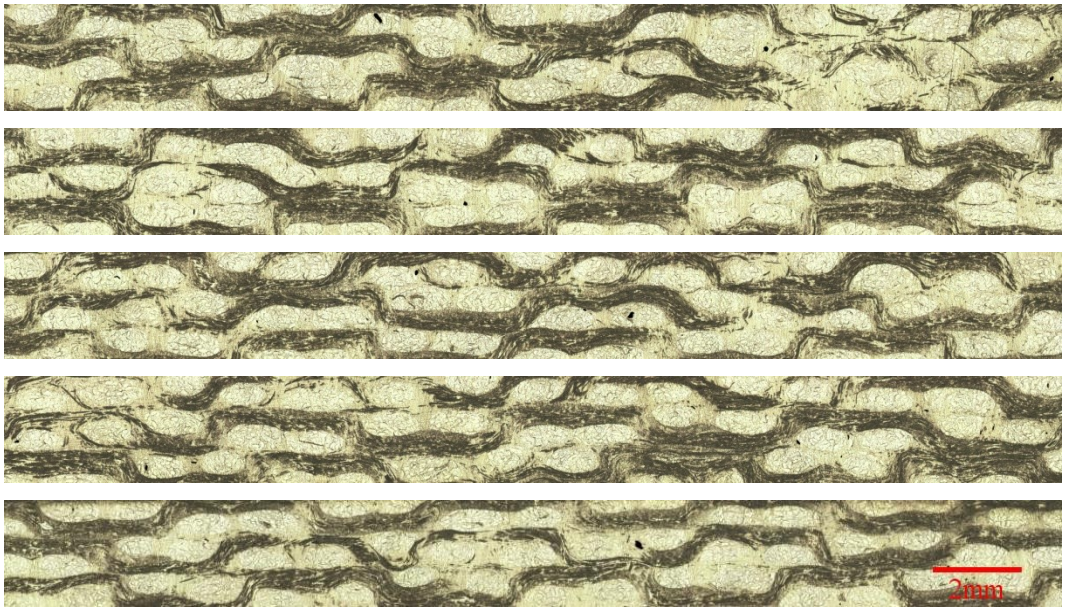

Appendix F: Force history data from drop-weight impact testing (Section 6.1.3.3)

SS (Dry)

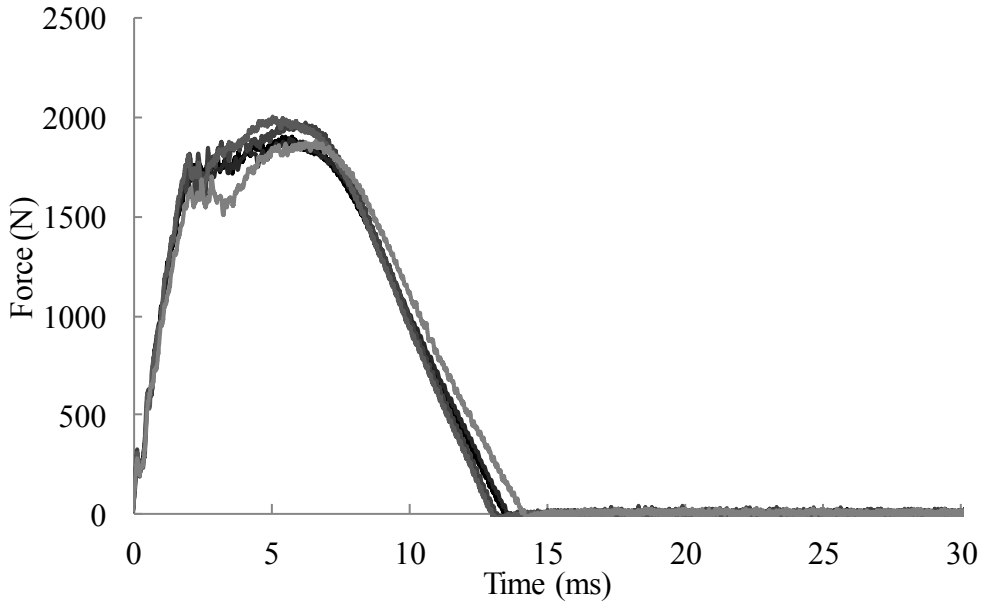

MS (Grafted)

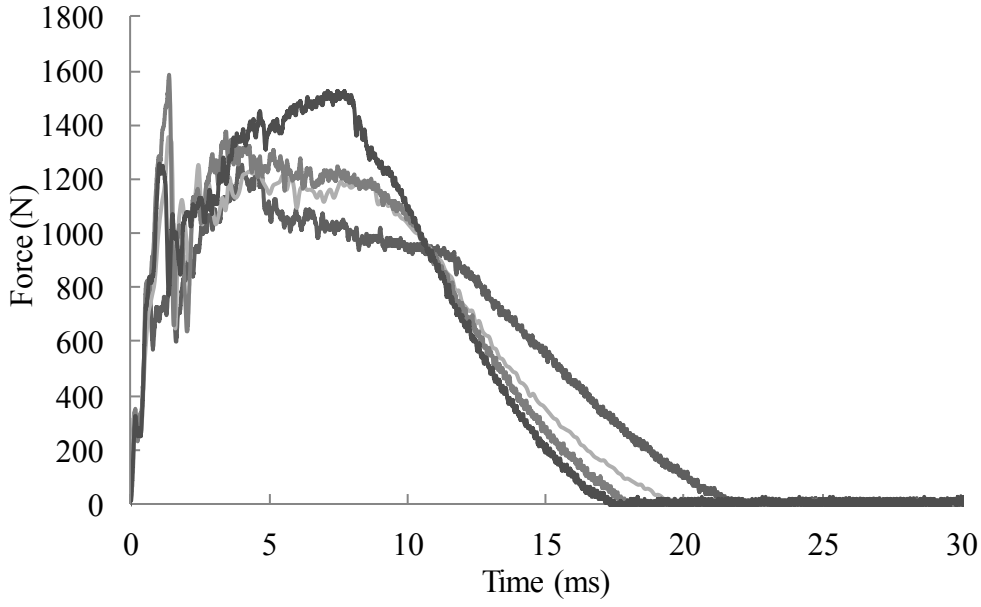

SS (Wet)

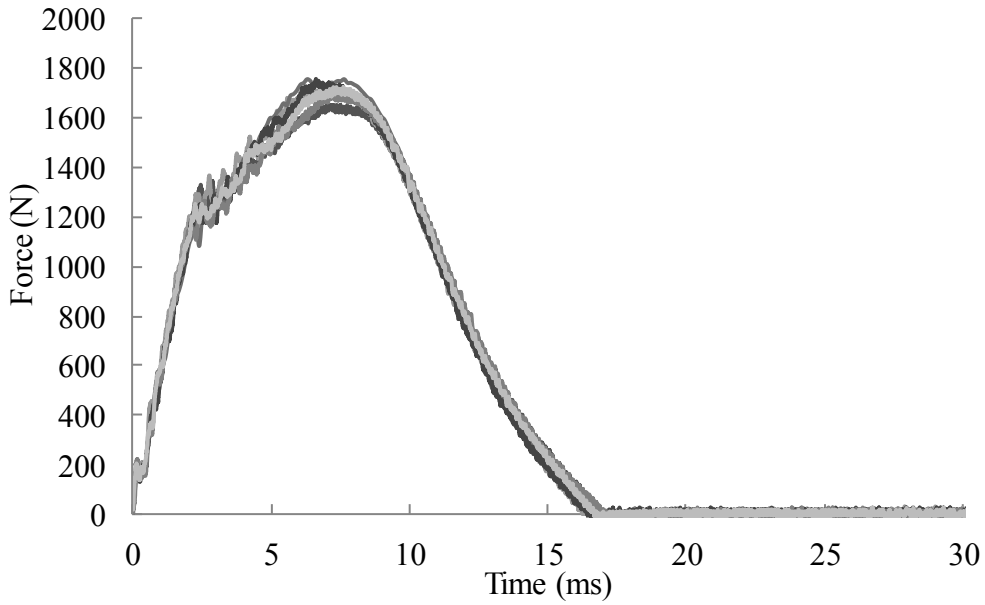

MS (Wet-layup)

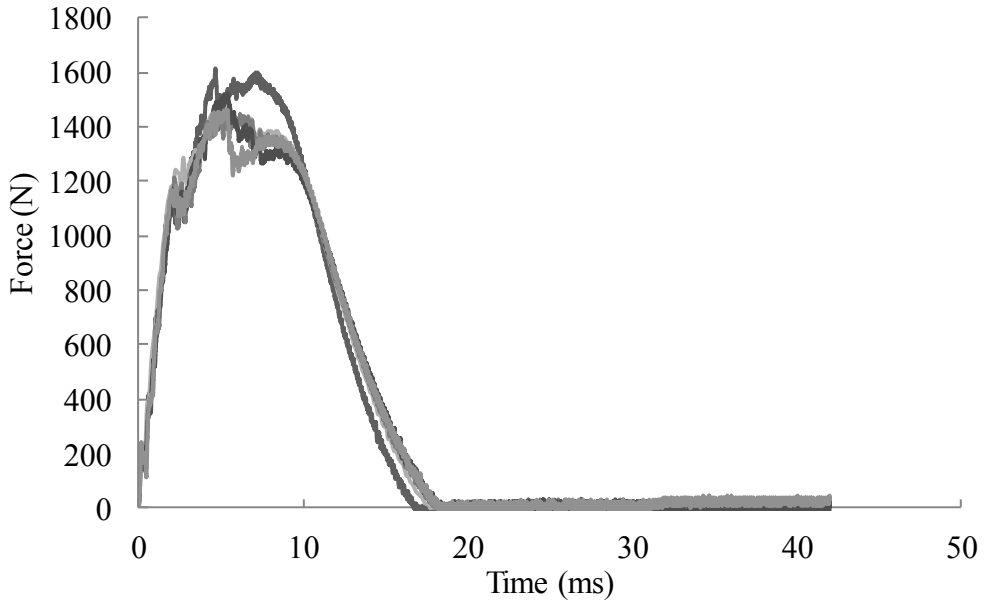

Appendix G: Stress-strain curves from tensile testing (Section 6.2)

Effect of pressure

	BL200	BL550
1 bar	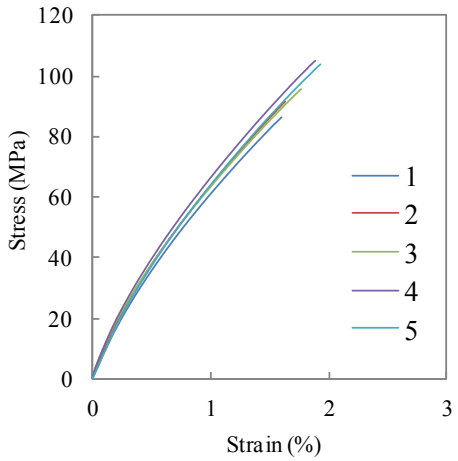	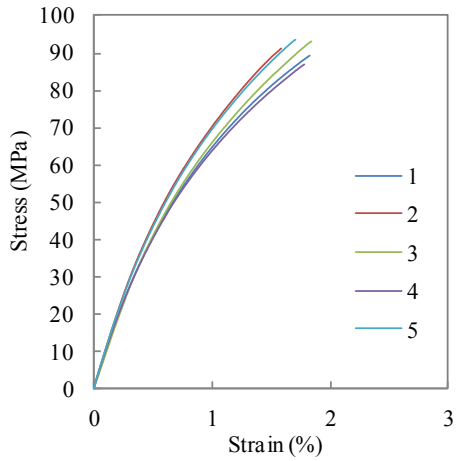
3 bar	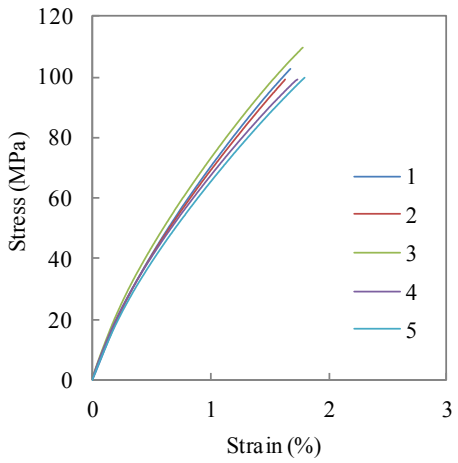	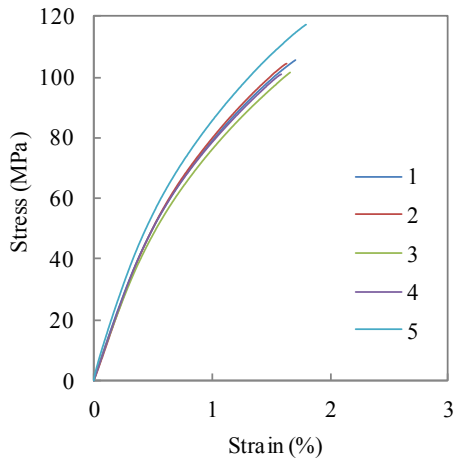
5 bar	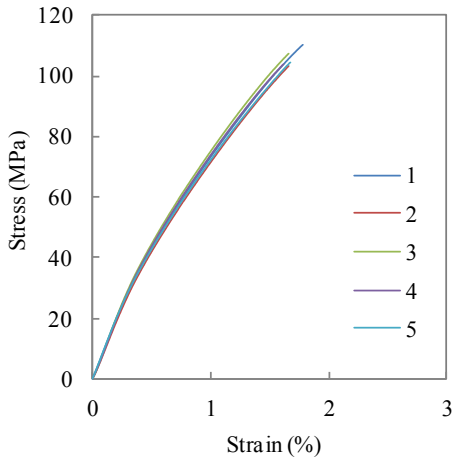	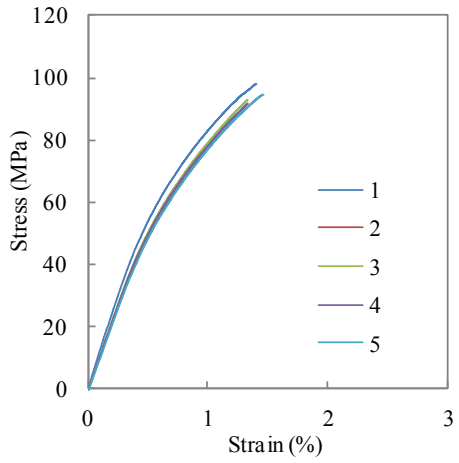

Effect of layup